

PRODUCTION AND CHARACTERIZATION OF ALKALI-FREE BOROSILICATE  
GLASS AND GLASS-CERAMICS FOR DISPLAY TECHNOLOGY



by  
Gökhan Nar

Submitted to Graduate School of Natural and Applied Sciences  
in Partial Fulfillment of the Requirements  
for the Degree of Master of Science in  
Materials and Nanotechnology Engineering

Yeditepe University  
2020

PRODUCTION AND CHARACTERIZATION OF ALKALI-FREE BOROSILICATE  
GLASS AND GLASS-CERAMICS FOR DISPLAY TECHNOLOGY

APPROVED BY:

Prof. Dr. Volkan Günay  
(Thesis Supervisor)  
(Yeditepe University)

.....

Prof. Dr. Şenol Yılmaz  
(Sakarya University)

.....

Assist. Prof. Dr. Mehmet Safa BODUR  
(Yeditepe University)

.....

DATE OF APPROVAL: ...../...../2020

## ACKNOWLEDGEMENTS

I would like to thank my supervisor Prof. Dr. Volkan GÜNAY for the opportunity to be supervised by him and valuable contributions throughout my thesis studies.

I would like to thank my co-supervisor Dr. Yusuf ÖZTÜRK for his patience and endless support in every stage of my thesis.

I would also like to thank Doç. Dr. Esin GÜNAY for acceptance of me in her research group and continuous support.

I would like to thank Chief Technician Bilal ALCAN for supporting in the experimental studies.

Finally, I would like to thank my family for their endless love and support, which makes everything more beautiful.

## ABSTRACT

### PRODUCTION AND CHARACTERIZATION OF ALKALI-FREE BOROSILICATE GLASS AND GLASS-CERAMICS

The rapid and continuous increasing in the development of display technologies and expansion of use these technologies in our daily social and business life have made these technology focus of attention. Glass materials that directly affects the performance of this systems with its properties are shown as the significant component in the display technology system. Within scope of this thesis, a composition was obtained at certain intervals from 32 patents with 912 compositions included glass substrates properties for display technologies by using data mining. Glass-ceramic materials were produced by adding of 1-2-3 wt. percent LiF as nucleating agent to obtained the glass composition. Adding of LiF (Lithium Fluoride) to alkali-free borosilicate glass substrate in order to produce glass-ceramic materials in the determined compositons will be first study in this field. In this sense, it is thought that it will contribute to the literature study in the field of producing glass-ceramics from glass substrate materials by using LiF as nucleating agent.

Physical (thermal expansion coefficient,  $T_g$  and softening temperture), chemical (crystal structure of glass-ceramics), optical (transmittance), microstructure (optical microscope, SEM) properties of parent glass composition without additive of LiF and doped 1-2-3 wt. percent LiF glass compositions was performed. Finally, the changes in the specified properties in the between glass and glass-ceramics materials were investigated.

## ÖZET

### **EKRAN TEKNOLOJİLERİNDE KULLANILAN ALKALİ İÇERMEYEN CAM VE CAM-SERAMİK MALZEMELERİN ÜRETİMİ VE KARAKTERİZASYONU**

Ekran teknolojilerindeki gelişimin hızla artması ve günlük sosyal ve iş hayatımızda bu teknolojilerin kullanımının genişlemesi ekran teknolojilerine olan ilgiyi artırmaktadır. Cam malzemeleri, ekran teknolojileri sisteminde bulunan ve özellikleri ile bu sistemin performansını direkt olarak etkileyen en önemli bileşen olarak gösterilmektedir. Bu tez kapsamında, ekran teknolojilerinde kullanılan alttaş camların yer aldığı 32 patent ve bu patentler içerisinde bulunan 912 adet kompozisyondan veri madenciliği gerçekleştirilerek belirli aralıklarda bir kompozisyon elde edilmiştir. Elde edilen cam kompozisyonu ve bu kompozisyona çekirdekleştirici olarak yüzde ağ. 1-2-3 LiF (Lityum Florür) ilave edilerek cam-seramik malzemeleri üretilmiştir. Alttaş camlardan çekirdekleştirici ajan olarak LiF kullanılarak elde edilen cam-seramik malzemeleri bu alanda ilk çalışma olacaktır. Bu anlamda alttaş cam kompozisyonlarından cam-seramik malzemeleri üretimi çalışmalarında literatüre bir katkı sağlayacağı düşünülmektedir.

Patentlerden elde edilen cam kompozisyonunun ve sonrasında yüzde ağ. 1-2-3 LiF katkılı kompozisyonların fiziksel (termal genleşme katsayısı,  $T_g$  ve yumuşama sıcaklıkları), kimyasal (oluşan fazların kristal yapısı), optik (geçirgenlik), mikroyapısal (optik mikroskop, Taramalı elektron mikroskobu) analizleri gerçekleştirilerek, LiF katkılama sonrasında elde edilen cam-seramik malzemelerinde belirtilen özelliklerde meydana gelen değişimler incelenmiştir.

## TABLE OF CONTENTS

ACKNOWLEDGEMENTS.....	iii
ABSTRACT .....	iv
ÖZET .....	v
LIST OF FIGURES .....	viii
LIST OF TABLES.....	xv
LIST OF SYMBOLS/ABBREVIATIONS.....	xvii
1. INTRODUCTION .....	1
1.1. DISPLAY TECHNOLOGY .....	1
1.1.1. Cathode Ray Tube (CRT).....	2
1.1.2. Vacuum Fluorescent Display (VFD).....	2
1.1.3. Plasma Display Panel (PDP) .....	3
1.1.4. Light Emitting Diodes (LED).....	3
1.1.5. Liquid Crystal Display (LCD).....	4
1.1.6. Organic Light Emitting Diodes (OLED) .....	4
1.2. GLASS AND GLASS-CERAMICS.....	6
1.3. GLASS SUBSTRATE FOR DISPLAY TECHNOLOGIES.....	9
1.4. MARKET RESEARCH OF GLASS SUBSTRATE MATERIALS.....	14
1.5. PRODUCTION METHOD OF GLASS SUBSTRATE.....	16
1.5.1. Float Process .....	16
1.5.2. Slot – Draw Process.....	17
1.5.3. Up – Draw Process .....	18
1.5.4. Re – Draw Process.....	19
1.5.5. Overflow Down – Draw Process .....	20
1.6. STRENGTHENING OF GLASS MATERIALS .....	22
1.6.1. Thermal Strengthening .....	22
1.6.2. Coating Technologies .....	23
1.6.3. Lamination Technologies .....	25

1.6.4. Chemical Strengthening.....	26
1.6.5. Crystallization Method .....	27
2. PRODUCTION AND CHARACTERIZATION OF GLASS MATERIALS.....	31
2.1. DETERMINATION OF GLASS COMPOSITION .....	31
2.2. PREPARATION AND PRODUCTION OF GLASS MATERIALS.....	40
2.3. CHARACTERIZATION OF GLASS MATERIALS .....	45
2.3.1. Crystallization Kinetics of Glass Materials .....	45
2.3.2. Thermal Expansion Coefficient of Glass Materials.....	60
3. PRODUCTION AND CHARACTERIZATION OF GLASS-CERAMIC MATERIALS .....	69
3.1. PRODUCTION OF GLASS-CERAMIC MATERIALS .....	69
3.1.1. X-Ray Diffraction Analysis.....	71
3.1.2. Optical Microscope Analysis.....	84
3.1.3. Scanning Electron Microscopy (SEM) Analysis.....	90
3.1.4. Transmittance Analysis of Glass-Ceramic Materials .....	93
3.1.5. Three Point Bending Test of Produced Glass-Ceramics .....	102
4. CONCLUSION.....	104
5. SUGGESTIONS AND FUTURE WORKS .....	107
REFERENCES .....	108

## LIST OF FIGURES

Figure 1.1. Structure of AMOLED and PMOLED display technologies.....	5
Figure 1.2. Tetrahedron structure of $\text{SiO}_4^{4-}$ [21].....	6
Figure 1.3. Crystal and amorphous structure of $\text{SiO}_2$ [21].....	7
Figure 1.4. Temperature – volume change of glass materials [20].....	7
Figure 1.5. From glass to glass-ceramic. (a) Nuclei formation, (b) Crystal growth on nuclei, and (c) glass-ceramic microstructure [27] .....	9
Figure 1.6. Thermal expansion of silicon, and Corning Codes 7059 and 1737 substrate glasses [34] .....	12
Figure 1.7. Shrinkage of a typical a-Si substrate in the 400-500°C range [37].....	13
Figure 1.8. The Redraw Process [41] .....	20
Figure 1.9. Overflow Down – Draw Production Method [47] .....	21
Figure 1.10. a) AFM image of glass produced by fusion method and b) AFM image of glass produced by fusion method and surface polished with cerium oxide [48].....	22
Figure 1.11. Differential CSB strength distributions of the heat-treated glasses (upper surface) with and without coating [52].....	24



Figure 1.12. Differential CSB strength distributions of the heat-treated glasses (lower surface) with and without coating [52] .....	24
Figure 2.1. a) Distribution of SiO <sub>2</sub> and b) Intensity range of SiO <sub>2</sub> obtained from patents ..	34
Figure 2.2. a) Distribution of Al <sub>2</sub> O <sub>3</sub> and b) Intensity range of Al <sub>2</sub> O <sub>3</sub> obtained from patents .....	35
Figure 2.3. a) Distribution of B <sub>2</sub> O <sub>3</sub> and b) Intensity range of B <sub>2</sub> O <sub>3</sub> obtained from patents.	36
Figure 2.4. a) Distribution of MgO and b) Intensity range of MgO obtained from patents	37
Figure 2.5. a) Distribution of CaO and b) Intensity range of CaO obtained from patents ..	38
Figure 2.6. a) Distribution of SrO and b) Intensity range of SrO obtained from patents ....	39
Figure 2.7. Performing the homogenization process in the ball mill.....	42
Figure 2.8. Melting process of prepared glass batch at elevator furnace.....	43
Figure 2.9. Casting of melted glass to graphite mold and produced glass samples.....	43
Figure 2.10. Color changing of the glass samples at 720°C for 2 hours annealing process	44
Figure 2.11. Cutting of produced glass samples with BUEHLER IsoMet Low Speed Raw device .....	45
Figure 2.12. SII Exstar TG-DTA thermo analyzer device.....	47
Figure 2.13. DTA curves of the parent glass composition at different heating rate.....	48

Figure 2.14. The plot of $\ln(T_c2/\phi)$ versus $1/T_c$ of parent glass composition .....	49
Figure 2.15. DTA curves of the doped 1 wt. percent LiF glass composition at different heating rate.....	50
Figure 2.16. The plot of $\ln(T_c2/\phi)$ versus $1/T_c$ of the doped 1 wt. percent LiF glass composition.....	51
Figure 2.17. The plot of $\ln(T_c2/\phi)$ versus $1/T_c$ of the doped 2 wt. percent LiF glass composition.....	52
Figure 2.18. The plot of $\ln(T_c2/\phi)$ versus $1/T_c$ of the doped 2 wt. percent LiF glass composition.....	53
Figure 2.19. DTA curves of the doped 3 wt. percent LiF glass composition at different heating rate.....	54
Figure 2.20. The plot of $\ln(T_c2/\phi)$ versus $1/T_c$ of the doped 3 wt. percent LiF glass composition.....	55
Figure 2.21. The plot of $\ln(\phi)$ versus $1/T_c$ of the parent glass composition.....	56
Figure 2.22. The plot of $\ln(\phi)$ versus $1/T_c$ of the doped 1 wt. % LiF glass composition..	56
Figure 2.23. The plot of $\ln(\phi)$ versus $1/T_c$ of the doped % 2 wt. LiF glass composition..	57
Figure 2.24. The plot of $\ln(\phi)$ versus $1/T_c$ of the doped 3 wt. % LiF glass composition.	57

Figure 2.25. Activation energy obtained by using the method of Kissinger and Ozawa ....	58
Figure 2.26. DTA curves of studied glasses by N. Salama S.et. al.[103].....	59
Figure 2.27. Netzch DIL 402C model dilatometer device.....	60
Figure 2.28. Dilatometer analysis result of the parent glass composition .....	63
Figure 2.29. Dilatometer analysis result of the doped 1 wt. % LiF glass composition .....	64
Figure 2.30. Dilatometer analysis result of the doped 2 wt. percent LiF glass composition .....	65
Figure 2.31. Dilatometer analysis result of the doped 3 wt. percent LiF glass composition .....	66
Figure 3.1. Softening of samples at 900°C for 3 hours.....	69
Figure 3.2. The samples nucleated at 730°C for 2h and crystallized at 830°C for 3h.....	70
Figure 3.3. Image of production process of glass-ceramics in the furnace .....	70
Figure 3.4. PANalytical X'Pert PRO MPD model X-ray diffractometer analyze device ...	71
Figure 3.5. XRD-Thin Film pattern of glass compositions without LiF nucleated at 630°C for 2h and crystallizaed at 640 for 3h-6h-9h-24h. ....	72
Figure 3.6. XRD-Thin Film pattern of the parent glass compositions nucleated at 680°C for 2h and crystallizaed at 690 for 3h-6h-9h-24h.....	73

Figure 3.7. XRD-Thin Film pattern of parent glass compositions nucleated at 730°C for 2h and crystallized at 740°C for 3h-6h-9h-24h-48h. ....	74
Figure 3.8. XRD-Thin Film pattern of glass compositions doped 1 wt. percent LiF nucleated at 630°C for 2h and crystallized at 640 for 3h-6h-9h-24h.....	75
Figure 3.9. XRD-Thin Film pattern of doped 1 wt. percent LiF glass compositions nucleated at 680°C for 2h and crystallized at 690°C for 3h-6h-9h-24h.....	76
Figure 3.10. XRD-Thin Film pattern of doped 1 wt. percent LiF glass compositions nucleated at 730°C for 2h and crystallized at 740°C for 3h-6h-9h-24h-48h.....	77
Figure 3.11. XRD-Thin Film pattern of doped 2wt. percent LiF glass compositions nucleated at 630°C for 2h and crystallized at 640 for 3h-6h-9h-24h.....	78
Figure 3.12. XRD-Thin Film pattern of doped 2 wt. percent LiF glass compositions nucleated at 680°C for 2h and crystallized at 690°C for 3h-6h-9h-24h. ....	79
Figure 3.13. XRD-Thin Film pattern of the doped 2 wt. percent LiF glass compositions nucleated at 730°C for 2h and crystallized at 740°C for 3h-6h-9h-24h-48h.....	80
Figure 3.14. XRD-Thin Film pattern of doped 3 wt. percent LiF glass compositions nucleated at 630°C for 2h and crystallized at 640°C for 3h-6h-9h-24h. ....	81

Figure 3.15. XRD-Thin Film pattern of doped 3 wt. percent LiF glass compositions nucleated at 680°C for 2h and crystallized at 690°C for 3h-6h-9h-24h. .... 82

Figure 3.16. XRD-Thin Film pattern of doped 3 wt. percent LiF glass compositions nucleated at 730°C for 2h and crystallized at 740°C for 3h-6h-9h-24h-48h. .... 83

Figure 3.17. OLYMPUS-BX53M optical microscope device..... 85

Figure 3.18. Materials used in preparing cold bakelite process..... 86

Figure 3.19. Samples placed on cold bakelite molds..... 86

Figure 3.20. Grinding process with METKON GRIPO 1V device ..... 87

Figure 3.21. ATA SAPHIR 530 polishing device ..... 88

Figure 3.22. Perkin Elmer UV-Visible-NIR spectrophotometer ..... 93

Figure 3.23. Transmittance of samples nucleated at 630°C for 2h and (a) crystallized at 640°C for 3h and (b) crystallized at 640°C for 6h..... 94

Figure 3.24. Transmittance of samples nucleated at 630°C for 2h and (a) crystallized at 640°C for 9h and (b) crystallized at 640°C for 24h..... 94

Figure 3.25. The transmittance value of samples nucleated at 630 °C for 2h and crystallized at 640°C for 3h-6h-9h-24h..... 96

Figure 3.26. Transmittance of samples nucleated at 680°C for 2h and (a) crystallized at 690°C for 3h and (b) crystallized at 690°C for 6h.....	96
Figure 3.27. Transmittance of samples nucleated at 680°C for 2h and (a) crystallized at 690°C for 9h and (b) crystallized at 690°C for 24h.....	97
Figure 3.28. The transmittance value of samples nucleated at 680 °C for 2h and crystallized at 690°C for 3h-6h-9h-24h.....	98
Figure 3.29. Transmittance of samples nucleated at 730°C for 2h and (a) crystallized at 740°C for 3h and (b) crystallized at 740°C for 6h.....	99
Figure 3.30. Transmittance of samples nucleated at 730°C for 2h and (a) crystallized at 740°C for 9h and (b) crystallized at 740°C for 24h.....	99
Figure 3.31. Transmittance of sample nucleated at 730°C for 2h and crystallized at 740°C for 48h.....	100
Figure 3.32. The transmittance value of samples nucleated at 730°C for 2h and crystallized at 740°C for 3h-6h-9h-24h-48h .....	101
Figure 3.33. Three point bending test of the produced glass and glass-ceramic materials nucleated at 730°C for 2h and crystallized at 740°C for 48h .....	102

## LIST OF TABLES

Table 1.1. Compositions of corning glasses proposed or sold for use as LCD Substrates [9] .....	11
Table 1.2. Major applications of glass substrate and forecast the size of these segments..	15
Table 2.1. Maximum and minimum range of chemical component obtained from patents	31
Table 2.2. Glass composition obtained from distribution and intensity range of components in the patents .....	40
Table 2.3. Chemical structure of glass frit produced by Gizem Frit .....	41
Table 2.4. Thermal parameters of the parent glass composition obtained from DTA results .....	48
Table 2.5. Thermal parameters of the doped 1 wt. percent LiF glass composition obtained from DTA results .....	50
Table 2.6. Thermal parameters of the doped 2 wt. percent LiF glass composition obtained from DTA results .....	52
Table 2.7. Thermal parameters of the doped 3 wt. percent LiF glass composition obtained from DTA results .....	54
Table 2.8. Thermal expansion coefficient of glass compositions.....	61

Table 2.9. Comparison of thermal expansion values of parent glass composition and doped 1-2-3 wt. percent LiF glass compositions with commercial display glass .....	62
Table 2.10. T <sub>g</sub> and dilatometer softening temperature for each composition .....	67
Table 3.1. Optical microscope image of crystallized samples.....	89
Table 3.2. SEM image of crystallized samples.....	91
Table 3.3. Transmittance value of the samples nucleated at 630°C for 2h and crystallized at 640°C for 9h-24h and at different LiF content .....	95
Table 3.4. Transmittance value of the samples nucleated at 680°C for 2h and crystallized at 690°C for 9h-24h and at different LiF content .....	98
Table 3.5. Transmittance value of the samples nucleated at 730°C for 2h and crystallized at 740°C for 3h-6h-9h-24h and at different LiF content .....	100



**LIST OF SYMBOLS/ABBREVIATIONS**

$\phi$	Heating rate
$T_g$	Glass transition temperature
$T_c$	Glass crystallization temperature
R	Constant
$^{\circ}\text{C}$	Centigrade
K	Kelvin
$E_a$	Crystallization activation energy
J	Joule
mm	Millimeter
$\mu\text{m}$	Micrometer
nm	Nanometer
XRD	X-Ray diffraction
SEM	Scanning electron microscopy
DTA	Differential thermal analysis
DSC	Differential scanning calorimetry
SLS	Soda lime silica
AFM	Atomic force microscopy
CSB	Centrosymmetric bending

# 1. INTRODUCTION

## 1.1. DISPLAY TECHNOLOGY

Display technology has gradually influenced the lifestyle of human beings. The technology is considered as an necessary part of the modern world. The display technology allow us to observe the planet or to access information in the worldwide [1]. The 21<sup>st</sup> century is considered as the digital age since digital age provide to us share information and create a communication network among the different society in the world. Today, display technologies have achieved to been in everywhere from our personal smartphones, computers to buildings, medical (ultrasound device), military (helmet, defend industry etc.) applications [2],[3]. Fundamentally, display is a computer, mobile phone, tablet etc. output surface and projecting mechanism that shows text and often graphic images to the user, by favour of cathode ray tube (CRT), liquid crystal display (LCD), light-emitting diode (LED), or other image projection technology. The displays technologies use analog signal as input. When the input information is supplied as an electrical signal, the display is called an electronic display [4].

History of display technology has begun with Cathode Ray Tube (CRT), which was made commercial in 1922 and developments in this field has gradually continued [5]. Cathode Ray Tube (CRT), technology has dominated the display industry up the late 20<sup>th</sup> century since its commercialization in 1922. But, new trends such as in mobile electronic devices induce to increase demands for display technology. Especially, demands of consumer are that the technology can be co-friendly, operated at any place and any time, less power consumption, and more display quality [6]. Through development in display technology to meet demands of consumers, Liquid Emitting Diodes (LED), Liquid Crystal Diodes (LCD) – Thin Film Transistor (TFT) etc. technology has been improved. Structure of latest display technologies is comprised of different component such as cathode, anode, organic layers, TFT mechanism, and glass substrate. Glass with excellent properties with compatible to display application such as transparency, thermal stability etc. is important component in the system and approximately 9.6 percent of the system costs come from the substrates [7],[8]. Display glass technology has gradually evolved since Code 0211 first glass substrate produced by

Corning Inc [9]. After that, studies in this field has been continued so as to improve glass substrate properties including alkali content, chemical durability etc. and more be compatible to display devices. Within the scope of the thesis, glass batch was prepared by taking into account the composition created by using patents include glass substrate for display technologies and glass-ceramics was produced at different crystallization time-temperature and with doped different LiF proportions (1-2-3 percent wt.) and then, optical properties (transmittance value at visible range), physical properties (thermal expansion coefficient, glass transition and softening point), chemical (crystal structure of formed phase) ve microstructural analysis (optical microscope and Scanning Electron Microscopy, SEM) produced glass and glass-ceramics was investigated.

Within the scope of generally display technology studies, historical development and working principle of the technology was explored. In the following section, information about these title is given in summary.

### **1.1.1. Cathode Ray Tube (CRT)**

Cathode Ray Tube was invented by German scientist Karl Braun in 1897. The cathode ray tube (CRT) is composed of vacuum tube that include electron guns and a phosphorescent screen is projected image[5]. Created images with CRT appear through electrical waveforms, pictures etc. Glasses used in CRT to cover out of surface are heavy, large, and fragile. If CRT is used as commercial product, glass used in the system involve lead and is produced as thick in terms of safety. Also, the glass has shatter-resistant and inhibit of X-ray emissions. CRT dominated 70 percent of the display market until 2000. After this time, in order to meet the evolving demands of the electronic-device user, a new technology in this field was enhanced as Vacuum Fluorescent Display (VFD) [6],[7].

### **1.1.2. Vacuum Fluorescent Display (VFD)**

The Vacuum Fluorescent Display is a vacuum tube and is similar to Cathode Ray Tubes. VFD was invented in 1915 by Georges Claude in France. The display is called as a gas-discharge display. In the Vacuum Fluorescent Display, anode that coated with phosphor exposed to electrons emitted from a cathode filament and controlled by a grid. The voltage

on the grid determines whether the electrons repelled or allowed to collide with a phosphor coated anode. Electrons striking the anode cause light to be emitted from the phosphor. The output light emission generates the specific wavelength light and output color associated with Vacuum Fluorescent technology [10].

### **1.1.3. Plasma Display Panel (PDP)**

Plasma Display Panel is results of needs as any invention. In 1960, in order to develop quality display was launched a project supporting of Prof. Donald L. Bitzer, Prof. H. Gene Slottow, and their graduate student Robert H. Wilson at the University of Illinois. After 4 years started the project, in 1964 the team was developed a plasma display panel. Plasma display panels (PDP) are a type of screen display that uses gases to emit light to form pixels on to a glass plate which displays an image. In plasma display panels, since each cell contains a light source, in the form of plasma, each pixel is light controlled. Compared to CRT screens, PDPs are much thinner and lighter weight but roughly consume the same amount of power [11]. Whereas intensive studies were conducting in this field, Light Emitting Diode (LED) technologies which emergence time is almost at the same time with PDP was developed. Summary information about the LED technologies is given below title.

### **1.1.4. Light Emitting Diodes (LED)**

LED stands for light emitting diode, was designed by Nick Holonyak in 1962. The semiconductor diode produce a light, when a voltage is applied to it. Due to the p-n junction diode, in other words p-n junction diode that emits light, when a voltage is applied to the diodes, electron recombine with electron holes within the device, releasing energy in the form of photons. This effect is known electroluminescence, and the color of the light determined by the energy band gap of the semiconductor [11],[12]. LEDs ensure high performance, uses less power because energy-efficient light emitting diodes for backlighting use less energy than cold cathode fluorescent lamp (CCFL). They can be used in wider temperature range (-20°C to 85°C). Also, due to the ultra high speed response, display quality of LEDs was improved [13],[14]. To met consumer demands, as a results of studies

conducted in this area triggered Liquid Crystal Display (LCD). With the LCD technologies, a step forward has been taken in this field.

### **1.1.5. Liquid Crystal Display (LCD)**

Liquid-crystal display (LCD) was invented in 1964 at RCA Laboratories in Princeton, NJ. Basically, the LCDs utilize the electro-optical characteristic of a liquid crystal to convert an electrical stimulus into a visual signal. When a high electrical-field is applied to two electrically conductive and transparent plates, the liquid crystal molecules move freely thus scatter a light incident on the plate making screen appear in a white colour. A major milestone occurred in 1988 when a 14-in active-matrix (AM) thin-film transistor (TFT) display was developed. TFTs are micro-switching transistors that are arranged in a matrix on a glass substrate to control each pixel. Active Matrix LCD display panels depend on the thin-film transistors (TFT) to maintain the state of each pixel between scans while improving response times. A TFT monitor refresh rate is very high resulting in display that can be used for video, gaming, and all forms of multimedia applications. These advances have made LCD's critical component in the field of display technologies and expanded the marketplace [15]. With the developed technologies in this field, display technologies have become an indispensable part of people's daily life. In order to enhance the performance of display technologies, a new era launched called Organic Light Emitting Diodes (OLED) technology.

### **1.1.6. Organic Light Emitting Diodes (OLED)**

Organic light emitting diode technology was invented by researcher at the Eastman Kodak company in 1987. Organic light emitting diodes (OLED) are monolithic, solid-state devices that is in the range of 100 to 500 nanometers thick and consist of a series of a conducting layer and an emissive layer, all layer together sandwiched between two electrodes and deposited on a substrate. The conducting layer is made of organic plastic molecules that transport holes from anode. The emissive layer is a film of organic compound that transport electrons from the cathode and emits light when exposed to an electricity. When electricity is applied to an OLED, electrons move from the electrodes into organic thin films until they recombine in the emissive zone forming excitons. With the excitons, the light is generated

from OLED system. OLED's are divide into two groups; active matrix light emitting diodes (AMOLED) and passive matrix light emitting diodes (PMOLED) displays in commercial products [16],[17]. The main difference between the two screens; pixel formation and how to control pixels. In PMOLEDs, the anodes and cathodes are arranged perpendicular to each other, their intersection create the pixels in which light is emitted, and which pixel is switched on and off is controlled by the current sent to the anode and cathode in the selected strips. In AMOLED displays, thin-film transistor (TFT) are used as switches to control the amount of current and thus the brightness of each pixel [18].

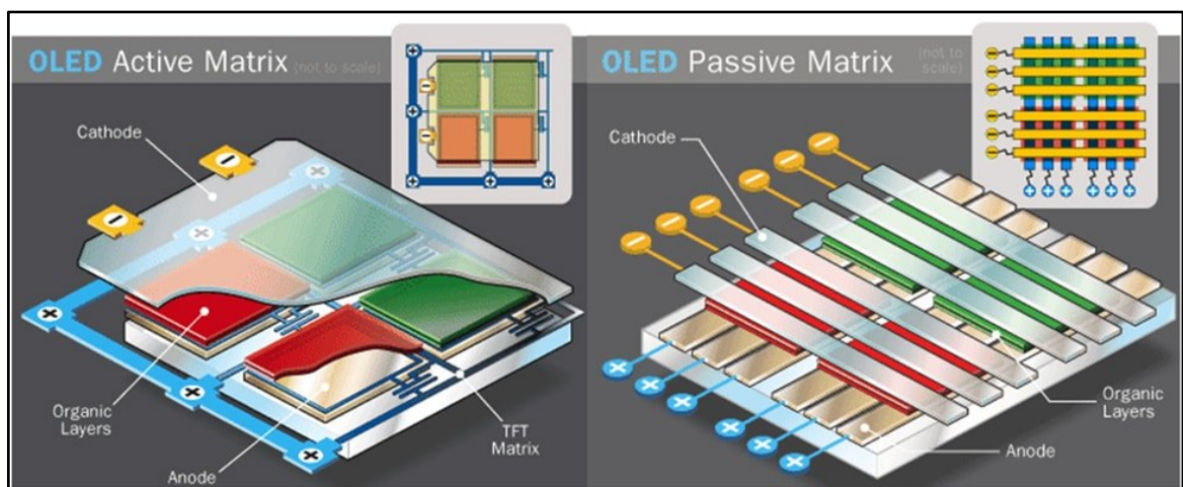


Figure 1.1. Structure of AMOLED and PMOLED display technologies

There are different materials chose in the systems as substrates such as plastic, glass, and metal. Although plastic, glass and metal can be used as substrates in display technologies; high permeability in the visible spectrum, optical advantages such as high homogeneity and high UV resistance at refractive index, thermal advantages such as high temperature and dimensional stability, low thermal expansion coefficient and no gas release, high chemical resistance, high barrier properties against water and oxygen vapor advantages such as scratch and scrubbing/washing resistance increase the tendency to use glass as substrates [19]. Other advantages of using glass substrates are; they enable compact device designs that provide brighter displays, higher resolution and longer battery life for the end user, while providing lower cost and increased design flexibility for manufacturers [20].

Glass is the only material that can be meet the demanding requirements display manufacturing process and operation. In the next section, the glass material which are main material of the thesis and glass-ceramics was described in detail.

## 1.2. GLASS AND GLASS-CERAMICS

Glasses are defined in various ways with their development. Some of those; non-crystalline solids, materials obtained by solidification of a liquid without crystallization, and all amorphous solids obtained by supercooling a liquid, regardless of chemical composition. ASTM (American Society for Testing Materials) as the glass, “crystalline inorganic melting product cooled to rigid conditions without crystallization” and a formal description of the glass has been made.

Glass is a flowable material composed of alkaline and alkaline earth metal oxides and some other metal oxides and its main component is silicon dioxide ( $\text{SiO}_2$ ). Figure 1.2 shows the silicon oxide ( $\text{SiO}_2$ ) compound, main component of the glass [21].

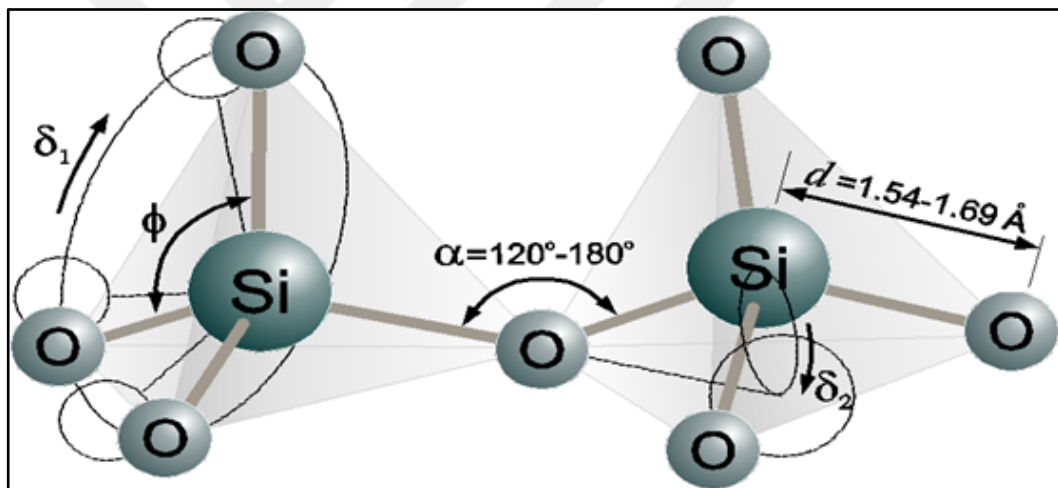


Figure 1.2. Tetrahedron structure of  $\text{SiO}_4^{4-}$  [21]

The crystalline compound exhibits tetrahedron symmetry to which four oxygen atoms are attached to each silicon atom. In the liquid phase, the gravitational force between  $\text{Si}^{4+}$  and  $\text{O}^{2-}$  ions are very high and therefore their mobility is very low and their viscosity is very high. When rapidly cooling below the melting temperature ( $1710^\circ\text{C}$  for  $\text{SiO}_2$ ) the ions do not have time to organize and maintain the amorphous (glassy structure) structure with irregular states in the liquid phase. The sequence and amorphous structure of the atoms of glass-forming  $\text{SiO}_2$  are shown in Figure 1.3.

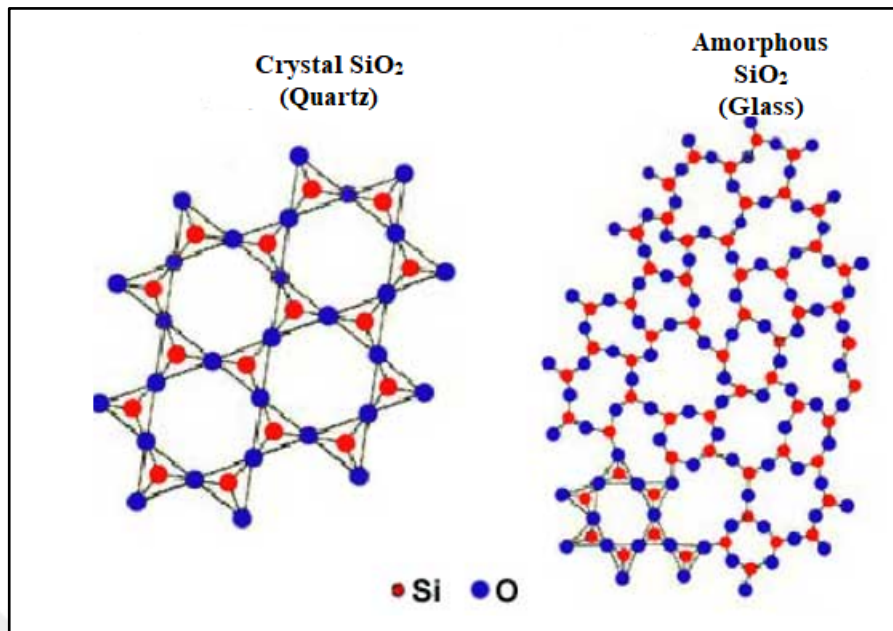


Figure 1.3. Crystal and amorphous structure of  $\text{SiO}_2$  [21]

If a substance is supplied with enough energy from the outside, it becomes liquid when cooled it solidifies. Linear solidification is observed below the melting temperature in a crystal material where they are arranged regularly and the volume decreases as it cools (Figure 1.4).

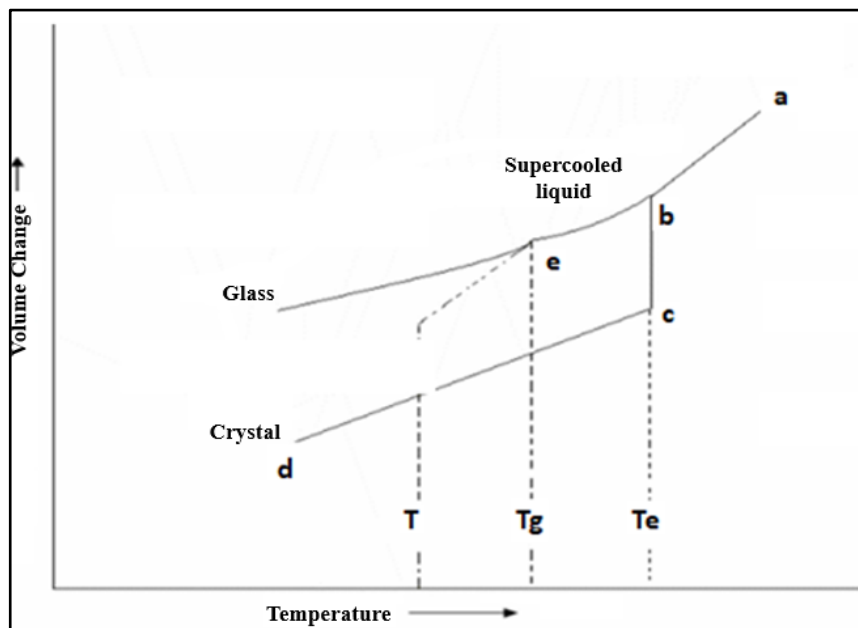


Figure 1.4. Temperature – volume change of glass materials [20]



For example, copper melts at  $1083^{\circ}\text{C}$  and becomes solid below this temperature. The glass materials do not have a constant melting temperature, but their liquid, supercooled liquid and glassy state are observed. The volume change is fast until the point  $T_g$  which is called the transition temperature, because the atoms cannot be constructed in a certain order, after this point is very slow. As a result, very dense and amorphous structure material called glass is obtained. The crystalline material cools down to point b in the liquid state and cools from point c and to point d. The  $T_e$  is the melting temperature of the solid. The glassy material cools as liquid up to point b and is in the supercooled liquid state between b-c. The point  $T_g$  is the glass transition temperature. From this point on, it takes the form of solid looking glass [22],[23].

Another subject about the title is glass-ceramic material. Glass-ceramic materials were produced in the thesis in order to observe the change in the crystallization behavior and other properties based on doped and crystallization temperature-time. Invention of glass-ceramics date from 1739 thanks to the studies of French Chemist Rene-Antoine Ferchault de Reaumur [24]. The French chemist mixed soda-lime-silica glass with sand and gypsum and then heated the mixture for many hours. As a result, he obtained crystallized porcelain materials. After extended period of time, while Stanley Donald Stookey, a research from Corning Inc., was working on host glasses lithium silicate glass compositions, discovered a glass-ceramics materials in 1953. Normally, glass temperature of their composition roughly at around  $450^{\circ}\text{C}$ . While the studies was been continuing, temperature of furnace was set up over to  $850^{\circ}\text{C}$  serendipitously. After the overheated temperature, Stookey observed that shape of obtained glass had not altered, thus recognized that it is a ceramic material. After the invention, many glass-ceramic materials were improved by scientist, glass manufacturers all over the world [25],[26].

Generally, glass-ceramic materials are produced via controlled nucleation and crystallization process of glass. Firstly, in the glass-ceramics production process, determined glass composition are melted, and then thermally process at different temperature and time is applied to the initial glass in order to obtained glass-ceramic material. The glass-ceramics production process is fundamentally a thermal process as illustrated in Fig 1.5 ,[23],[27].

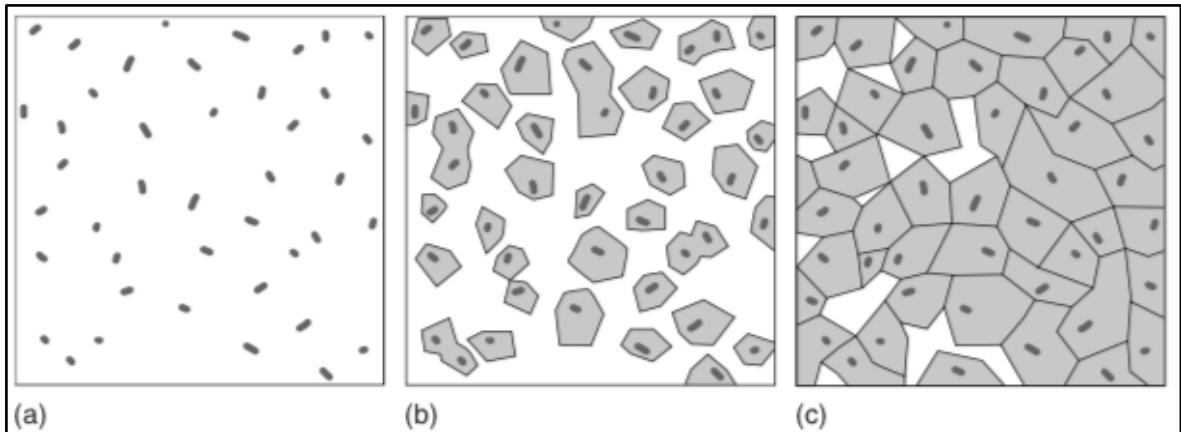


Figure 1.5. From glass to glass-ceramic. (a) Nuclei formation, (b) Crystal growth on nuclei, and (c) glass-ceramic microstructure [27]

Glass-ceramic materials have several advantages such as having zero or low porosity, combining a different of desired properties, designing their nano-microstructure for a application. Currently, glass-ceramics materials have been widely used in white LEDs, electrode materials for rechargeable batteries, armor, and machinable applications [28]. There are several required properties of substrate glass used in display technologies, in the following section, the properties of the glasses was described.

### 1.3. GLASS SUBSTRATE FOR DISPLAY TECHNOLOGIES

Excellent properties of glass such as high chemical, corrosion resistance, thermal stability at elevated temperature, high UV-transparency etc. compare to other plastic, metal materials make it the substrate in display technologies. In addition to these properties of glass, there are several requirements in the processing of the glass as substrate in display devices. For example, substrate glass should contain less alkaline earth, be low thermal expansion coefficient etc. [29],[30],[31].

The first flat glass produced by Corning was Code 0211 alkali zinc borosilicate glass. The glass reduced the TFT device lifetime owing to sodium content. Then, second sample of Corning was Code 7740 alkali borosilicate which has less sodium content than previous one. Experiments conducted by customers showed that less sodium content improved device life time but it was not satisfactory. Producing alkali-free glass studies continued extensively. In 1956, Code 7059 alkali-free barium borosilicate glass was developed by George Hares from

Corning, but, the glass was using in resistor applications. In the mid-1970 Alpha and Dumbaugh point out that an alkali-free glass would be proper for TFT applications, and proposed alkaline earth borosilicate glass. Proposed glass by them was suitable in terms of free of alkalis, high strain point, and compatible with thermal expansion coefficient value of silicon. Thanks to the improvements in TFT applications make the first alkali free glass code 7059 invented by George Hares became suitable for TFT applications [9],[32],[33]. Historical development of glass used as substrate can be seen in Table 1.1.



Table 1.1. Compositions of corning glasses proposed or sold for use as LCD Substrates [9]

Code	Description	Strain Point(°C)	CTE (x10 <sup>-7</sup> /°C)	Density (g/cm <sup>3</sup> )	Year developed	Reference
0211	Alkali zinc borosilicate	508	74	2.53	1953	First LCD product
7740	Alkali borosilicate	510	32.5	2.23	1982	Sampled (invented 1934, but not substrate)
1724	Alkaline earth borosilicate	675	43.5	2.64	1981	
7059	Barium borosilicate	595	46.7	2.76	1956	First alkali-free
1733	Alkaline earth borosilicate	643	36	2.48	1990	
1734	Alkaline earth borosilicate	661	48	2.70	1992	
1735	Alkaline earth borosilicate	665	49	2.70	1992	
1737	Alkaline earth borosilicate	666	37.8	2.54	1993	
1737G	As-free alkaline earth borosilicate	668	36.7	2.54	1997	Third LCD product
Eagle <sup>2000</sup>	Alkaline earth borosilicate	666	31.8	2.38	2000	Fifth LCD product
Eagle XG <sup>TM</sup>	Alkaline earth borosilicate	669	32	2.38	2006	Sixth LCD product
Jade <sup>TM</sup>	Alkaline earth borosilicate	740	37.5	2.63	2008	Low-T p-Si product

Normally, alkaline are added to glass batch as flux, it promote to lower the melting temperature of the glass. However, glasses used in display technologies it has been realized that alkaline content of the substrates, particularly sodium, diffusion bring about contamination of the TFT's. Migration of alkali at elevated temperature from the glass substrate into the silicon TFT will cause problems such as undesirable leakage currents and effect performance of the glass negatively. Therefore, the glass needs to be alkali-free and sodium levels have been reduced to 100 ppm and the content of sodium seems acceptable. Also, in order to prevent diffusion from glass into the transistor circuits, introducing of boron and aluminum to glass composition is another option [33],[34],[35].

Thermal expansion of glass substrates is another critical property. The thermal expansion coefficient of various components in a display technology system including the glass, sealants, silicon chips, and other components should be match with each other and be lower.

Matching the thermal expansion of the glass to silicon supply to assembly of silicon-based devices directly on the glass substrates. Secondly, Lower thermal expansion coefficient of substrates provide ability to against thermal shock when it exposed to some heating and cooling process. Also, low coefficient of thermal expansion has different benefit, including prevent breakage because of thermal shock or minimize dimensional distortion during temporal thermal process [34], [36]. In the Figure 1.6, thermal expansion value of silicon, Code 1737, and Code 7059 materials is shown. It can be seen that thermal expansion value of silicon and Code 1737 is more match than Code 7059.

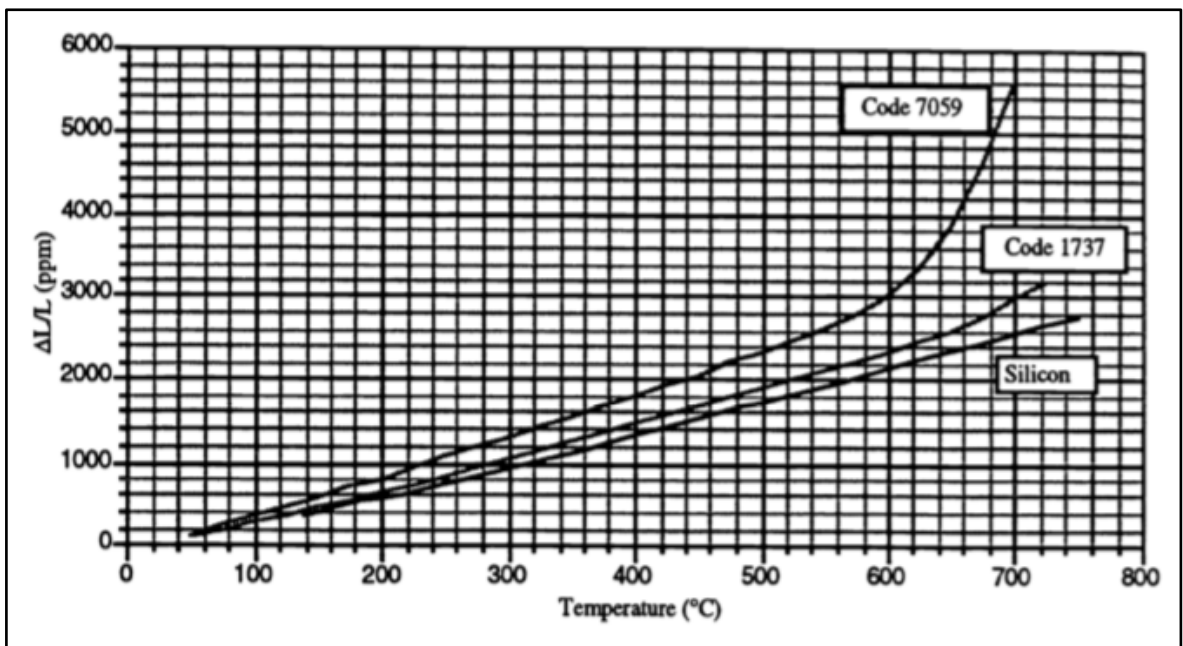


Figure 1.6. Thermal expansion of silicon, and Corning Codes 7059 and 1737 substrate glasses [34]

Another concern about thermal property of glass substrate is thermal stability. When a glass is exposed to higher temperatures in a TFT process, relaxation occurred in glass structure can cause notable dimensional change.

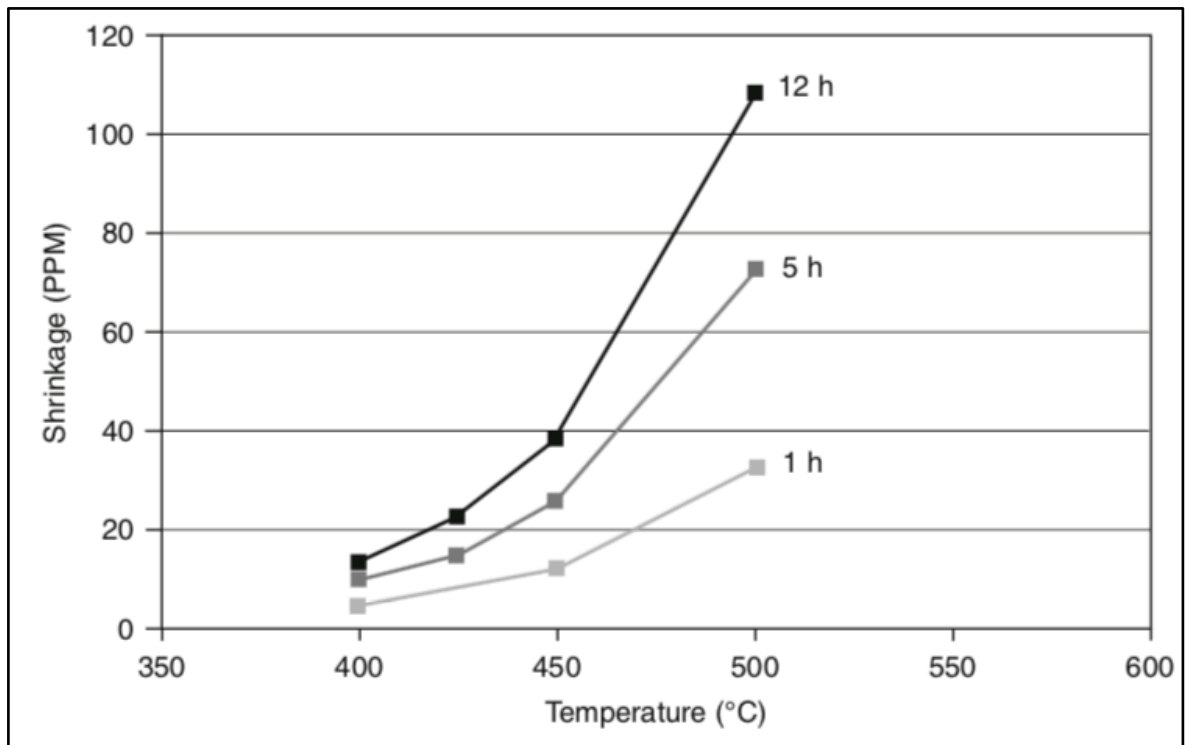


Figure 1.7. Shrinkage of a typical a-Si substrate in the 400-500°C range [37]

While the TFT process can utilize enlargement during photolithographic exposure to compensate for the variance of thin-film features due to the thermal shrinkage, this has practical limitations. For production lithographic equipment, the limit for thermal shrinkage should be in the range of 10-20 ppm. In addition, the thermal shrinkage must be uniform within the sheet.

In order to reduce thermal shrinkage desired in the range of 10-20, controlling the tendency of the glass to thermal relaxation at higher temperatures, additional high-temperature pre-treatment step providing pre-shrinking will be useful. Other option is increasing the glass high temperature viscosity by designing glass composition for thermal durability [37].

During photolithography processing, an glass substrate is exposed to numerous chemical solutions for cleaning, etching or patterning. These solutions are pH ranges from basic to acidic including nitric acid, hydrogen peroxide, hydrochloric acid, sulfuric acid and fluoride solutions (HF) each of which could affect the integrity of the glass surface. In the case of acid attack, dissolving of silica from the surface of the glass, lead to defects at the visual appearance. On the other hand, fluorides and bases attack the silica network of the glasses, which dissolves the glass uniformly, but lead to roughening of the surface, especially

polished surface. It is necessary to deal with these attacks without any visual degradation for the glass [34],[37].

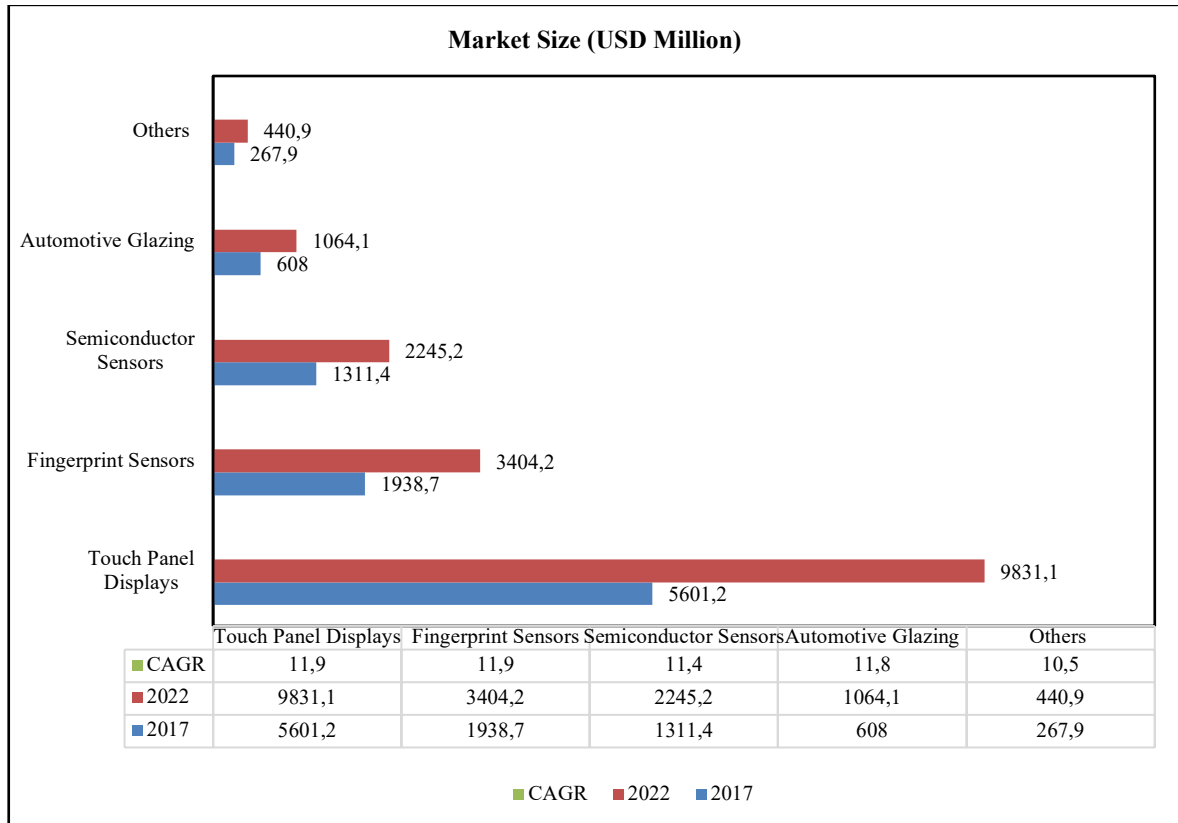
These properties are critical for a glass substrate. In order to improve these properties, and expand the use of glasses as substrate, glass manufacturing in worldwide has been investing in the field. This situation enlarge marketing area and use of glass substrate. After giving the characteristics properties of substrate glass, market research was carried out in order to emphasize the importance of the substrate glass and the added value it can provide in the case of production. The next section, the related study was given.

#### **1.4. MARKET RESEARCH OF GLASS SUBSTRATE MATERIALS**

The glass substrate market is divided into five different categorize; semiconductor substrate, touch panel displays, fingerprint sensors, and automotive glazing. Glass is used in several applications because of its properties such as electrical conductivity, sensitivity, lightweight, and flexibility.

Table 1.2. Major applications of glass substrate and forecast the size of these segments

[19]



Semiconductor glass substrates are used in across electronic and solar cells applications. According to the World Semiconductor Trade Statistics (WSTS) organization, the global semiconductor market is forecasted to witness a 3.3 percent of growth in 2017 and reach USD 346.1 billion from USD 335.0 billion in 2016. Glass is used in semiconductors as substrates due to its electroconductivity and lightweight. The electroconductivity and lightweight of the glass became semiconductor substrates for microelectronic devices such as TFT-LCD and solar cells. Hence, the rising of the glass substrate is directly proportional to the growth of semiconductor industry. Companies such as Corning (US), Asahi Glass (Japan), and SCHOTT (Germany) are produced glass materials used in semiconductor substrates [19].

Production of these substrate is complex, and the properties mentioned above are crucial. Glass production method is also very critical to provide all the desired features. Therefore, different production method has been developed since its used as substrate to meet requirements. In the next section, production methods of glass substrate is explained.



## 1.5. PRODUCTION METHOD OF GLASS SUBSTRATE

There are different production method of glass substrate. Float process, Slot-draw process, Up-draw process, Redraw process, Overflow Down-draw process are known as glass substrate production methods. The methods will be described in the section respectively.

### 1.5.1. Float Process

Float process was developed by A. Pilkington and K. Bickerstaff in England at between 1953-1957. Glass produced with Float process has high quality flatness in terms of surface smoothness, parallelism and defect rate. Float process generally is used in the production of large scale glasses such as windows and automotive windshield. In the continuous production systems with this process, soda-lime-silicate glasses are melted  $\approx 1600^{\circ}\text{C}$ . After melting process, the glass which has low viscosity value is floated by spreading on the molten tin with high density. In order to prevent oxidation of tin that is in the process over time, flotation is carried out in a pressurized nitrogen atmosphere. During the flotation, the glass has a lower viscosity is thinned spreading on the tin bath, and its thickness is adjusted according to the desired production specifications by pressing or stretching with various apparatus. Glass becomes almost solidified and the viscosity increases due to the floating the molten glass on the tin bath. After floatation of the glass, following step is annealing. Aim of the annealing process is to eliminate internal stresses which occur by compressing and stretching of the glass to adjust its thickness. In the annealing process, glass is reheated to  $\approx 600^{\circ}\text{C}$  and the internal stress in the structure are eliminated by gradually cooling from this temperature. After annealing, cutting the glass to desired dimensions is carried out with diamond-tipped cutters at  $60^{\circ}\text{C}$  and made glass ready for use [38].

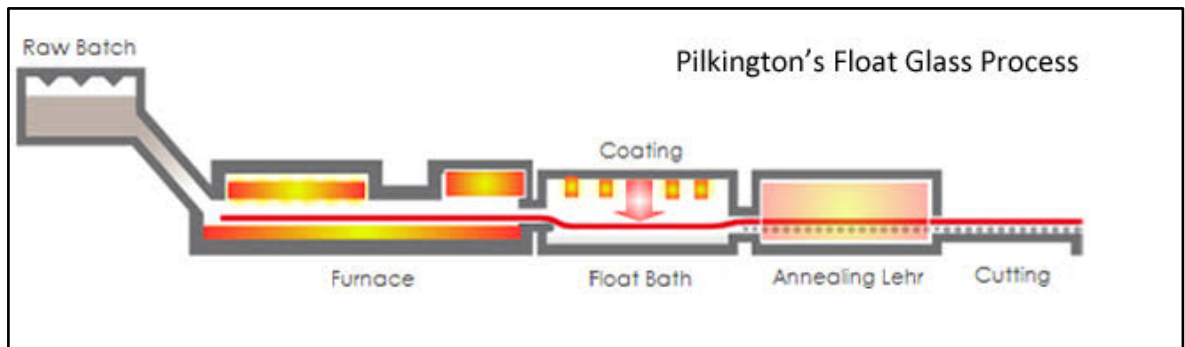


Figure 1.8. Pilkington's Float Glass Process

### 1.5.2. Slot – Draw Process

Slot-Draw Process was invented by Dan Brown at Corning Incorporated in the mid 1940s. In the slot-draw process, molten glass is carried to refractory melting tank with a rectangular opening in the bottom. Rectangular opening has V-shaped slot and angled slot edges and the slots is clamped to the bottom of the glass tank by screws. When the molten glass fills the tank, slots on the bottom of the tank is opened and the glass appear through the slot as a sheet. V-shaped glass is cooled by air blown and through nozzle and then to form a thin sheet and control the sheet thickness, the glass is pulled by rollers [39].

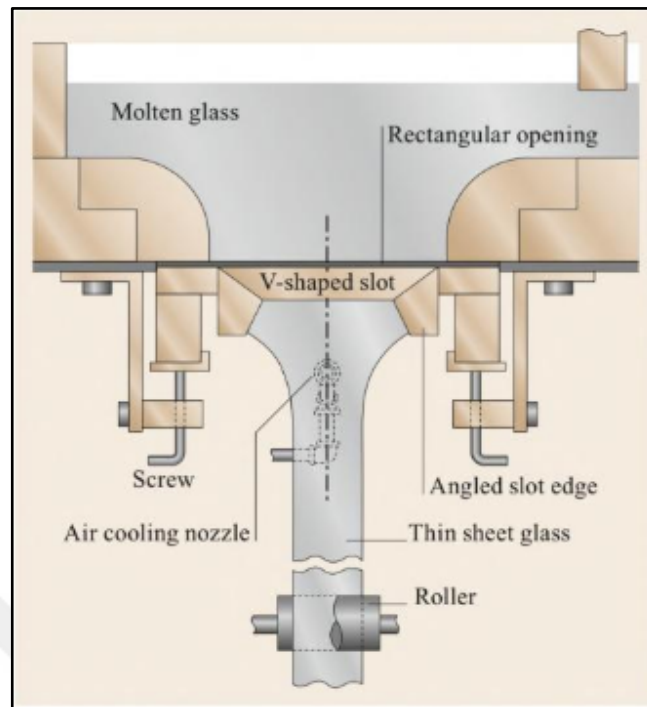


Figure 1.9. The Slot Draw Process [39]

### 1.5.3. Up – Draw Process

Up-draw process was developed by SCHOTT AG to produce thin glasses and ultra-clear flat glasses. In the Up-Draw process, the glass preform is pulled from the bottom with roller and then preforms are annealed at certain temperatures. After annealing process, the glass preforms is cooled and obtained the glass sheet desired thickness [40].

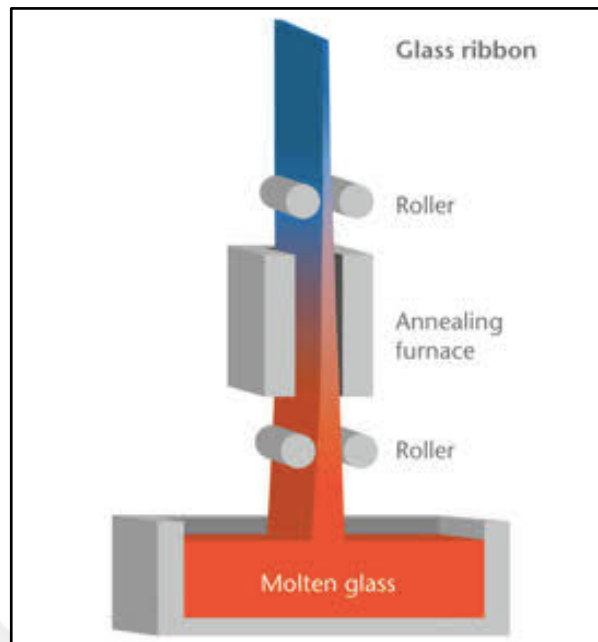


Figure 1.10. The Up-Draw Process [41]

#### 1.5.4. Re – Draw Process

Redraw process is based on the heating - softening of flat glass with a certain thickness and the simultaneous drawing and elongation. Redraw process is consist of five different part. These parts; in the upper region of the device, fixing zone in which the preformed glass is fixed, the preheating zone where the glass is heated to a certain temperature, the forming zone or deformation zone where the glass heated to a certain temperature, the cooling zone where the shaped glass is cooled to certain temperature, and finally it is called the drawing zone where the glass is brought to desired thickness.

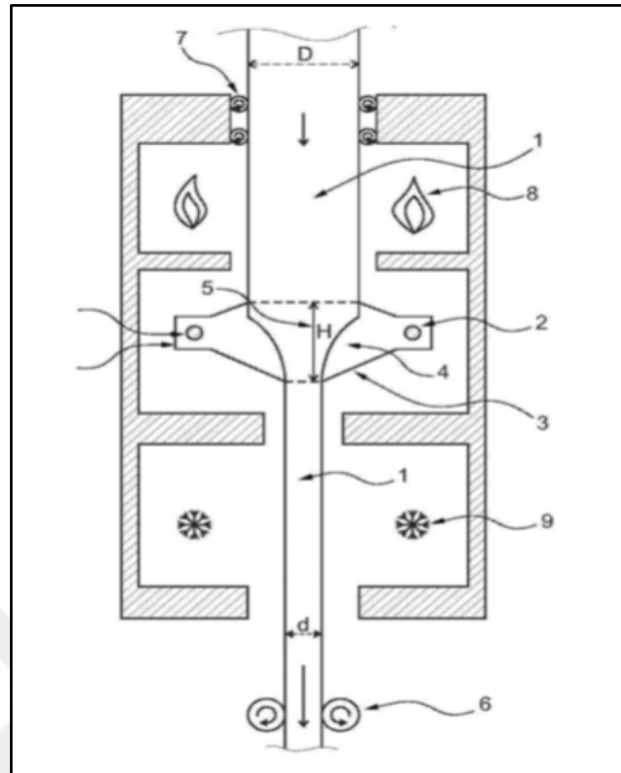


Figure 1.8. The Redraw Process [41]

The glass preform is heated up to a range of  $10^{10}$  dPas to  $10^{14}$  dPas viscosity value by a pre-heating system indicated by (1), before reaching the flat glass forming zone. There are two opposing zones (2) in the middle section of redraw device. During production, the deformation can occur in the zone indicated by the number 4 in the heating zone is shown by dashed line. The preformed glass is heated to temperatures in the deformation zone (4) with a viscosity of at least  $10^4$  dPas and at most  $10^8$  dPas. Also, the height of the deformation zone is defined by H, which is indicated by the number 5. After shaping the glass in the deformation zone, the next step is the cooling zone, which is symbolized by the ice crystal (9). In the cooling zone, the glass is cooled with a maximum speed of  $230^\circ\text{C}/\text{min}$ . Finally, the glass is pulled into the sheet by the pulleys indicated by the number 6 [41].

### 1.5.5. Overflow Down – Draw Process

Overflow Down-Draw process was developed by Stuart Dockert and Clint Shay from Corning Inc to produce automotive windshield glass in the 1960s. The main advantage of this process than float method is that the glass can be produced without any contacting with

tin bath means that both surfaces have a similar composition and do not require a second polishing process after production [42],[43]. In the overflow down-draw process, the glass which is melted in the melting unit is transferred to the refining unit. In order to reduce the viscosity and to eliminate bubbles in the molten glass, it is recommended the temperature of the gas treatment tank should equal to or higher than the melting tank temperature. It is desirable that the melt glass separated from the glass treatment tank is cooled in a controlled on the way to the mixing tank and the mixing tank temperature is  $\approx 150\text{-}300^\circ\text{C}$  lower than the gas treatment tank. At this stage, the concentration differences in the molten glass are eliminated and homogenized. Until the stage the method is similar with the float technology, after which the production method differs. The glass separated from the mixing unit is conveyed to the casting unit and after waiting there, it flows down and reaches the forming unit. The melting becomes form of glass by cooling during flowing from the forming unit (isopipe) and there may be various design differences in the system [44]. The forming unit called as isopipe has a section in which the melt fills, overflows and flows down the sides to join at the bottom of the unit (the fusion name is given due to this junction) [45],[46].

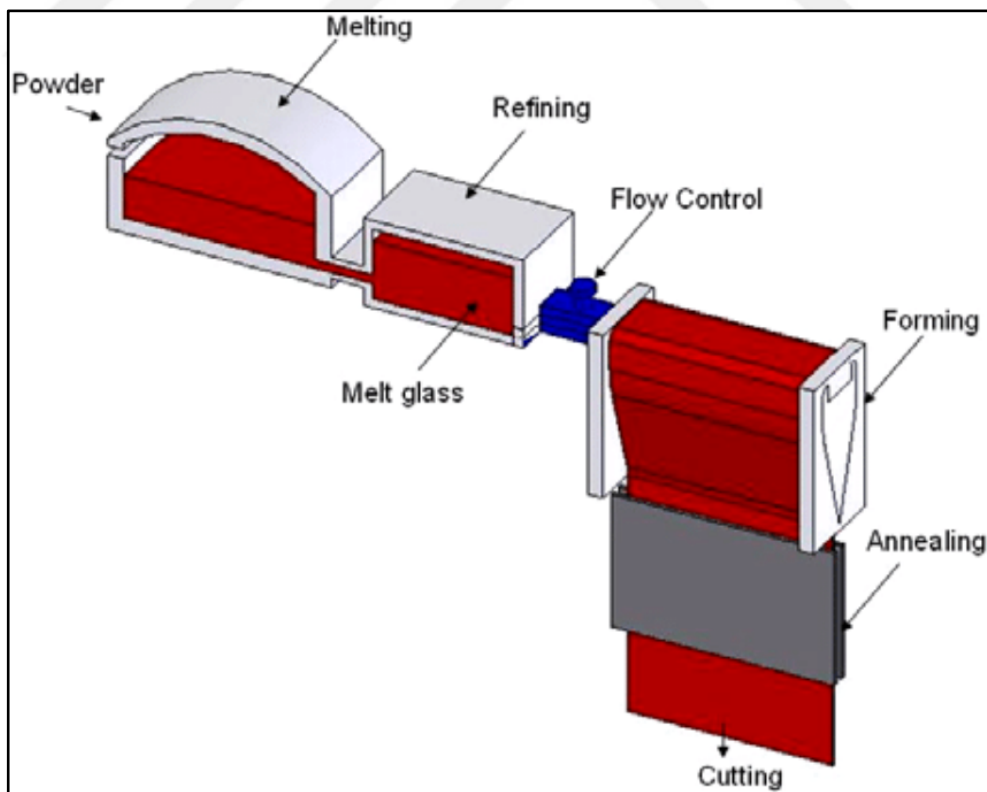


Figure 1.9. Overflow Down – Draw Production Method [47]

The most important advantage of this process over other methods are; high quality, smooth surfaces that do not contact with any process apparatus [47]. For example, Takashi Murada et al.[48], reported that the surface roughness of the glass obtained using the process is in the range of 0.1 – 0.2 nm and this roughness value is lower than a polished glass surface.

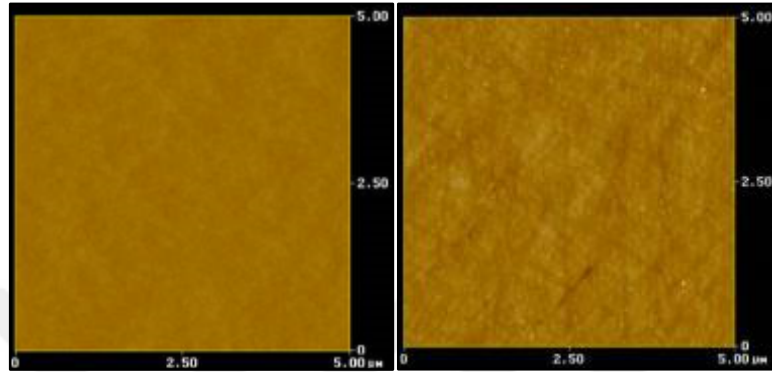


Figure 1.10. a) AFM image of glass produced by fusion method and b) AFM image of glass produced by fusion method and surface polished with cerium oxide [48]

Glass sheets having a thickness of about 0.6 mm and a width of 3000 mm can be produced with this method. There are  $\approx 150$  kinds of products produced with this method with production capacity of approximately 30 million tons and this ratio corresponds to  $\approx 35$  percent of the total glass production [49].

Finally, in the next section, the study of the strengthening of glass, including the crystallization method to be applied within the scope of the thesis is given.

## 1.6. STRENGTHENING OF GLASS MATERIALS

### 1.6.1. Thermal Strengthening

Thermal strengthening means that glass is cooled rapidly from a temperature above  $T_g$ . This process also is known as quenching the glass with air, liquid or fluidized air. Cooling rapidly of the glass lead to cools surface of glass than interior part of glass. A certain part of the glass surface is elastic solid while interior of glass still undergo thermoelastic stress relaxation. All surface and edges of thermally tempered glass become to come under compression stress. In this way, all compression are equal and the process make glass more

durable. Also, due to the fractures of thermally strengthened glass are not sharp and dangerous, the glasses is known as safety glass.

Generally, 3 mm glass thickness is request in the thermal strengthening process. Recent progress has examined to strengthening only 2 mm thick glass using cooling process. Other limitations are maximum practical cooling rate achievable, geometrical considerations, the relatively high thermal expansion of glass and the quality of the glass. In order to improve mechanical strength of glass <2mm thickness, coating or chemical etc. different process is applied [50].

### **1.6.2. Coating Technologies**

There generally are defects on the glass surface such as microcraks, break-down of chemical bonds and the segregation of compositions in service environments such as corrosion, high temperature and the radiation of high-energy particles. These defects affect mechanical properties of glasses negatively. Therefore, eliminating the defects by surface treatments becomes an significant method to enhance mechanical properties of glasses.

Ormosil and epoxy polymeric coatings, gas-thermal nitriding with nanosized silica particle, titania film coating etc. methods are used in improving mechanical properties of glass as surface modifications [51].

S.V. Es'kin et.al.[52] developed a strengthening coating based on silicate nanoparticles for soda-lime-silica glass, examined conditions for the synthesis of fractal SiO<sub>2</sub> particles and application of coating of necessary thickness to glass through adsorption from solution, and optimized heat treatment of the coated glass.

According to their results, the coating increased the centrosymmetric bending (CSB) strength of the glasses by 26 percent of both their upper and lower sides.



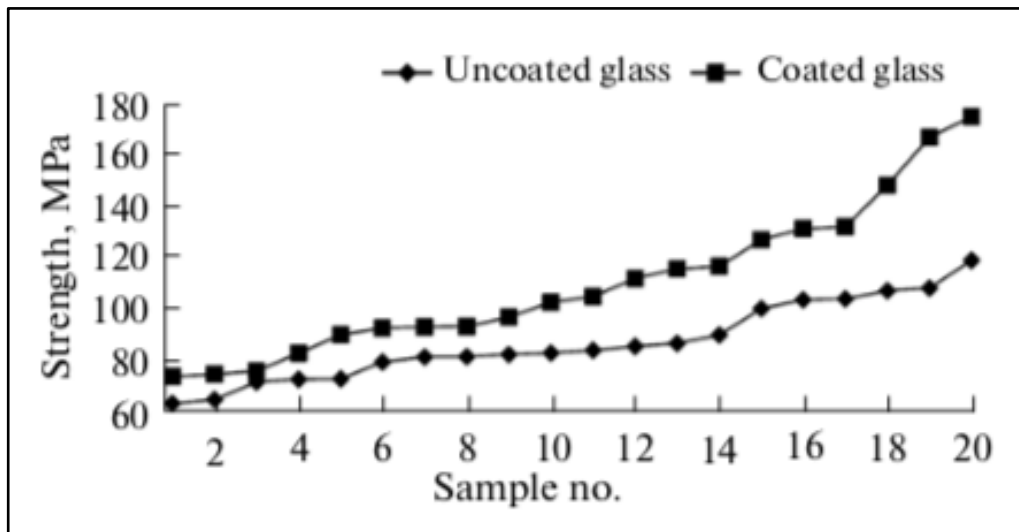


Figure 1.11. Differential CSB strength distributions of the heat-treated glasses (upper surface) with and without coating [52]

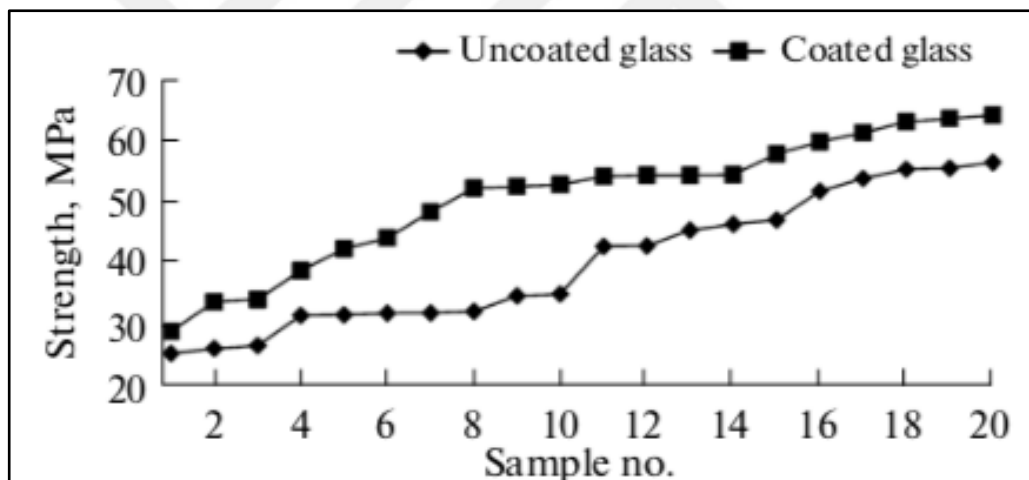


Figure 1.12. Differential CSB strength distributions of the heat-treated glasses (lower surface) with and without coating [52]

Coating 85 to 95 nm in thickness enhanced CSB strength of the float glass at 26 percent of both its upper and lower surfaces. It seems likely that  $\text{SiO}_2$  nanoparticles from the coating penetrate into cracks and scratches on the glass surface and that heat treatment produces strong siloxane bonds between the nanoparticles and glass. This can be interpreted as elimination of surface flaws [52].

Kırtay and et.al.[53], strengthened mechanical properties of SLS (Soda-Lime-Silica) glasses by using hybrid ormosil coating method. In their work, the ormosil resin solution consist of silane, epoxy resin and hardener based on Al-alkoxide. Mechanical measurement of

strengthened samples were investigated with Ring-on-Ring (ROR) tests. According to their results, flexural strength of commercial SLS glasses were improved over 3 times response to uncoated glasses by an hybrid (organic-inorganic) sol-gel coating.

To sum up, glass strengthening can be enhanced by applying a coating capable of eliminating sub- and microcracks on the glass surface and preventing crack development during the service of the material.

### 1.6.3. Lamination Technologies

Glass can be had different properties by combining with other materials. For example, laminated glass is a glass-plastic film (polyvinyl butyral (PVB) or ethylene vinyl acetate (EVA))-glass sandwich. Glass-plastic film-glass sandwich is processed by autoclaving at 1400°C and pressure up to 14 bar.

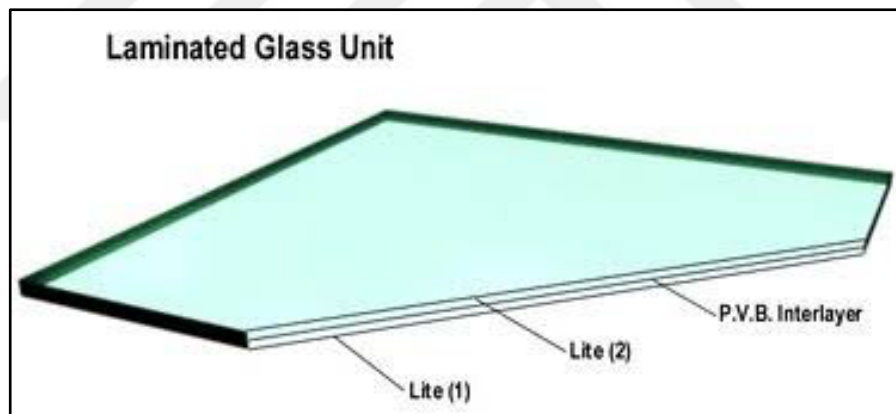


Figure 1.16 Structure representation of laminated glass

Due to the plastic film, when the glass breaks, its fragments keeps the glass fragments together and the laminated glass remains in the frame. The characteristic of laminated glasses makes it useful for automotive windshields since it provides significantly safety in a accident. Alternative transparent plastic film or interlayers can be used in laminated glass to obtain special properties, such as solar control, thermal insulation, fire protection etc. Laminated glass also has satisfactory structural behaviors under severe loading conditions such as explosions. One of the main reasons why laminated glass are used in building is its safe compared to float glass and tempered glass [54],[55].

#### 1.6.4. Chemical Strengthening

Chemical strengthening process generally is known as exchanging small ions in a glass surface by larger ions. The successful use of chemical ion-exchange was first conducted by Kistler in 1962 for soda-lime-silica glass treated in potassium nitrate. An alkali-containing glass is immersed in alkali salt such as  $\text{KNO}_3$  at temperatures well below the glass annealing point and at different time. When a small ion is replaced by a larger ions on the glass surface, the larger ions is compressed onto the surface. Thus, compression stresses occur on the surface and the strength of glass increases [56]. Generally, most commonly used chemical strengthening method is the replacement of  $\text{Na}^+$  ions in the glass structure with  $\text{K}^+$  ions in the salt bath. Introducing different ions size which differ from available in the glass structure change the structure of materials. While chemical strengthening process prevent defects occurred on the surface, strengthening and thermal shock resistance of glass are increased [57].

Güzel A. S. et.al. [58] improved the mechanical properties differences in between the air and tin surface of thin soda-lime-silicate float glasses that subjected to ion exchange uttering  $\text{KNO}_3$  salt bath. According to their results, chemically tempering developed the hardness of float soda-lime silicate glasses to roughly 18 percent. After all ion exchange process conditions, the hardness of both surface of glasses was improved. In the ion exchange experiments at different temperatures for the 12-h time, the hardness values increased until  $435^\circ\text{C}$  and then gradually decreased with increasing temperature for both surface. At the 12 h -  $435^\circ\text{C}$  process conditions, the maximum hardness value was achieved as 8.25 GPa with an increase of  $\approx 18$  percent with respect to the raw glass on the tin surface.

Shim et.al. [59] enhanced mechanical properties of borosilicate glass via ion-exchange method for lightweight, transparent, and thin bulletproof windows. The optimized ion exchange conditions of borosilicate glass 3, 4 and 6 mm thick at  $560^\circ\text{C}$  were 10, 12, and 15 min, respectively. The flexural strength of the strengthened borosilicate glass via ion exchange (3, 4 and 6 mm) were  $0.745\pm 0.018$ ,  $0.783\pm 0.017$  and  $0.810\pm 0.014$  GPa, respectively, the values were roughly 2.8 times higher than base glass. The transmittance of bulletproof windows was more than 86.1 percent and all samples satisfied the conditions (over 78 percent) of the standards in this field.

### 1.6.5. Crystallization Method

Improving mechanical properties of glass with crystallization technique has two different kind of methods. These methods are surface crystallization and bulk crystallization. In order to create crystallization on the glass surface, glass materials are heated to crystallization temperature, heat treatment is performed in this stage and on the glass surface, crystallization layer which has a lower thermal expansion than bulk glass has no crystallization on the surface is obtained. On the cooling from crystallization temperature, surface of glass and internal structure behave differently. Internal structure prone to expand than surface and compression stress occurs on the glass surface. This mechanism provides to improve mechanical properties of glass [60].

Another crystallization method is bulk crystallization. Glass-ceramics obtained with bulk crystallization exhibit stronger properties than conventional glass. The strength of glass-ceramics increases with increasing crystallization temperature, reaching a maximum over a particular temperature range. Increasing with crystallization temperature, crystals appear on the glass structure and mechanical properties is improved. The glass structure which increases crystallization temperature further, will become a ceramic structure and the glass properties will be lost. Therefore, bulk crystallization process of the glass occurs in the certain temperature and time range [61].

In the crystallization process, in order to launch crystallization in the glass structure different nucleation such as  $\text{TiO}_2$ ,  $\text{P}_2\text{O}_5$ ,  $\text{ZrO}_2$ ,  $\text{Sb}_2\text{O}_3$  agents are used. There are advantages and disadvantages of nucleation agent compared to each other. For example, adding of  $\text{TiO}_2$  or  $\text{ZrO}_2$  as nucleating agent cause volume crystallization. Purple to blue colored glass-ceramics are obtained if  $\text{TiO}_2$  is used as nucleating agent [62],[63]. Unlike the given examples, Liu J. et.al. [64] have prepared alkali-free glass and glass-ceramics system by using  $\text{MgF}_2$  nucleating agent. They observed that  $\text{MgF}_2$  promotes bulk crystallization in glass. In addition nucleating properties of  $\text{MgF}_2$ , it is a refining agent at high temperature in glass system. Generally,  $\text{As}_2\text{O}_5$ ,  $\text{Sb}_2\text{O}_5$ ,  $\text{Na}_2\text{SO}_4$  are used refining agent in glass production process. However, it has been observed that  $\text{As}_2\text{O}_5$ ,  $\text{Sb}_2\text{O}_5$ , are more effective at between 1150 – 1500 °C, when the temperature are increased to higher temperatures ( $\geq 1500$  °C) these agents are not effective like lower temperatures. For this reason, chlorides such as  $\text{CaCl}_2$ ,  $\text{BaCl}_2$ ,  $\text{CeCl}_3$ ,  $\text{NbCl}_3$ ,  $\text{ErCl}_2$  and  $\text{PrCl}_3$  are given as an alternative to these agents, which are more

compatible for temperatures above 1600°C. As another alternative to the mentioned chlorides, it is stated that fluorides such as LiF, NaF, KF, ZnF<sub>2</sub>, MgF<sub>2</sub>, BaF<sub>2</sub>, CeF<sub>2</sub> can be used refining agent in glass system at high temperature ( $\geq 1600$  °C) [65],[66].

LiF, which is among the alternative chlorides for refining agent is also used as nucleating agents in glass systems. ElBatal et. al. synthesized binary SrO-B<sub>2</sub>O<sub>3</sub> glasses doped with LiF (2 mol percent). They observed that LiF acts as a nucleating agent to cause formation or conversion of the same structural oxide into crystalline phase [67]. Additionally, Hamzawy and El-Meligy [68] conducted a research with regard to LiF effect on glass composition. In their studies, Na<sub>2</sub>O-CaO-Al<sub>2</sub>O<sub>3</sub>-SiO<sub>2</sub> glass composition was prepared and they state that doped with 3 wt. percent LiF reduces the expansion coefficient and improve the microstructure uniformity.

Also, LiF has optical properties. Due to the wide bandwidth of LiF, its crystals are more transparent than any other substance against short ultraviolet radiation wavelength [69]. For this reasons, LiF was used as nucleating agent for crystallization and effect of it on different properties of glass and glass-ceramics was investigated.

Apart from the study, after crystallization process at different time and temperature, light transmittance of prepared glass and glass-ceramics nucleated with LiF was observed. Light transmittance of substrate glass is important properties. Recent years, many glass-ceramics have been prepared with high transmittance. Lei Han et.al [70] have studied high crystallinity transparent glass-ceramics based on MgO-Al<sub>2</sub>O<sub>3</sub>-SiO<sub>2</sub>-P<sub>2</sub>O<sub>5</sub>. In this study, the optimal heat treatment schedule of parent glass is 840°C/36h + 1050°C/3h. Different properties of the glasses after heat treatment process is given in Table 1.3.

Table 1.3. Density, TEC, refractive index, Vickers hardness, bending strength, and compressive strength of parent glass and glass ceramics [70]

Sample	Density(g/cm <sup>3</sup> )	TEC(x10 <sup>-6</sup> °C,25-600°C)	Refractive index(n <sub>D</sub> )	Vickers hardness (GPa)	Bending strength (MPa)	Compressive strength (MPa)
PG	2.584±0.005	2.757±0.188	1.572±0.002	6.8±0.2	92±0.92	250±2.50
GC2	2.501±0.005	3.012±0.151	1.567±0.002	8.0±0.2	175±1.75	312±3.12
GC3	2.486±0.005	2.062±0.103	1.566±0.002	8.4±0.2	201±2.01	454±4.54
GC4	2.475±0.005	1.676±0.084	1.564±0.002	8.7±0.2	210±2.10	506±5.06
GC5	2.468±0.005	1.628±0.081	1.561±0.002	9.1±0.2	223±2.23	553±5.53
GC6	2.461±0.005	1.508±0.075	1.557±0.002	9.3±0.2	236±2.36	594±5.94

Properties of the parent glass and glass-ceramics after heat treatment process is shown in Table 1.3. It is concluded that light transmittance of the sample is depending on crystallization schedule. For example, whereas light transmittance of the parent glass is up to 85 – 95 percent, light transmittance of glass-ceramics (b-c-d-e-f) decreases to 60 percent.

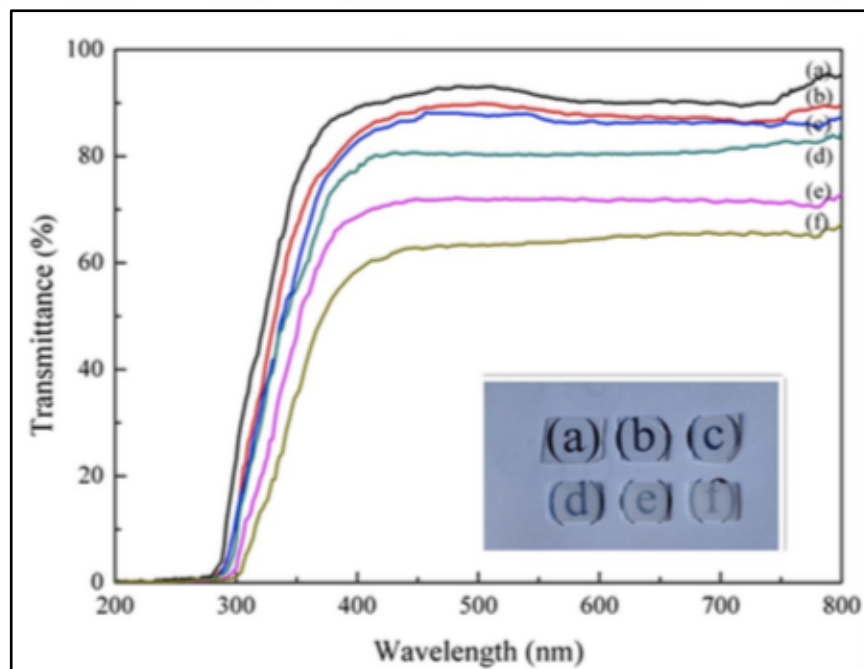


Figure 1.17. Transmittance spectra and photographs of (a) parent glass and glass-ceramics nucleated at 840 °C for 36 h and crystallized at 1050 °C for 2h, 3h, 4h, 5h and 6h [70].

Zhao M. et.al [71]. revealed that transparent glass-ceramics containing  $\text{Na}_{3.6}\text{Y}_{1.8}(\text{PO}_4)_3$  crystals were successfully synthesized. Heat treatment of the glasses coded as GC1, GC2, and GC3 is  $650^\circ\text{C}$  for 2h,  $670^\circ\text{C}$  for 2h, and  $690^\circ\text{C}$  for 2h respectively. In the visible region, the transmittance of glass ceramics produced with  $650^\circ\text{C}$  for 2h heat treatments is up to 85 percent. Optical transmittance spectra of PG, GC1, GC2 and GC3 glass samples is shown in Figure 1.18. It is found that transmittance value of these samples is decreased based on heat treatment schedule.

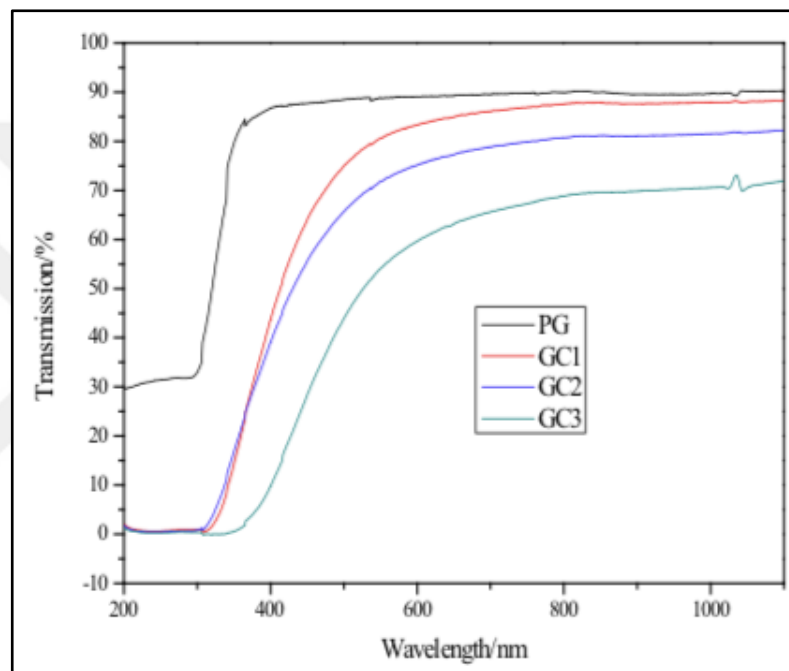


Figure 1.18. The optical transmittance spectra of PG, GC1, GC2, and GC3 [71].

Unlike the given studies, LiF was added as nucleating agent to developed glass composition by created data mining from patents to produce glass-ceramic. Then, crystallization behavior chemical (crystal structure of formed phase), physical (thermal expansion coefficient, glass transition and softening temperature), optical (transmittance) and microstructure (optical microscope and SEM analysis) of the glass and glass-ceramics was investigated.

Firstly, glass composition from patents included glass substrate for display technologies was determined, adding of LiF to determined glass was performed, thermal expansion coefficient and crystallization activation energy of parent glass composition and glass compositions doped 1-2-3 wt. percent LiF was analyzed. The aim of the crystallization process performed in this stage is to determine crystallization temperatures for producing glass-ceramics.

## 2. PRODUCTION AND CHARACTERIZATION OF GLASS MATERIALS

### 2.1. DETERMINATION OF GLASS COMPOSITION

In the determination of glass composition, international published/patents which is with regard to alkali-free borosilicate glass used as substrates for display technologies have been investigated and optimum component range determined.

32 patents and 921 composition which include alkali-free borosilicate glass composition and used as substrate on display technologies examined and a composition was obtained by creating intensity map for each composition and performing reverse engineering. Firstly, in order to have general information with regard to the usage rates of the components, maximum-minimum limits are determined for each component in patent. Secondly, intensity maps were created. In this process, maximum-minimum limits showed at Table 2.1 was divided into certain intervals, and number of composition been at the certain intervals was calculated. Therefore, distribution and intensity maps were created.

Table 2.1. Maximum and minimum range of chemical component obtained from patents

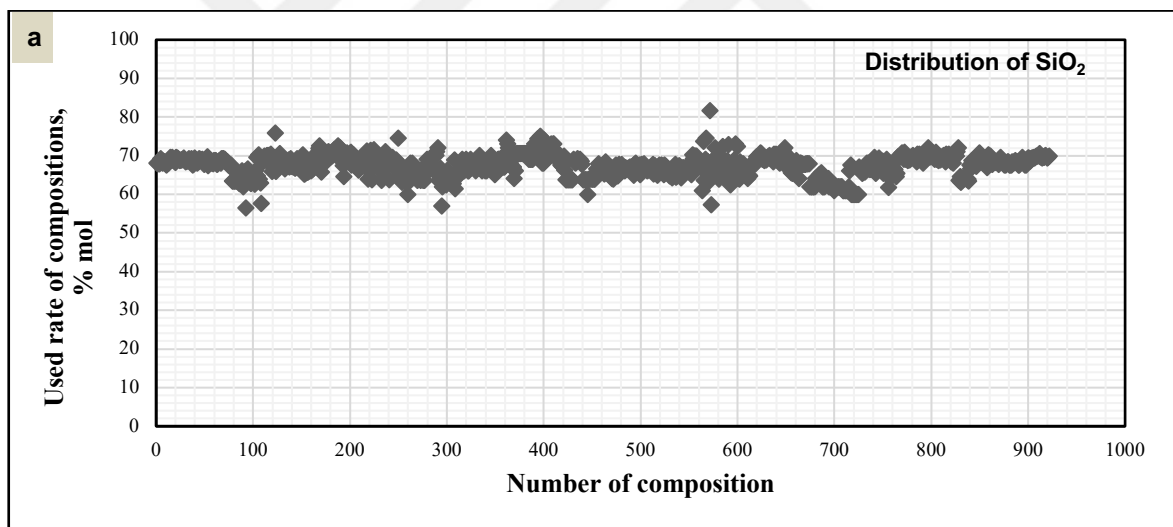
Patent No / Year	SiO <sub>2</sub>	Al <sub>2</sub> O <sub>3</sub>	B <sub>2</sub> O <sub>3</sub>	MgO	CaO	SrO
	Min. Max.	Min. Max.	Min. Max.	Min. Max.	Min. Max.	Min. Max.
US8598056 /2013	67,62	11,74	3,28	4,07	4,84	1,73
	69,56	14,47	4,92	5,54	6,68	3,60
US7534734 /2009	67,10	10,04	8,16	0,30	7,42	0,46
	69,75	11,13	10,11	2,98	10,70	5,51
US5116788 /1992	62,80	8,01	2,13	2,22	4,91	2,45
	66,00	10,70	16,10	9,22	21,70	6,13
US5770535 /1998	61,91	9,39	4,59	8,08	7,68	0,00
	63,12	11,52	4,69	9,39	8,08	0,00
US5811361 /1998	57,00	5,91	4,93	0,51	2,50	0,66
	70,25	18,00	13,21	6,54	13,47	8,14
US5851939 /1998	65,88	7,44	4,91	0,33	0,57	0,31
	75,76	13,44	10,68	11,19	8,81	5,99
WO20081490221A2 /2008	63,52	9,21	4,68	3,10	1,13	0,06
	72,53	18,70	9,13	12,31	5,78	1,97



<b>US6329310</b>	66,82	10,50	0,90	5,71	1,29	0,33
<b>/2001</b>	74,59	14,14	4,16	12,50	9,37	1,84
<b>US5885914</b>	57,00	10,00	9,00	0,50	0,50	2,00
<b>/1994</b>	72,00	20,00	14,00	3,50	5,30	11,50
<b>US6096670</b>	61,43	9,23	3,74	3,35	2,28	1,25
<b>/2000</b>	68,83	11,87	9,66	15,83	12,03	3,89
<b>US6169047</b>	65,00	1,00	5,00	1,00	1,00	2,00
<b>/2001</b>	70,00	14,00	10,00	12,00	11,00	9,30
<b>US6537937</b>	64,00	5,00	6,00	1,40	0,90	0,50
<b>/2003</b>	75,00	14,00	10,50	16,50	11,20	5,00
<b>US20070232478A1</b>	67,30	10,21	9,17	0,33	5,51	0,51
<b>/2007</b>	69,85	11,25	9,92	4,57	9,16	0,51
<b>US20050101469A1</b>	63,80	9,42	4,51	10,17	5,14	3,21
<b>/2005</b>	66,27	11,01	5,79	14,01	6,26	3,21
<b>US201201355853</b>	59,92	7,19	9,79	0,25	1,25	0,48
<b>/2012</b>	69,28	13,18	18,31	6,25	9,25	5,49
<b>US20090294773A1</b>	63,94	11,42	3,99	3,02	4,51	1,22
<b>/2009</b>	68,39	13,07	8,41	7,00	8,84	4,95
<b>US8883665/2014</b>	57,27	2,08	1,42	3,68	1,27	2,43
	81,65	10,17	4,59	23,10	11,36	5,12
<b>WO2001000538A2/2001</b>	68,00	9,00	7,00	5,00	2,00	0,30
	72,00	13,00	9,00	13,50	4,00	0,40
<b>US6546753</b>	62,42	7,39	5,25	0,50	0,97	0,32
<b>/2003</b>	73,02	13,83	16,27	8,16	7,70	6,15
<b>US7157392</b>	63,85	9,12	6,25	6,57	0,48	0,62
<b>/2007</b>	68,45	14,55	9,30	11,91	8,06	3,89
<b>US7358205</b>	67,85	9,97	8,94	0,02	6,58	3,98
<b>/2008</b>	68,36	10,44	9,74	0,03	6,78	4,05
<b>US6831029</b>	68,00	9,33	9,00	0,12	0,50	0,50
<b>/2004</b>	72,00	11,00	11,00	9,30	10,50	3,42
<b>US7968482</b>	64,13	4,81	6,71	1,61	4,76	0,63
<b>/2011</b>	69,25	11,27	9,80	5,21	9,55	4,51
<b>US7888276</b>	67,77	9,98	9,14	11,05	1,13	0,61
<b>/2011</b>	67,84	9,99	9,15	11,06	1,14	0,61
<b>US7838451</b>	60,00	5,00	5,00	3,50	2,00	2,00
<b>/2010</b>	67,50	11,50	9,00	8,00	16,00	16,00
<b>US7763559/2010</b>	65,33	8,28	7,91	1,32	5,83	0,19
	69,52	12,48	15,73	3,10	7,21	2,27
<b>US20020183188A1</b>	65,44	9,15	5,64	5,02	5,36	0,50

/2002	68,99	11,77	9,57	8,78	9,55	1,29
US8835335	61,80	9,20	10,87	0,81	4,50	0,64
/2014	67,87	11,63	15,53	10,17	9,91	0,64
US7365038	68,00	9,33	9,00	0,12	5,68	0,50
/2008	72,00	11,00	11,00	1,25	10,50	4,55
US7524784	68,00	9,33	9,00	0,12	5,68	0,50
/2009	72,00	11,00	11,00	1,25	10,50	4,55
US7754631	63,00	10,50	7,50	7,00	6,00	2,30
/2010	64,50	11,60	8,50	8,00	8,00	3,50
US7833919	66,58	11,75	1,25	0,84	2,99	0,68
/2010	70,69	13,51	4,96	7,48	5,89	4,29

Data obtained given patents and compositions are shown in the following figures as distribution and intensity range of components.



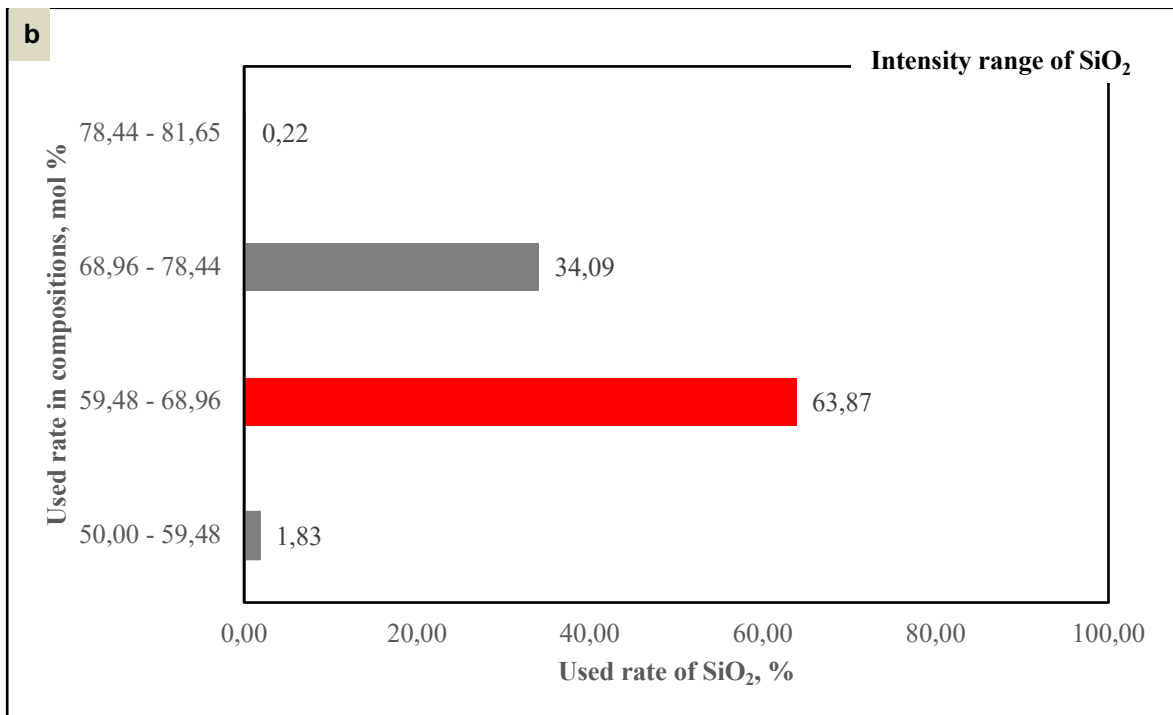


Figure 2.1. a) Distribution of SiO<sub>2</sub> and b) Intensity range of SiO<sub>2</sub> obtained from patents

It is concluded that the intensity range of SiO<sub>2</sub> calculated from the patents which involve glass substrate for display technologies is in the between 59,48 – 68,96 mol percent with 63,87 mol percent.

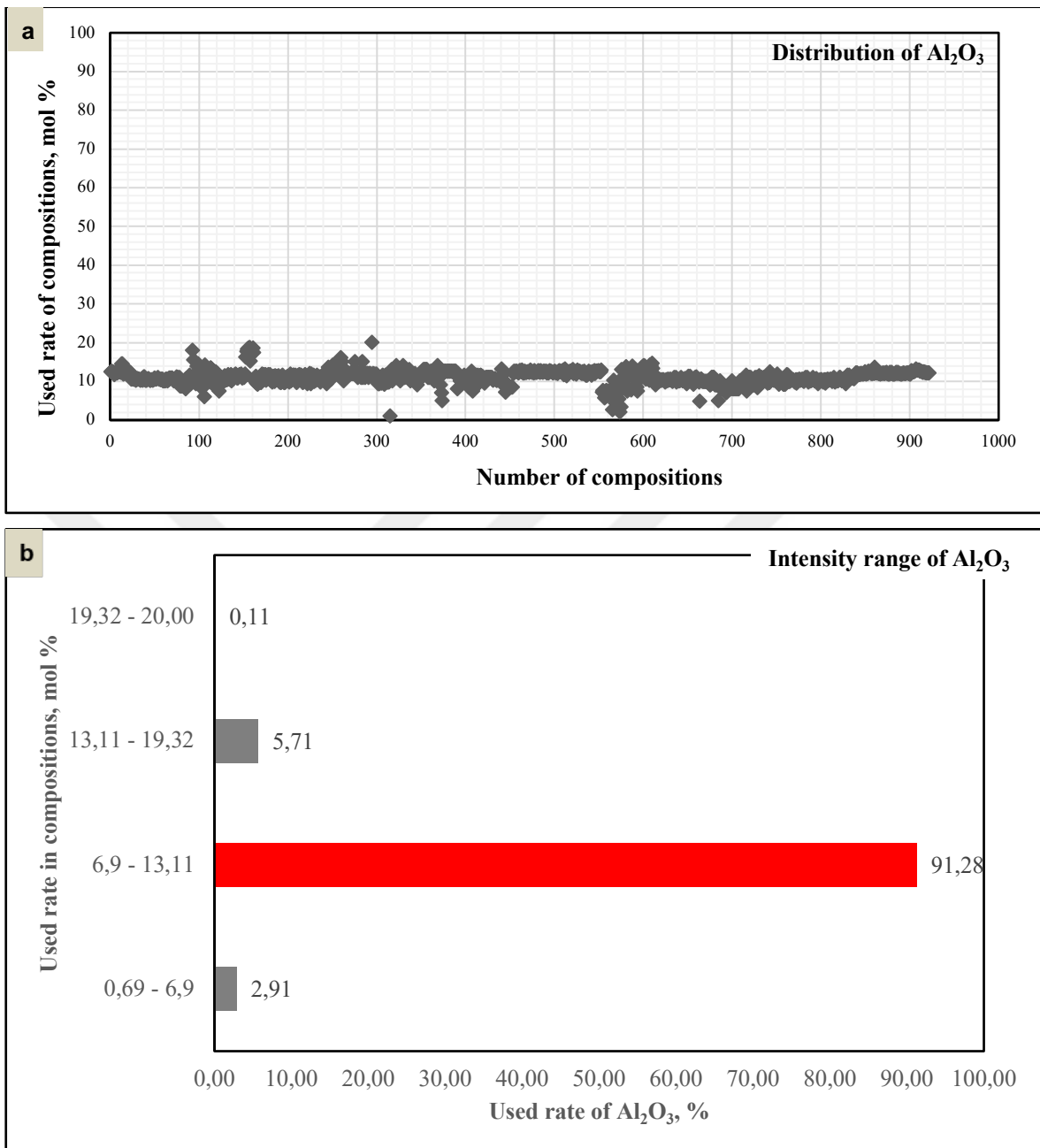


Figure 2.2. a) Distribution of  $\text{Al}_2\text{O}_3$  and b) Intensity range of  $\text{Al}_2\text{O}_3$  obtained from patents

It is concluded that the intensity range of  $\text{Al}_2\text{O}_3$  calculated from the patents which involve glass substrate for display technologies is in the between 6,9 – 13,11 mol percent with 91,28 mol percent.

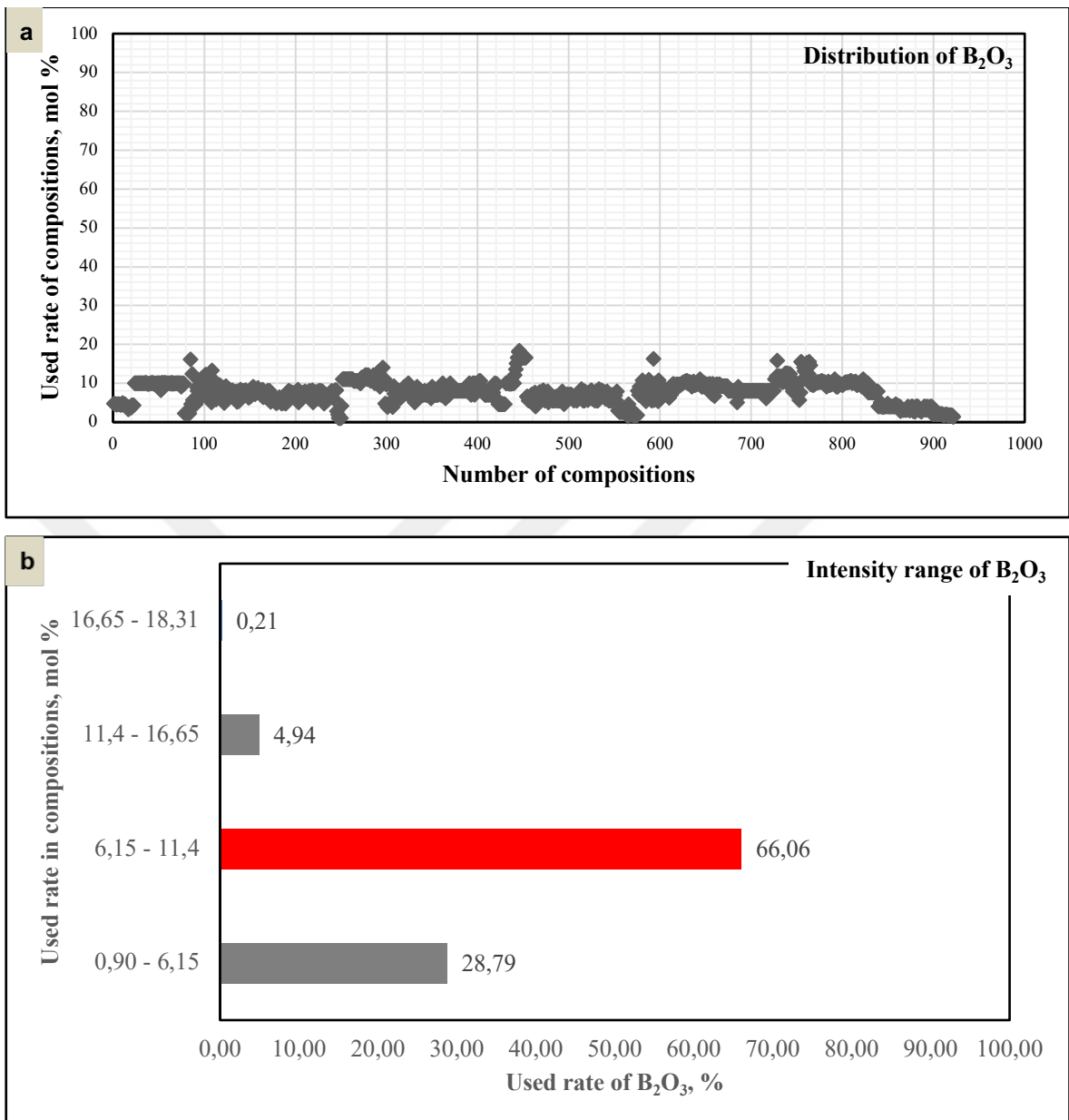


Figure 2.3. a) Distribution of B<sub>2</sub>O<sub>3</sub> and b) Intensity range of B<sub>2</sub>O<sub>3</sub> obtained from patents

It is concluded that the intensity range of B<sub>2</sub>O<sub>3</sub> calculated from the patents which involve glass substrate for display technologies is in the between 6,15 – 11,4 mol percent with 66,06 mol percent.

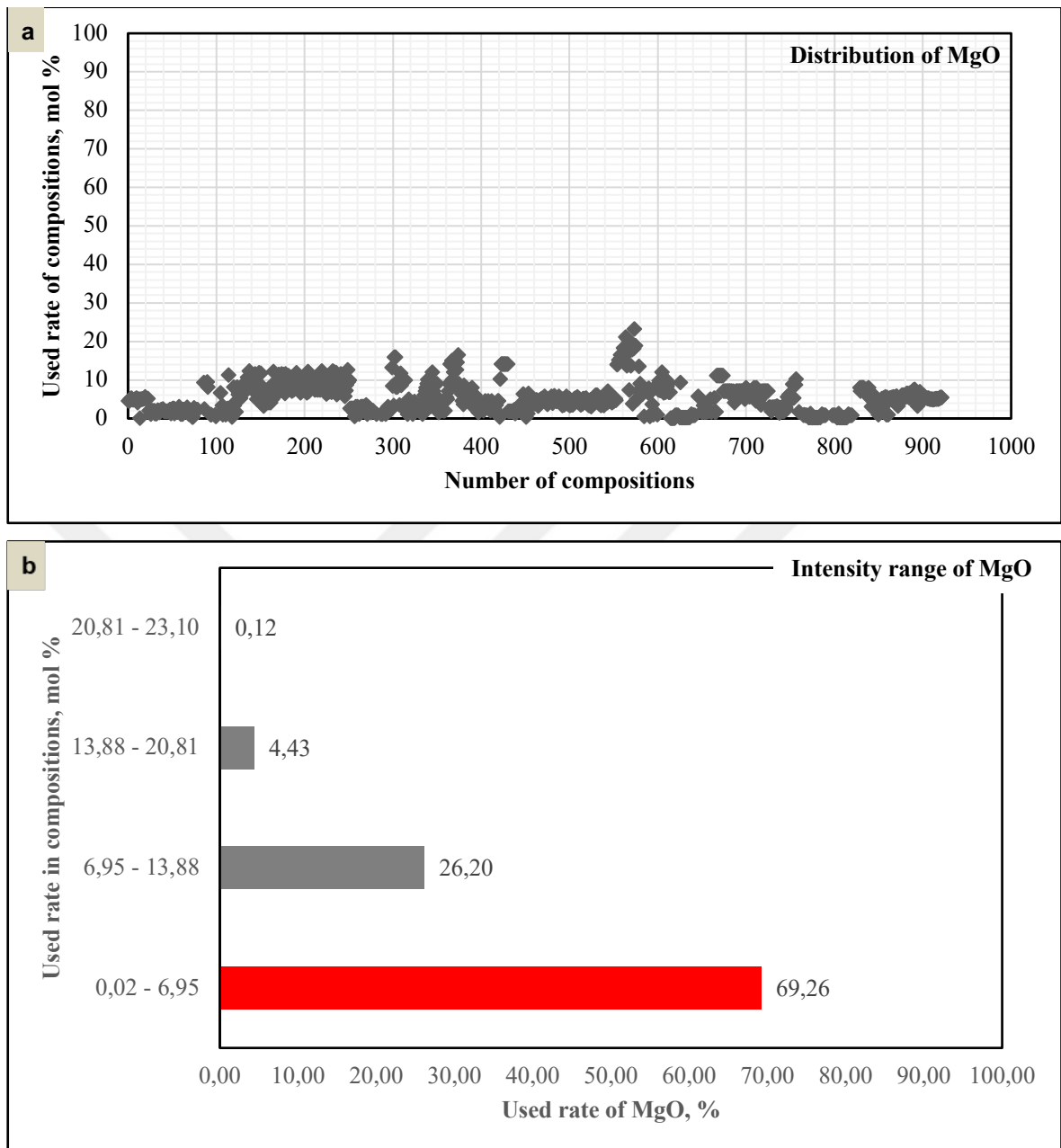


Figure 2.4. a) Distribution of MgO and b) Intensity range of MgO obtained from patents

It is concluded that the intensity range of MgO calculated from the patents which involve glass substrate for display technologies is in the between 0,02 – 6,95 mol percent with 69,26 mol percent.

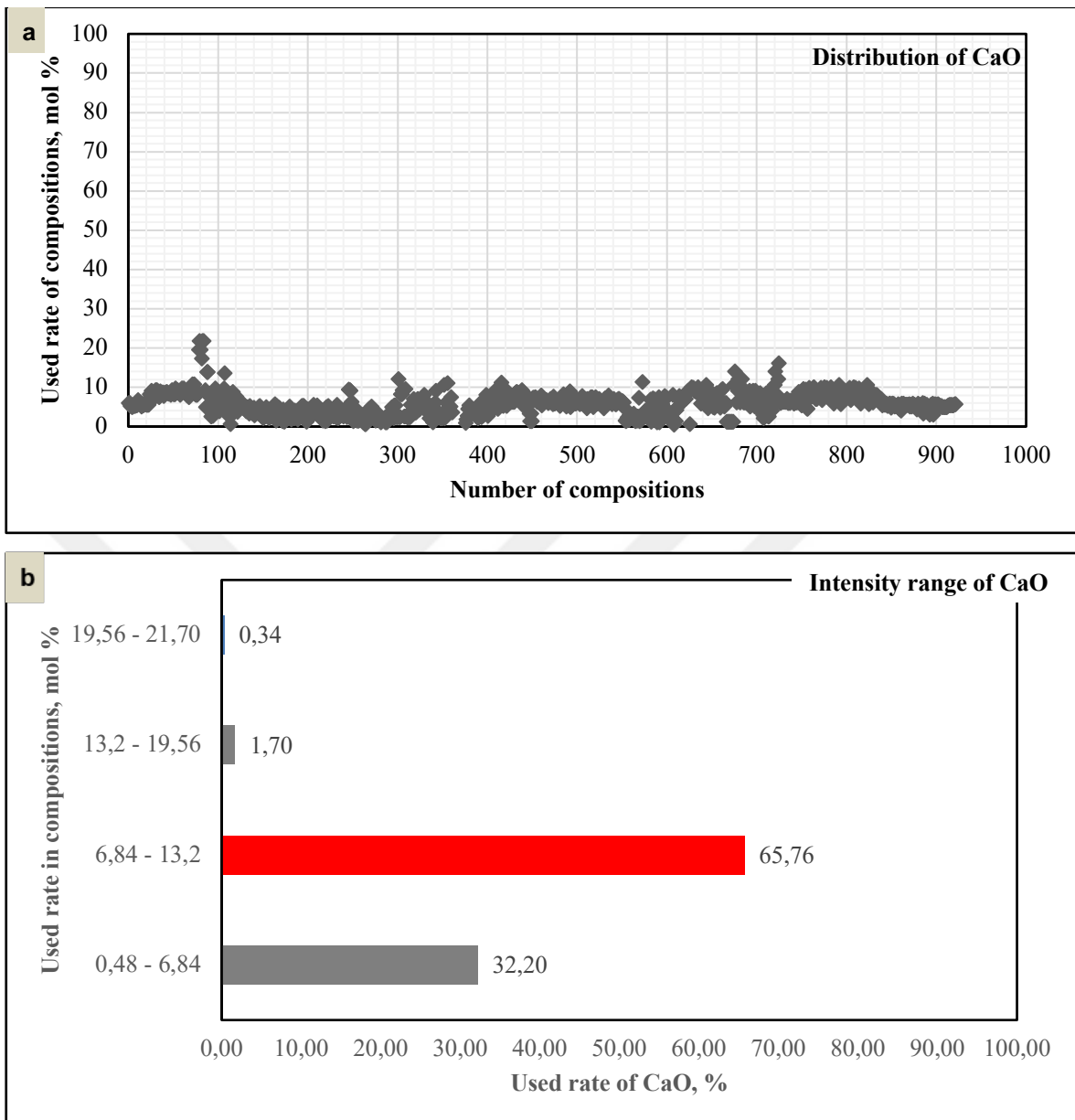


Figure 2.5. a) Distribution of CaO and b) Intensity range of CaO obtained from patents

It is concluded that the intensity range of CaO calculated from the patents which involve glass substrate for display technologies is in the between 6,84 – 13,2 mol percent with 65,76 mol percent.

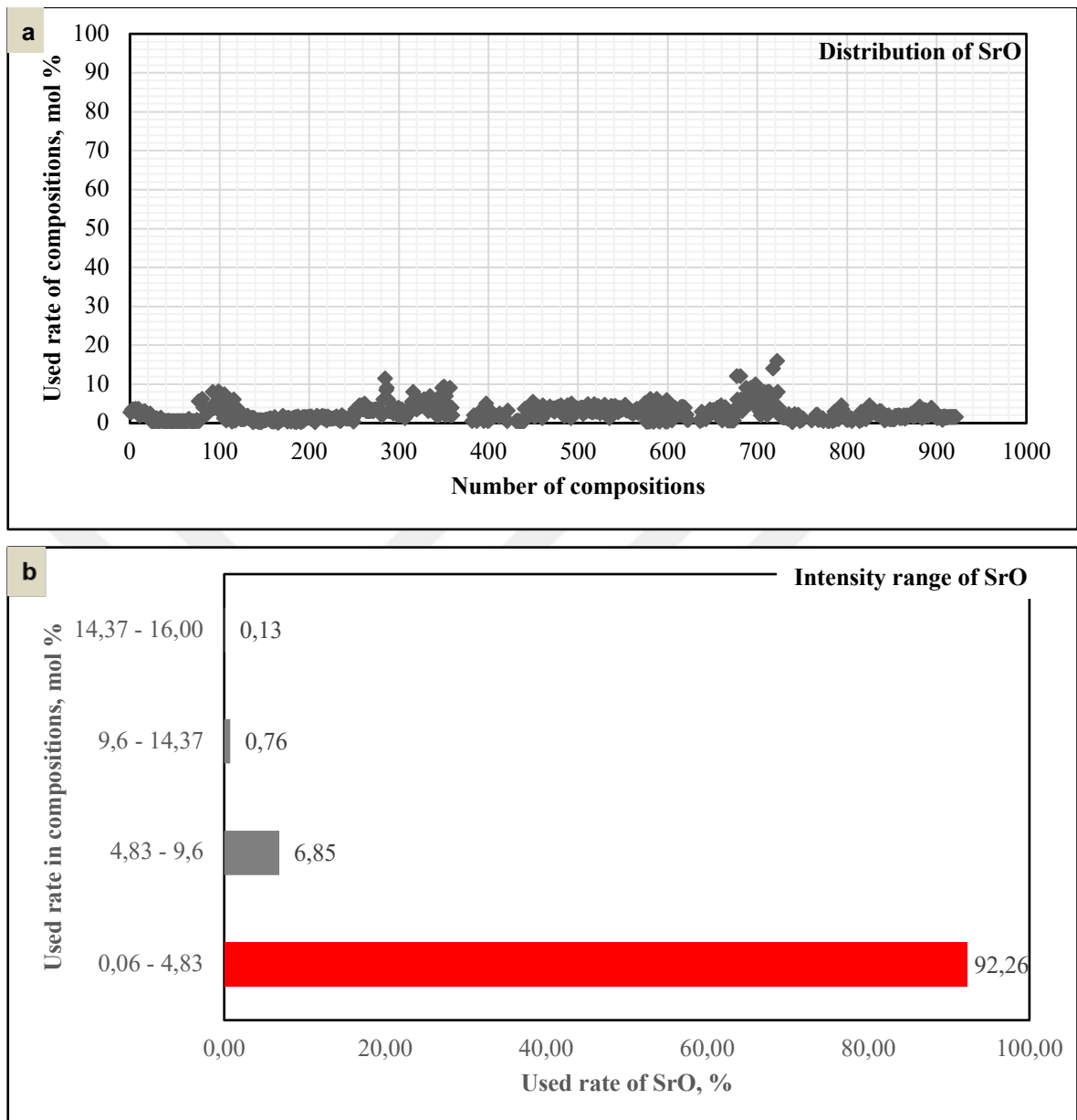


Figure 2.6. a) Distribution of SrO and b) Intensity range of SrO obtained from patents

It is concluded that the intensity range of SrO calculated from the patents which involve glass substrate for display technologies is in the between 0,06 – 4,83 mol percent with 92 ,26 mol percent.

When all these compositions were examined, the greatest difference in usage rate was observed in SiO<sub>2</sub> (57 - 81.65 mol percent) and Al<sub>2</sub>O<sub>3</sub> (1 – 20 mol percent) respectively. In other words, SiO<sub>2</sub> and Al<sub>2</sub>O<sub>3</sub> in the glass compositions are preferred in a wide range. Using rate of other components, is preferred in a lower range relatively.



Table 2.2. Glass composition obtained from distribution and intensity range of components in the patents

<b>Components</b>	<b>Contents, mol%</b>
SiO <sub>2</sub>	59,48-68,96
Al <sub>2</sub> O <sub>3</sub>	6,9-13,11
B <sub>2</sub> O <sub>3</sub>	6,15-11,4
MgO	0,02-6,95
CaO	6,84-13,02
SrO	0,06-4,83

Main components of glass structure and using rate of the components is determined by examined 32 patents and 912 composition in concordance with glass substrates.

## **2.2. PREPARATION AND PRODUCTION OF GLASS MATERIALS**

After determination of the compositions obtained from patents related to display technology glass, the next step is to prepare the appropriate glass batch for the production of the glasses in specified composition. In the study, glass frit material was chosen as raw material. Because of the lower melting temperature, high homogenization of glass frit, it is thought that it will provide ease in glass production process in laboratory conditions.

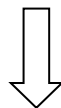
The production of glass frits in the desired compositions was requested from Gizem Frit, and chemical analysis of the glass frit sample produced by Gizem Frit is given in Table 2.3.

Table 2.3. Chemical structure of glass frit produced by Gizem Frit

Components	% mol
SiO <sub>2</sub>	62,06
Al <sub>2</sub> O <sub>3</sub>	12,20
B <sub>2</sub> O <sub>3</sub>	8,17
MgO	6,04
CaO	9,18
SrO	1,58
ZrO <sub>2</sub>	0,16
Fe <sub>2</sub> O <sub>3</sub>	0,08
BaO	0,06
K <sub>2</sub> O	0,06
TiO <sub>2</sub>	0,01
P <sub>2</sub> O <sub>5</sub>	0,002
ZnO	0,005
MnO	0,005
CuO	0,41

Generally, glass production process are composed of five different production step including (1) preparation of glass batch, (2) homogenization, (3) melting at high temperature, (4) casting into graphite mold, (5) annealing of produced glass, and preferably, cutting in desired measurement.

Preparation of glass batch

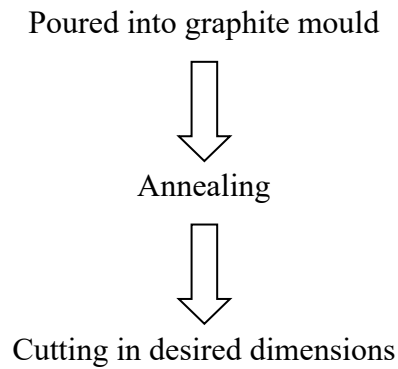


Homogenization



Melting Process





First step in the production method, the parent glass frit ve glass frit doped 1-2-3 wt.percent LiF, was homogenized. Homogenization process was done in ball milling for 8 hours.



Figure 2.7. Performing the homogenization process in the ball mill

After homogenization process, homogenized glass batch was melted at high temperature. In determination of melting temperature of the composition, Liu J. et.al [64] melted non-alkali borosilicate glass at 1600°C for 2 hours. Hence, it was decided that melting temperature of prepared glass compositions in the study would appropriate 1650°C with heating rate of 5°C/min for 2 hours at elevator furnace.

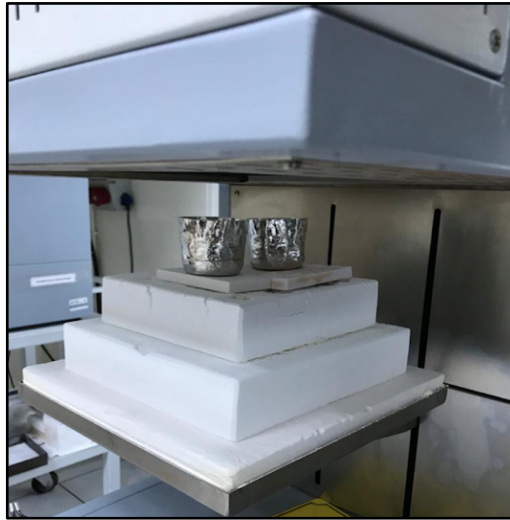


Figure 2.8. Melting process of prepared glass batch at elevator furnace

After completing of the determined temperature regime at elevator furnace, the casting process of the melted glass was poured into graphite molds and as shown in Figure 2.9 glass samples were produced.

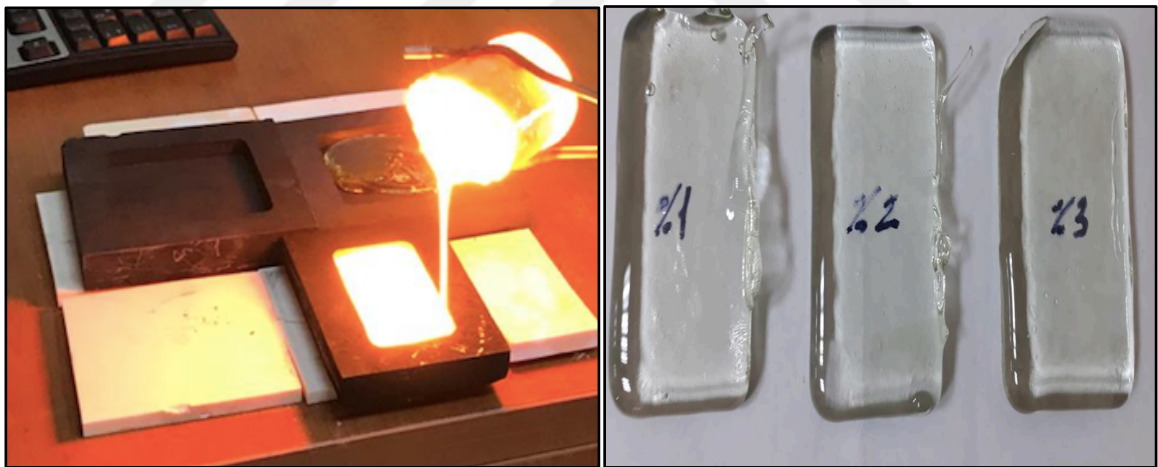


Figure 2.9. Casting of melted glass to graphite mold and produced glass samples

Annealing process of parent glass composition and doped 1 – 2 – 3 wt. percent LiF glass composition was performed at different temperature. When the annealing temperature of glass samples was performed at 720°C for 2h, color changing was observed at 2 and 3 wt. percent LiF doped glass composition (Figure 2.9).

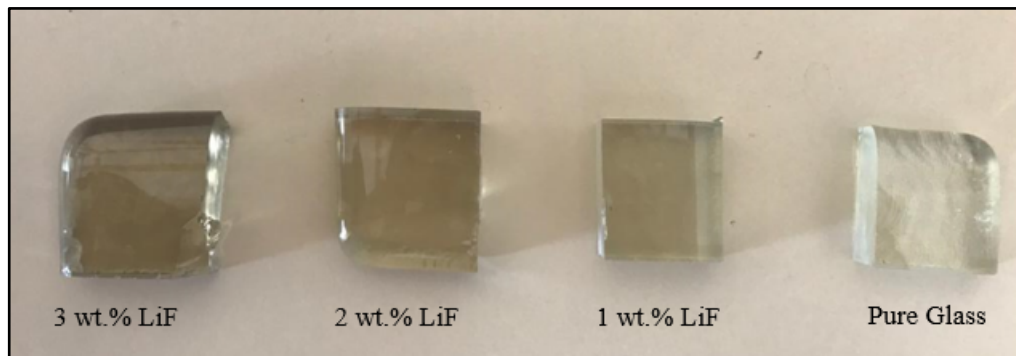


Figure 2.10. Color changing of the glass samples at 720°C for 2 hours annealing process

In addition to the color changing of the samples, appropriate annealing and crystallization temperature was determined from crystallization kinetic studies performed simultaneously with production process. Annealing temperature for parent glass composition and doped 1 – 2 – 3 wt. percent LiF glass composition was determined as 720°C, 600°C 2h, 570°C and 550°C 2h respectively. Crystallization kinetics studies are described in following section in detail.

After the annealing process, glass samples are ready to cut in desired size and to be produced glass – ceramic material. Sizing process of glass samples was made according to characterization tests to be carried out with the BUEHLER IsoMet Low Speed Raw device.



Figure 2.11. Cutting of produced glass samples with BUEHLER IsoMet Low Speed Raw device

Crystallization kinetics studies have been completed in order to determine the temperatures in which the ceramic structures will be obtained from the annealed samples at the specified temperatures for each composition doped 1 – 2 - 3 wt. percent LiF before glass-ceramic production process. After crystallization process, thermal expansion coefficient of parent glass composition and glass composition doped 1 - 2 - 3 wt. percent LiF was analyzed within scope of characterization of the glass batch.

## 2.3. CHARACTERIZATION OF GLASS MATERIALS

### 2.3.1. Crystallization Kinetics of Glass Materials

Crystallization of a liquid or amorphous solid consists of two different process as called nucleation and crystallization. Crystallization process of amorphous solid is commenced with crystal nucleation. Nucleation process is divided into two categories; homogeneous or primary nucleation and heterogenous or secondary nucleation. In the homogeneous process, nucleation takes place without adding of any foreign agents to main phase structure, while

heterogeneous occurs with a foreign substance introduced to main phase. Then, the nucleation process is trailed by growth of the crystal nuclei to macroscopic dimensions, which is classified crystal growth.

Structure and kinetics of crystallization in the crystallization mechanism of amorphous materials are significant parameters. How much energy is required to create a nuclei and growth of the nuclei is necessary for the crystallization of the structure. Crystallization kinetics of amorphous materials is examined isothermal and non-isothermal analysis techniques. In the isothermal techniques, the sample is heated above the glass transition temperature and the heat absorbed during the crystallization process is evaluated as a function of time. On the other hand, in the non-isothermal method, the sample is heated at a fixed rate and then the change in the enthalpy is measured as a function of temperature. The thermal analysis techniques are differential thermal analysis (DTA) and differential scanning calorimetry (DSC) [101],[102].

Within the scope of the thesis, Ozawa and Kissinger method was used to calculate crystallization activation energy of glass materials doped with 1-2-3 wt. percent LiF in order to have a idea crystallization behavior of the glass materials.

The crystallization behavior of glasses under non-isothermal conditions were determined by differential thermal analysis (DTA) method which was performed in a SII Exstar Tg/DTA 6300 thermo analyzer using 30 mg powdered samples heated from 30°C to 1250°C with different heating rates (5, 10, 15, and 20°C/min).

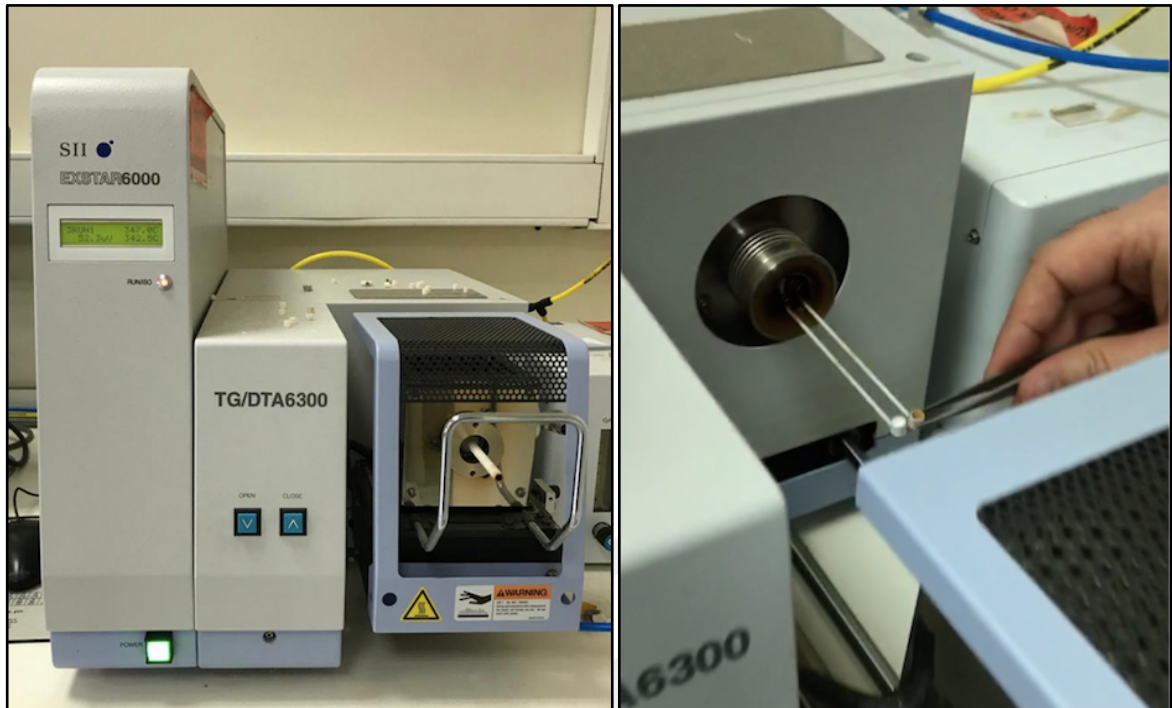


Figure 2.12. SII Exstar TG-DTA thermo analyzer device

Non-isothermal investigation of crystallization in amorphous materials is explained by the Kissinger-Ozawa equation as given in Equation 2.1 and 2.2 respectively.

$$\ln(T_c^2 / \phi) = E/R \cdot T_c + C \quad (2.1)$$

$$\ln \phi = -E/R \cdot T_c + C \quad (2.2)$$

Where  $T_c$  is the crystallization peak temperatures obtained from the DTA curves,  $\phi$  is the heating rate,  $R$  is the gas constant ( $R=8,314 \text{ J}/(\text{mol}\cdot\text{K})$ ), and  $C$  represents a constant. Based on Equation (2.1) proposed by Kissinger, the plot  $\ln(T_c^2 / \phi)$  versus  $1/T_c$  is expected to be linear, and according to the slope, the crystallization activation energy  $E_a$  can be calculated. Firstly, crystallization activation energy was calculated by using Kissinger Method. In the Figure 2.13. DTA curves performed at 5, 10, 15, 20°C/min with heating rate of the parent glass composition is shown.



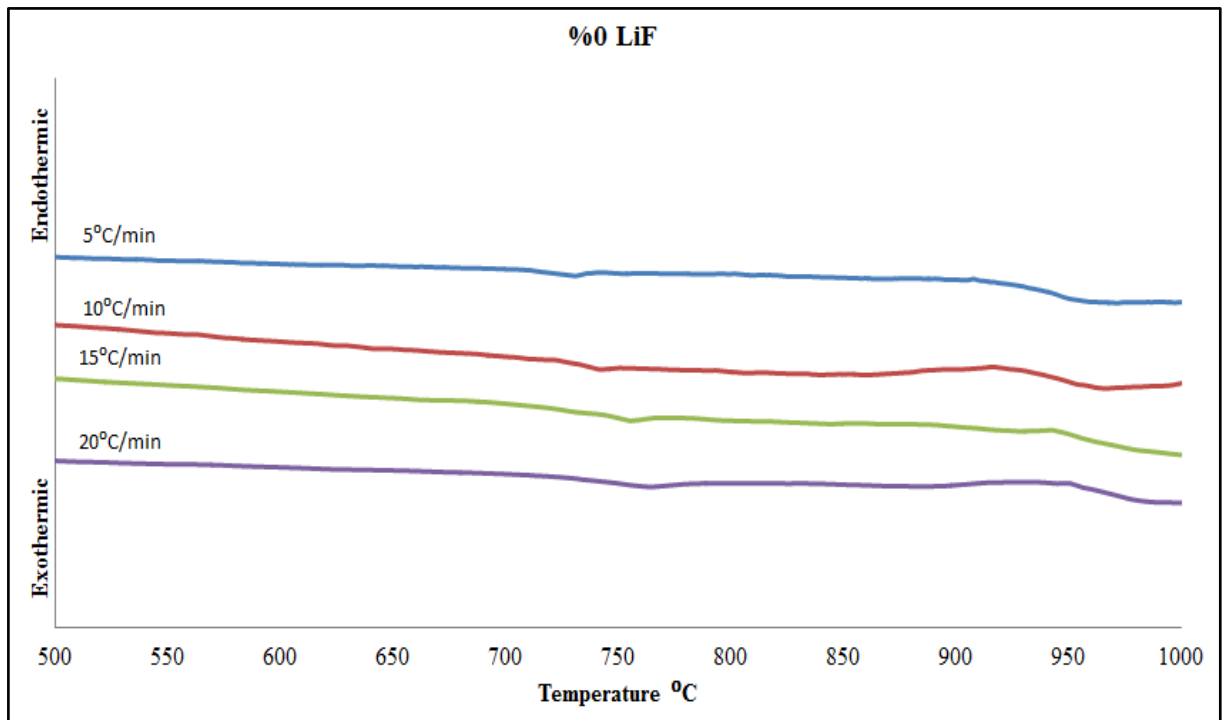


Figure 2.13. DTA curves of the parent glass composition at different heating rate

From the DTA curves of parent glass composition,  $T_g$  (glass-transition) temperatures of parent glass composition are determined as 1004 K, 1013 K, 1029 K, and 1041 K at different heating rate, (5°C/min, 10°C/min, 15°C/min, and 20°C/min.) respectively. Also, crystallization peak temperature  $T_c$ , corresponding to DTA curves, are determined as 1181 K, 1201 K, 1211 K, and 1221 K at different heating rate (5°C/min, 10°C/min, 15°C/min, and 20°C/min.) respectively.

Table 2.4. Thermal parameters of the parent glass composition obtained from DTA results

$\phi$ (°C/min.)	$T_g$ (K)	$T_c$ (K)
5	1004	1181
10	1013	1201
15	1029	1211
20	1041	1221

Crystallization activation energy of the parent glass composition by using  $T_g$  and  $T_c$  temperature determined DTA curves can be calculated. According to  $T_g$  and  $T_c$  temperature

obtained from DTA curves of parent glass composition as given in Table 2.4, activation energy is calculated from the slope of the plot of  $\ln(T_c^2 / \phi)$  versus  $1/T_c$  (Figure 2.14).

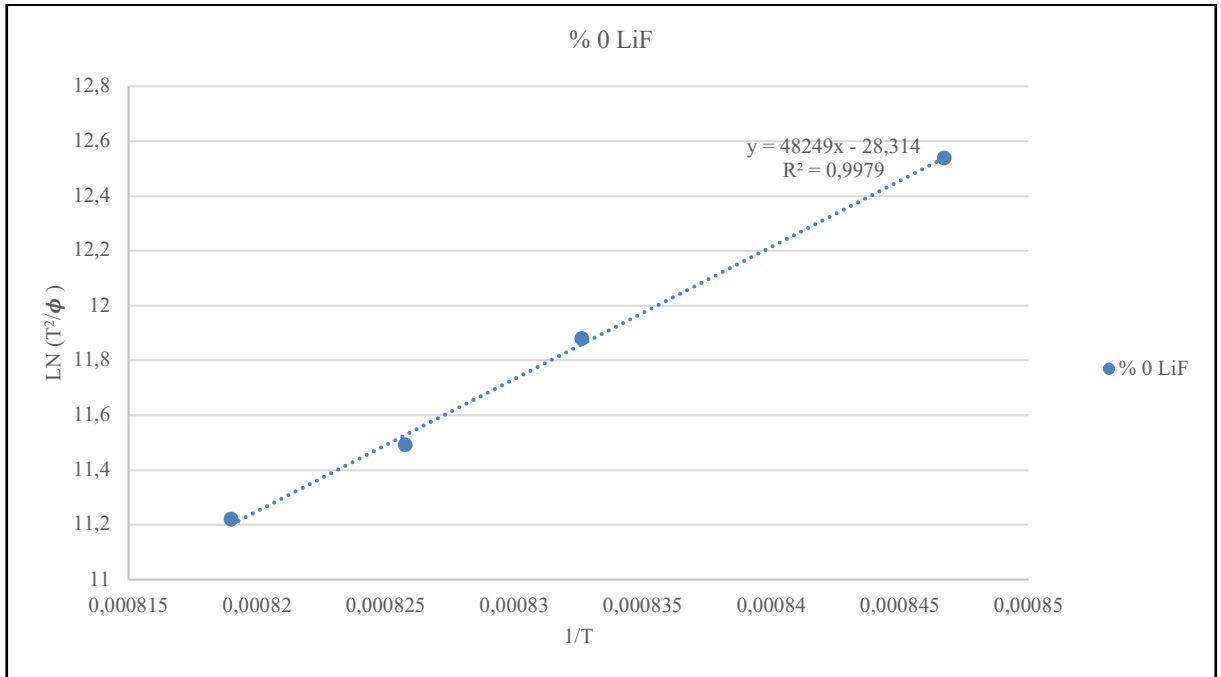


Figure 2.14. The plot of  $\ln(T_c^2 / \phi)$  versus  $1/T_c$  of parent glass composition

According to the slope of the plot of  $\ln(T_c^2 / \phi)$  versus  $1/T_c$  of parent glass composition, crystallization activation energy is calculated as 401 kJ/mol. In the Figure 2.15. DTA curves performed at 5, 10, 15, 20°C/min with heating rate of the doped 1 wt. percent LiF glass composition is shown.

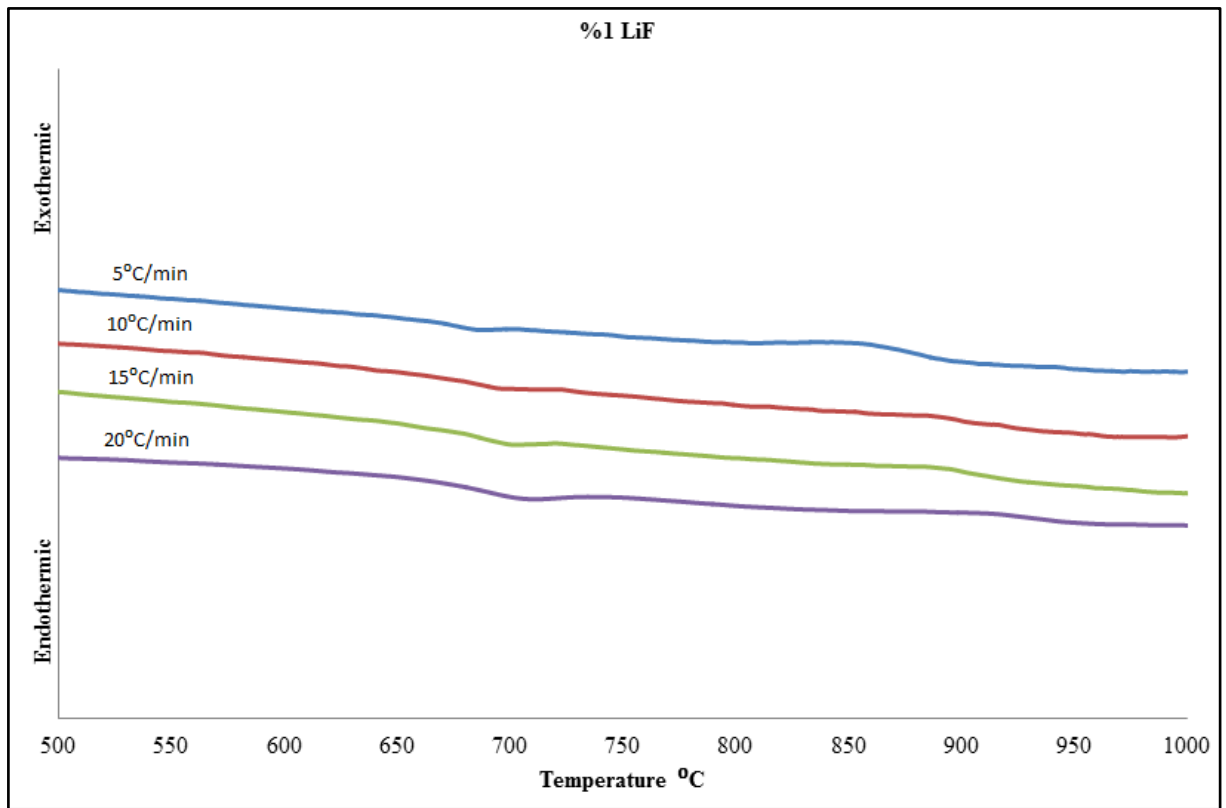


Figure 2.15. DTA curves of the doped 1 wt. percent LiF glass composition at different heating rate

From DTA curves of the doped 1 wt. percent LiF glass composition,  $T_g$  (glass-transition) temperature are determined as 957 K, 967 K, 974 K, and 987 K value at different heating rate (5°C/min, 10°C/min, 15°C/min, and 20°C/min.) respectively. Also, crystallization peak temperature  $T_c$ , corresponding to DTA curves, are determined as 1141 K, 1161 K, 1170 K, and 1182 K at different heating rate (5°C/min, 10°C/min, 15°C/min, and 20°C/min.) respectively.

Table 2.5. Thermal parameters of the doped 1 wt. percent LiF glass composition obtained from DTA results

$\phi$ (°C/min)	$T_g$ (K)	$T_c$ (K)
5	957	1141
10	967	1161
15	974	1170
20	987	1182

Crystallization activation energy of the doped 1 wt. percent LiF glass composition by using  $T_g$  and  $T_c$  temperature determined DTA curves can be calculated. According to  $T_g$  and  $T_c$  temperature obtained from DTA curves of the doped 1 wt. percent LiF glass composition as given in Table 2.5, activation energy is calculated from the slope of the plot of  $\ln(T_c^2 / \phi)$  versus  $1/T_c$  (Figure 2.16).

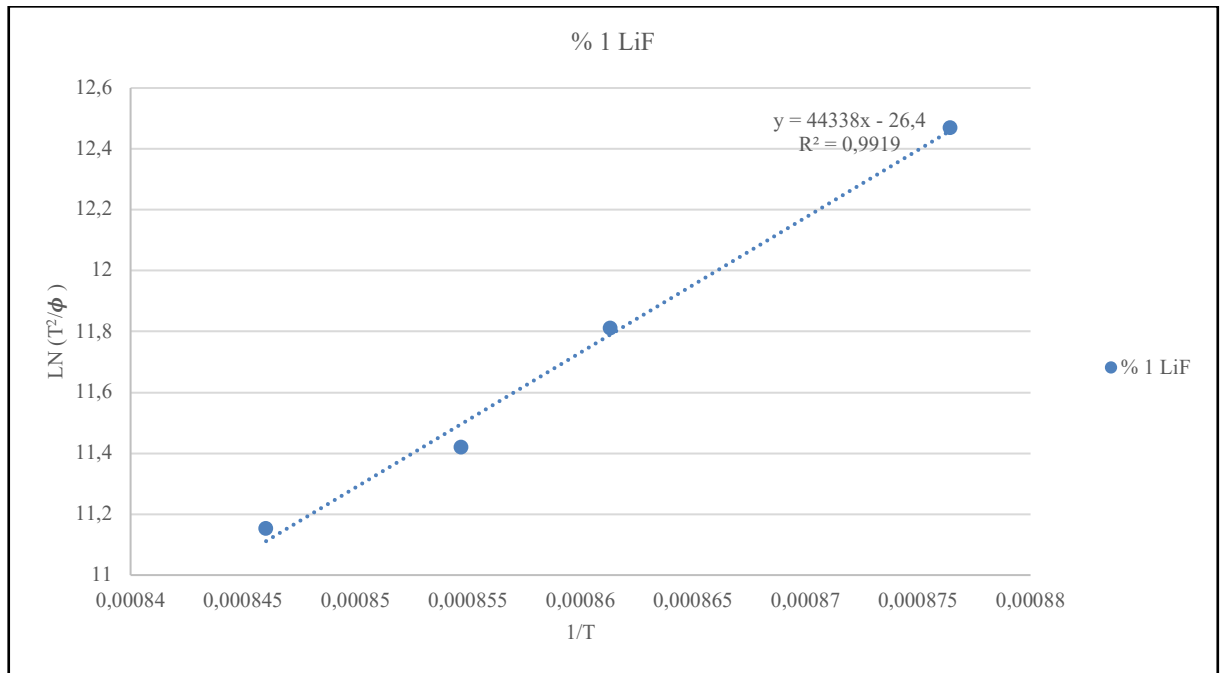


Figure 2.16. The plot of  $\ln(T_c^2 / \phi)$  versus  $1/T_c$  of the doped 1 wt. percent LiF glass composition

According to the slope of the plot of  $\ln(T_c^2 / \phi)$  versus  $1/T_c$  of the doped 1 wt. percent LiF glass composition, crystallization activation energy is calculated 369 kJ/mol. In the Figure 2.17. DTA curves performed at 5, 10, 15, 20°C/min with heating rate of the doped 2 wt. percent LiF glass composition is shown.

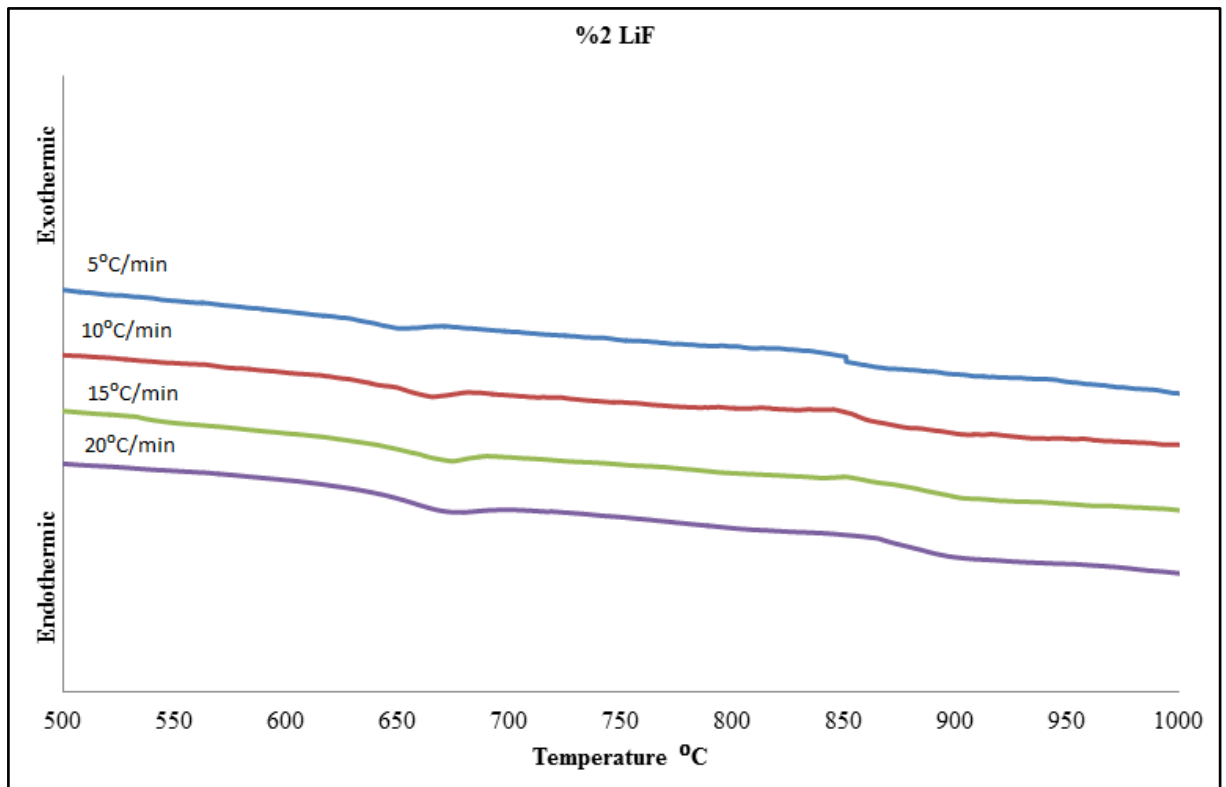


Figure 2.17. The plot of  $\ln(T_c^2 / \phi)$  versus  $1/T_c$  of the doped 2 wt. percent LiF glass composition

From DTA curves of the doped 2 wt. percent LiF glass composition,  $T_g$  (glass-transition temperature) of the doped 2 wt. percent LiF glass composition are determined as 922 K, 938 K, 949 K, and 955 K value at different heating rate (5°C/min, 10°C/min, 15°C/min, and 20°C/min.) respectively. Also, crystallization peak temperature  $T_c$ , corresponding to DTA curves, are determined as 1102 K, 1119 K, 1130 K, and 1142 K at different heating rate (5°C/min, 10°C/min, 15°C/min, and 20°C/min.) respectively.

Table 2.6. Thermal parameters of the doped 2 wt. percent LiF glass composition obtained from DTA results

$\phi$ (°C/min)	$T_g$ (K)	$T_c$ (K)
5	922	1102
10	938	1119
15	949	1130
20	955	1142

Crystallization activation energy of the doped 2 wt. percent LiF glass composition by using  $T_g$  and  $T_c$  temperature determined DTA curves can be calculated. According to  $T_g$  and  $T_c$  temperature obtained from DTA curves of the doped 2 wt. percent LiF glass composition as given in Table 2.6, activation energy is calculated from the slope of the plot of  $\ln(T_c^2 / \phi)$  versus  $1/T_c$  (Figure 2.18).

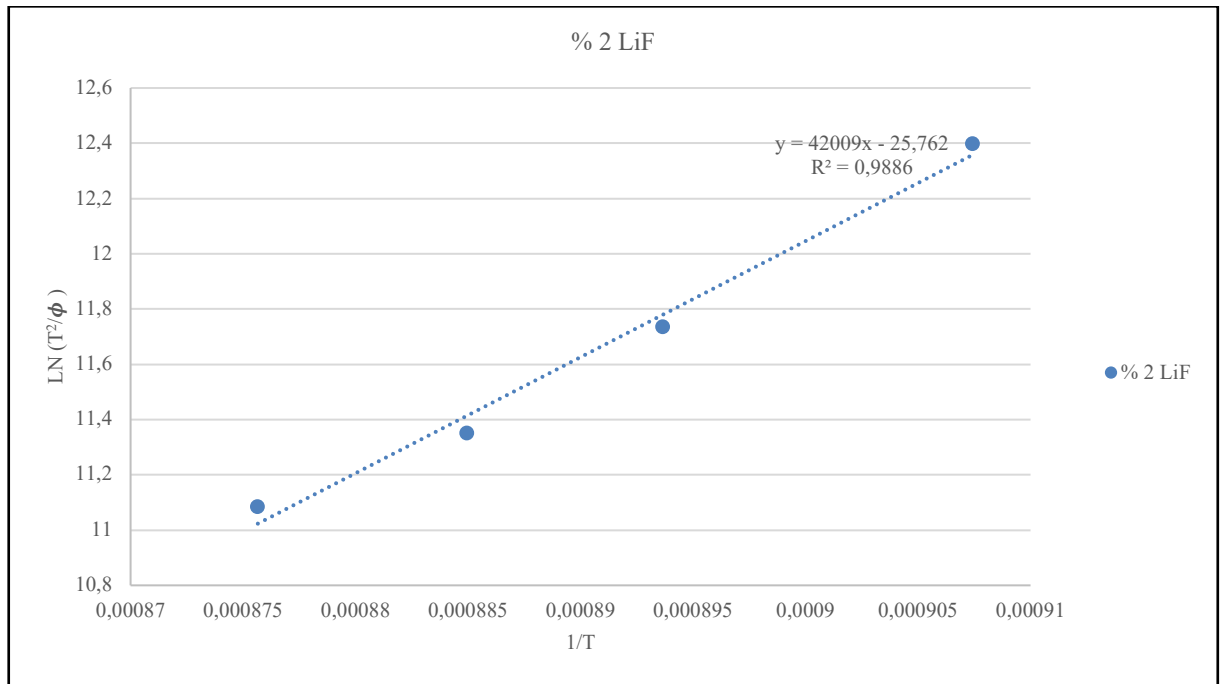


Figure 2.18. The plot of  $\ln(T_c^2 / \phi)$  versus  $1/T_c$  of the doped 2 wt. percent LiF glass composition

According to the slope of the plot of  $\ln(T_c^2 / \phi)$  versus  $1/T_c$  of the doped 2 wt. percent LiF glass composition, crystallization activation energy is calculated 349 kJ/mol. In the Figure 2.19. DTA curves performed at 5, 10, 15, 20°C/min with heating rate of the doped 3 wt. percent LiF glass composition is shown.

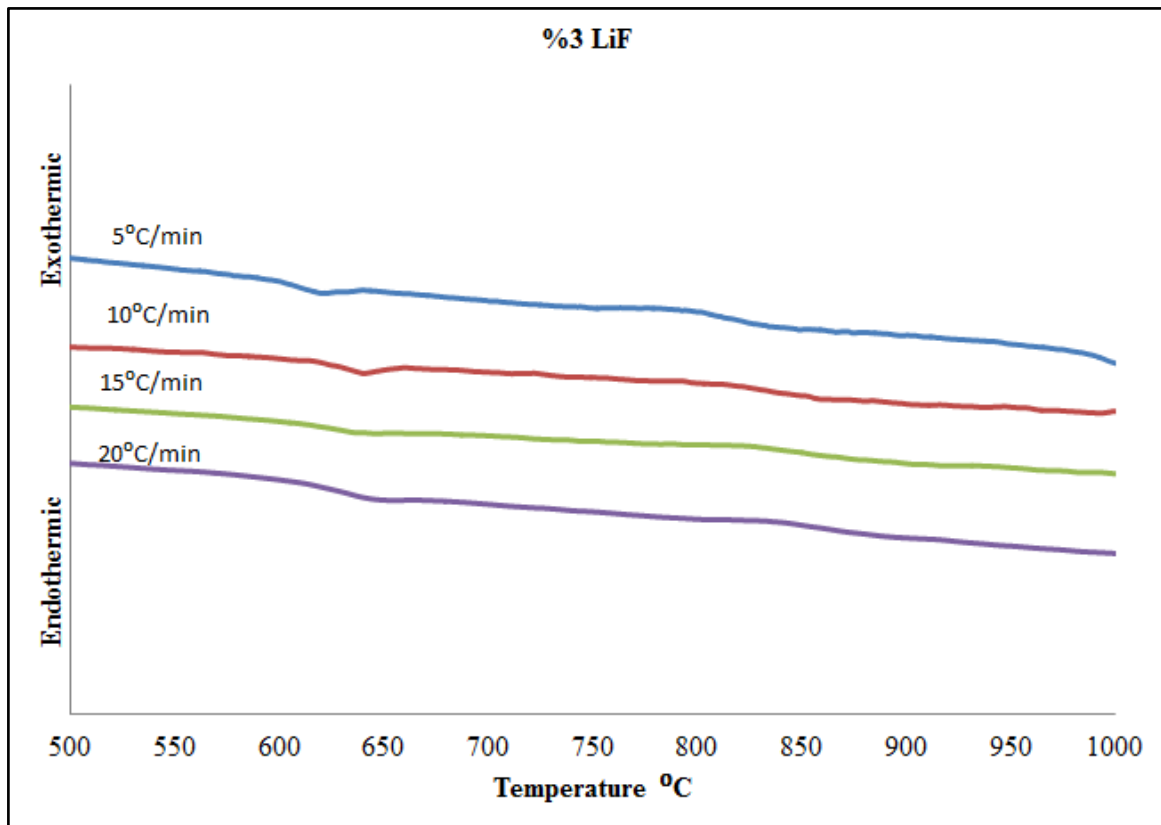


Figure 2.19. DTA curves of the doped 3 wt. percent LiF glass composition at different heating rate

From DTA curves of the doped 3 wt. percent LiF glass composition,  $T_g$  temperatures of the doped 3 wt. percent LiF glass composition are determined as 897 K, 906 K, 918 K, and 928 K value at different heating rate (5°C/min, 10°C/min, 15°C/min, and 20°C/min.) respectively. Also, crystallization peak temperature  $T_c$ , corresponding to DTA curves, are determined as 1065 K, 1085 K, 1098 K, and 1111 K at different heating rate (5°C/min, 10°C/min, 15°C/min, and 20°C/min.) respectively.

Table 2.7. Thermal parameters of the doped 3 wt. percent LiF glass composition obtained from DTA results

$\phi$ (°C/min)	$T_g$ (K)	$T_c$ (K)
5	897	1065
10	906	1085
15	918	1098
20	928	1111

Crystallization activation energy of the doped 3 wt. percent LiF glass composition by using  $T_g$  and  $T_c$  temperature determined DTA curves can be calculated. According to  $T_g$  and  $T_c$  temperature obtained from DTA curves of the doped 3 wt. percent LiF glass composition as given in Table 2.7, activation energy is calculated from the slope of the plot of  $\ln(T_c^2 / \phi)$  versus  $1/T_c$  (Figure 2.20).

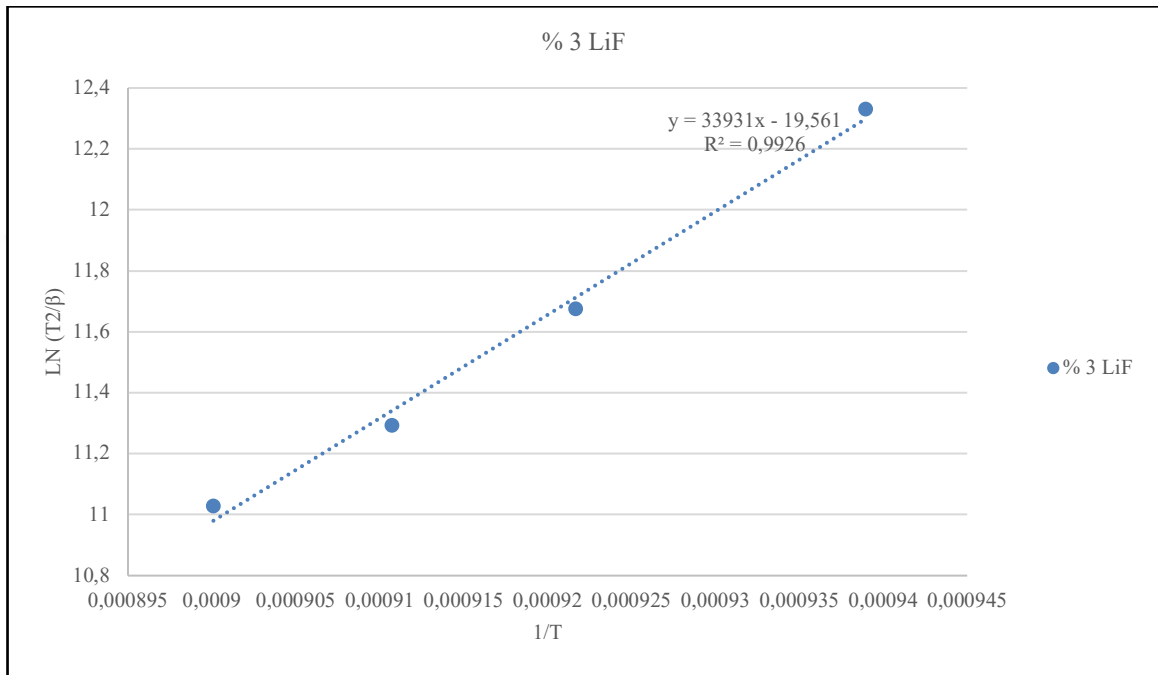


Figure 2.20. The plot of  $\ln(T_c^2 / \phi)$  versus  $1/T_c$  of the doped 3 wt. percent LiF glass composition

According to the slope of the plot of  $\ln(T_c^2 / \phi)$  versus  $1/T_c$  of the doped 3 wt. percent LiF glass composition, crystallization activation energy is calculated 282 kJ/mol.

Based on Eq. (2.2) proposed by Ozawa, crystallization activation energy  $E_a$  can be calculated from the slope of the plot of  $\ln(\phi)$  versus  $1/T_c$ . Determined  $T_g$ , and  $T_c$  temperature obtained from DTA curves at different heating rate (5°C/min, 10°C/min, 15°C/min, and 20°C/min.) equaled to the parent glass composition and doped 1-2-3 wt.% LiF glass compositions was used in Ozawa Eq. as well.



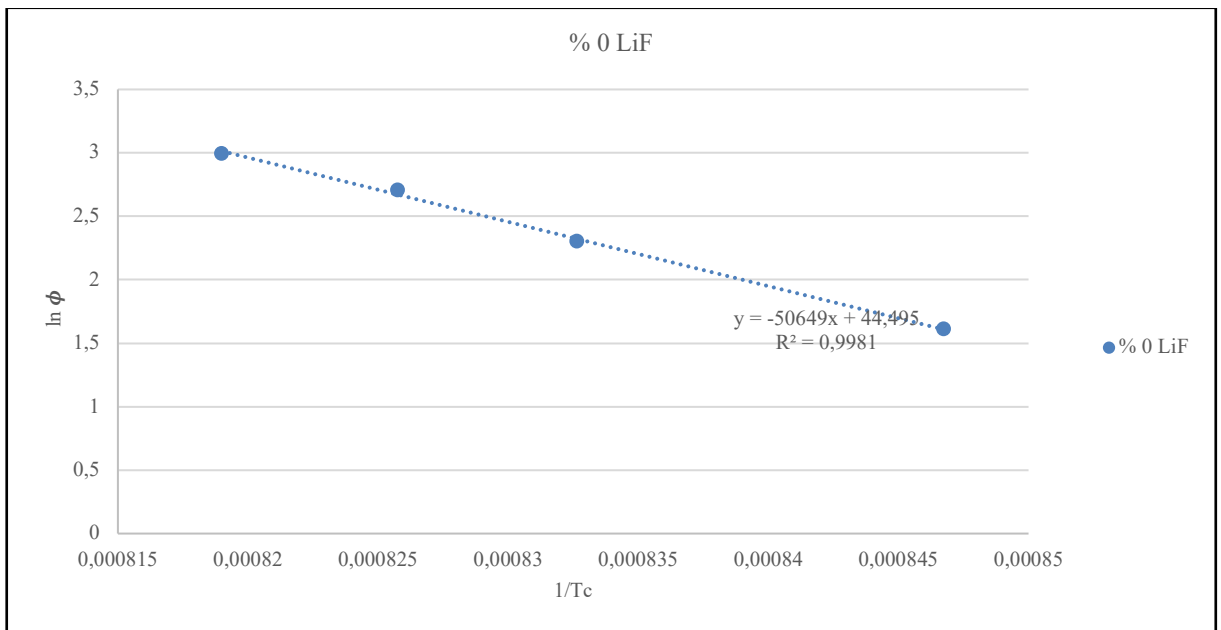


Figure 2.21. The plot of  $\ln(\phi)$  versus  $1/T_c$  of the parent glass composition

According to the slope of the plot of  $\ln(\phi)$  versus  $1/T_c$  of the parent glass composition, crystallization activation energy of the glass was calculated as 421 kJ/mol.

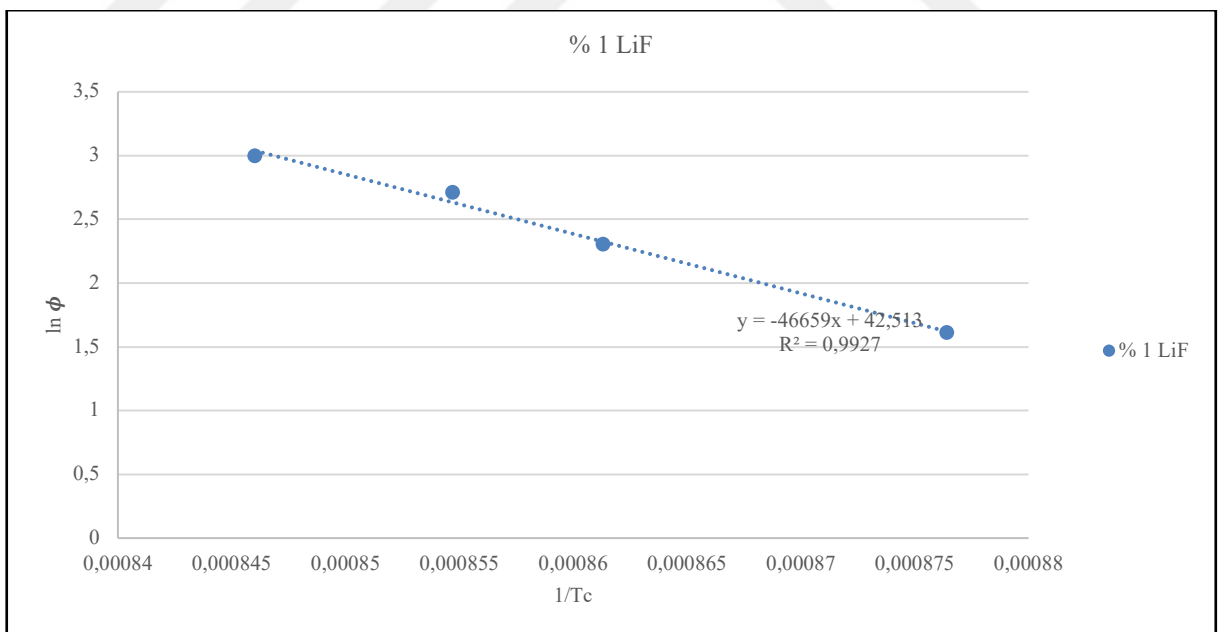


Figure 2.22. The plot of  $\ln(\phi)$  versus  $1/T_c$  of the doped 1 wt. % LiF glass composition

According to the slope of the plot of  $\ln(\phi)$  versus  $1/T_c$  of the doped 1 wt. percent LiF glass composition, crystallization activation energy of the glass was calculated as 388 kJ/mol.

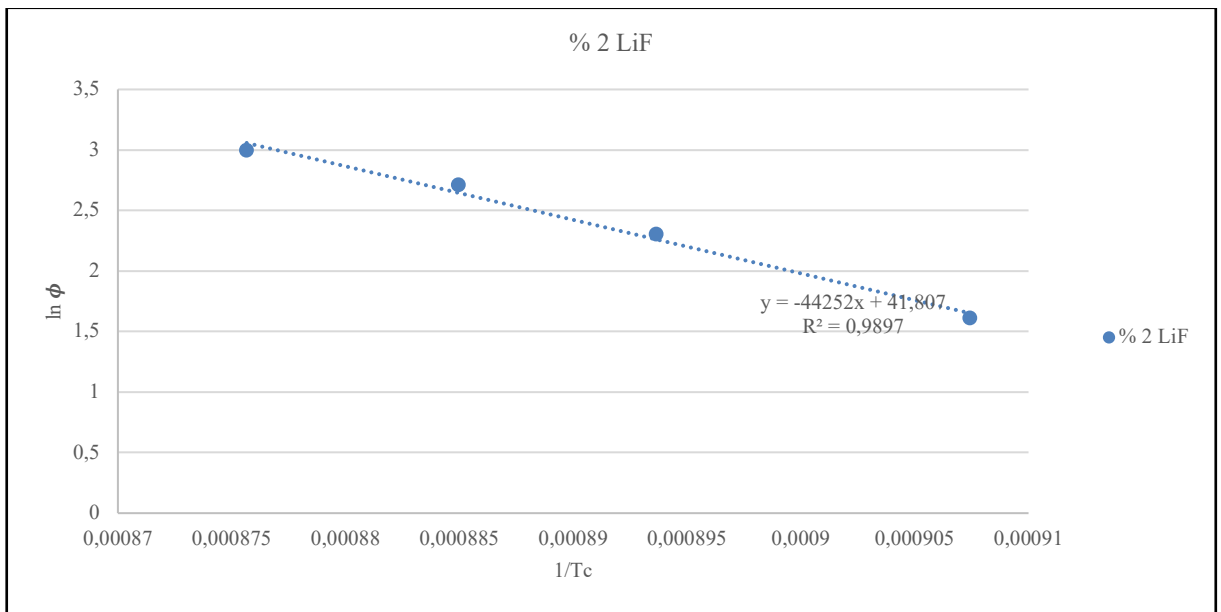


Figure 2.23. The plot of  $\ln(\phi)$  versus  $1/T_c$  of the doped % 2 wt. LiF glass composition. According to the slope of the plot of  $\ln(\phi)$  versus  $1/T_c$  of the doped 2 wt. percent LiF glass composition, crystallization activation energy of the glass was calculated as 368 kJ/mol.

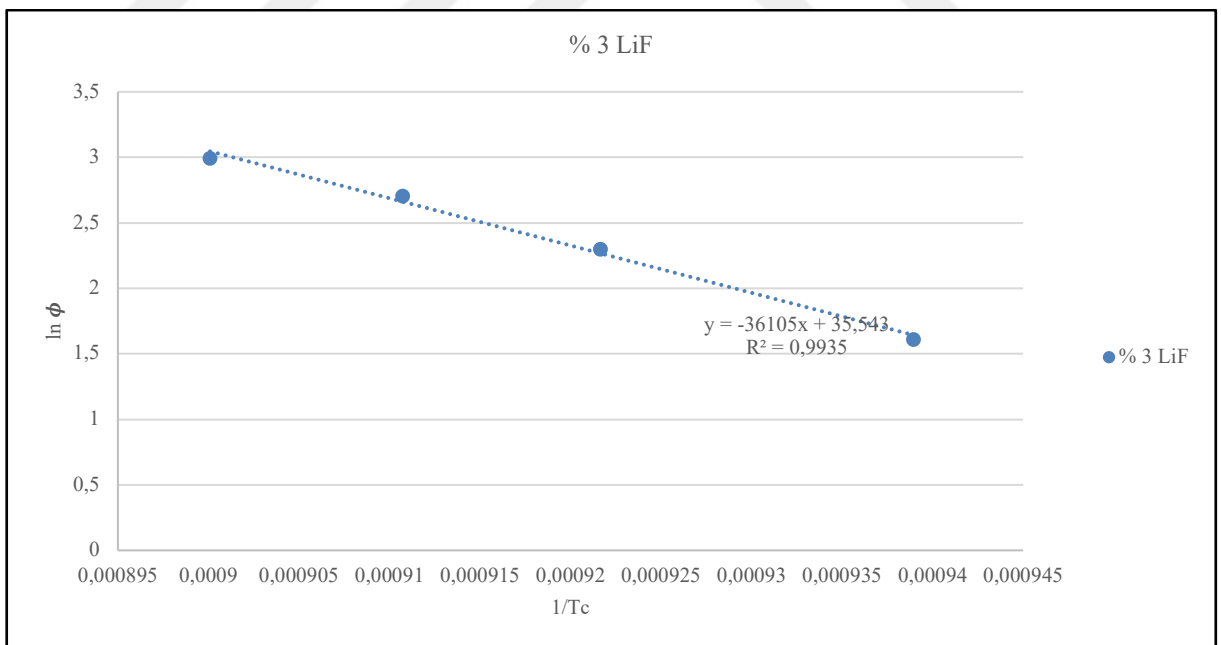


Figure 2.24. The plot of  $\ln(\phi)$  versus  $1/T_c$  of the doped 3 wt. % LiF glass composition. According to the slope of the plot of  $\ln(\phi)$  versus  $1/T_c$  of the doped 3 wt. percent LiF glass composition, crystallization activation energy of the glass was calculated as 300 kJ/mol.

It can be seen that the activation energy of different glass composition decrease with adding of LiF content. When the LiF rate increase from 0 to 3 wt. percent, the activation energy of the glass 401 kJ/mol, 369 kJ/mol, 349 kJ/mol and 282 kJ/mol, respectively according to Kissinger method.

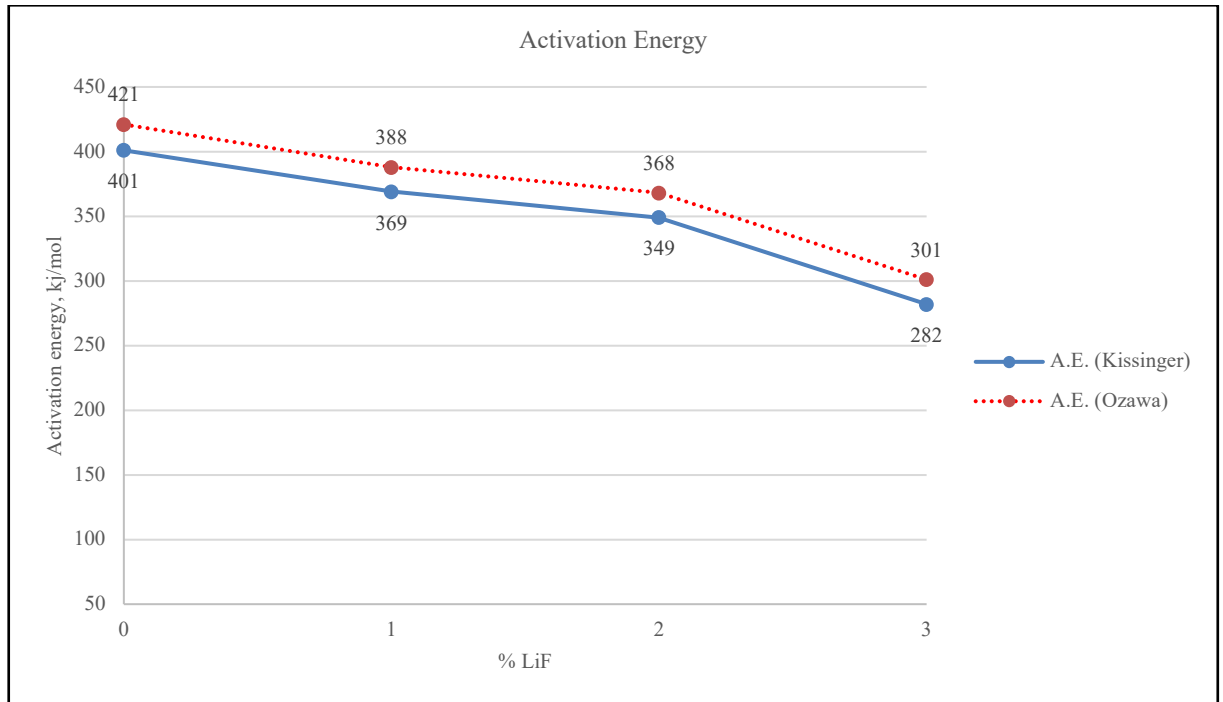


Figure 2.25. Activation energy obtained by using the method of Kissinger and Ozawa

According to Ozawa method similar to Kissinger, LiF rate effects activation energy and increasing of LiF from parent glass without LiF to doped 3 wt. percent LiF glass composition the activation energy of glasses were obtained as 421 kJ/mol, 388 kJ/mol, 368 kJ/mol and 301 kJ/mol, respectively.

Literature studies about effect of LiF on glass composition shows that LiF reduces the T<sub>g</sub> and softening temperature of glass materials. To illustrate, N. Salama S.et. al.[106] investigated crystallization characteristics of different nucleation agent including LiF on aluminosilicate glasses. It can be seen that LiF content lead to decrease of T<sub>g</sub> temperature to 585°C from 780-750°C in the Figure 2.26. They concluded that adding of 6 wt. percent LiF into the glasses decreases the temperature of both melting and beginning of crystallization.

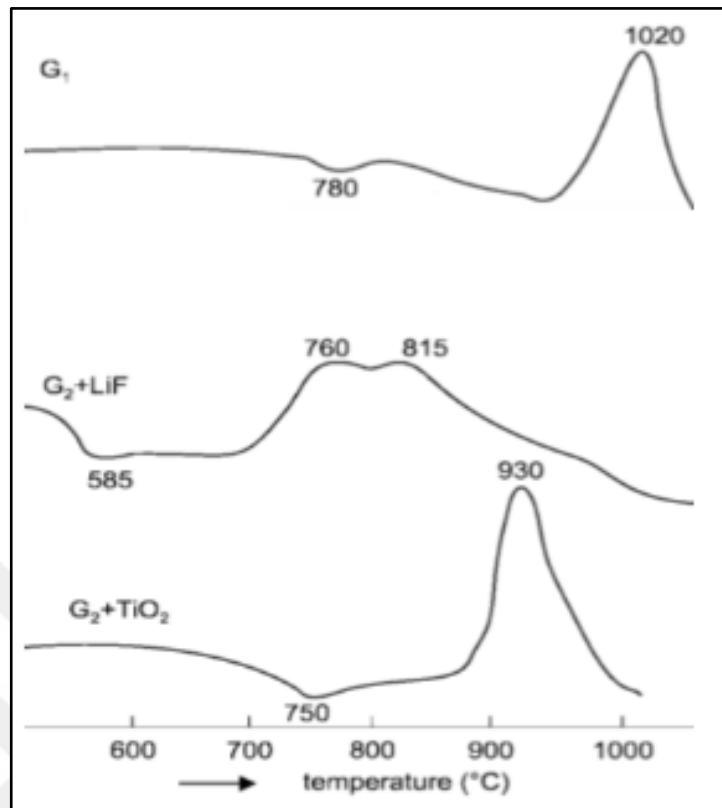


Figure 2.26. DTA curves of studied glasses by N. Salama S.et. al.[103]

As mentioned in crystallization section, Hamzawy E. and El-Meliegy E. [68] observed LiF effect in the  $\text{Na}_2\text{O}-\text{CaO}-\text{Al}_2\text{O}_3-\text{SiO}_2$  glass composition. In general, adding of LiF to such glass composition has a lowering effect on  $T_g$  (transition temperature) and  $T_s$  (softening temperature). Also, LiF acts nucleation agent in the observed of nepheline phase.

When thermal analysis of the parent glass composition and the doped 1-2-3 wt. percent LiF glass compositions results are compared with the given two different studies, it has been observed that  $T_g$  and crystallization temperature of each composition decreased. Because of the lowering of both  $T_g$  and crystallization temperature it made easier to produce glass-ceramic structure. Before the glass-ceramic production method, in order to determine the thermal expansion coefficient and dilatometer softening temperature of the glass compositions, dilatometer analysis is performed. Detail information about the dilatometer analysis is given in the next section.

### 2.3.2. Thermal Expansion Coefficient of Glass Materials

In the determination of thermal expansion coefficient of the parent glass composition and doped 1-2-3 wt. percent LiF, Netzch DIL 402C model dilatometer device shown in Figure 2.27 within TUBITAK-MRC, Institute of Materials was used. Generally, thermal expansion coefficient of a material is calculated with rate of change in volume depending on the temperature. Mathematical expression of the thermal expansion coefficient is given in the Equation 2.3.

$$\delta_v = \frac{1}{V} \left( \frac{\Delta V}{\Delta T} \right) \quad (2.3)$$

According to Eq. 2.3,  $\Delta V$  represents the change in the volume, and  $\Delta T$  denotes the temperature interval over which the sample is heated. From this given equation, a graph is created with L/Lo values representing the change in the volume in the X axis and the temperature in the Y axis.



Figure 2.27. Netzch DIL 402C model dilatometer device

Before the analysis, glass samples were cut into 5x25x10 mm with the IsoMet-Low Speed Saw device according to ISO 7991 Glass – Determination of coefficient of mean linear

thermal expansion standard. The thermal expansion analysis of the glass samples was carried out in the temperature range of 30 – 600°C with 10°C/min heating range.

Obtained thermal expansion coefficient values for each composition are given in Table 2.8.

Table 2.8. Thermal expansion coefficient of glass compositions

Temperature (°C)	Parent Glass Composition	%1 LiF	%2 LiF	%3 LiF
	Thermal expansion coefficient, 10 <sup>-6</sup> / °K	Thermal expansion coefficient, 10 <sup>-6</sup> / °K	Thermal expansion coefficient, 10 <sup>-6</sup> / °K	Thermal expansion coefficient, 10 <sup>-6</sup> / °K
50	4,6823	4,2004	5,2564	9,1923
100	4,1616	4,0809	4,7601	6,2913
150	4,1979	4,2290	4,8335	5,7152
200	4,2917	4,3935	4,9566	5,5803
250	4,3331	4,4850	5,0297	5,5076
300	4,3421	4,5329	5,0641	5,4496
350	4,3403	4,5648	5,0857	5,3960
400	4,3347	4,5813	5,1047	5,3493
450	4,3202	4,5900	5,1216	5,3104
500	4,3110	4,6032	5,1582	5,2948
550	4,3088	4,6283	5,2275	5,3106
600	4,3145	4,6768	5,3794	5,3730

Thermal expansion coefficients are generally specified based on the value in the range of 0-300°C. Therefore, thermal expansion coefficient value for the parent glass composition and doped 1-2-3 wt. percent LiF glass compositions is 4,3421x10<sup>-6</sup>/K, 4,5329 x10<sup>-6</sup>/K, 5,0641 x10<sup>-6</sup>/K, and 5,5803 x10<sup>-6</sup>/K respectively.

There are different kind of commercial display glass produced by leading glass manufacturers, Corning, SCHOTT, NIPPON. It is seen that thermal expansion of these glasses are in the range of 3,17 x10<sup>-6</sup>/°C and 7,2 x10<sup>-6</sup>/°K as given in Table 2.9. These glasses

are used in display application such as glass substrate, LCD, Active matrix display AMLCD, TFT. When the thermal expansion coefficient of parent glass and doped 1-2-3 wt. percent LiF glass compositions compared to commercial glasses, it is found that thermal expansion coefficient values that vary between  $4,3 \times 10^{-6}/K$  and  $5,1 \times 10^{-6}/K$  are in the range of thermal expansion coefficient of commercial display glasses used in display technologies.

Table 2.9. Comparison of thermal expansion values of parent glass composition and doped 1-2-3 wt. percent LiF glass compositions with commercial display glass

Description of Glass	Thermal expansion coefficient (0-300°C)
Produced with parent glass composition	$4,3 \times 10^{-6}/K$
Produced 1% wt. LiF glass	$4,5 \times 10^{-6}/K$
Produced 2% wt. LiF glass	$5,5 \times 10^{-6}/K$
Produced 3% wt. LiF glass	$5,1 \times 10^{-6}/K$
Corning Eagle XG	$3,17 \times 10^{-6}/K$
SCHOTT AF32 eco	$3,2 \times 10^{-6}/K$
NIPPON OA-10G	$3,8 \times 10^{-6}/K$
SCHOTT AF 45	$4,5 \times 10^{-6}/K$
SCHOTT D 263 T	$7,2 \times 10^{-6}/K$

Glass transition and dilatometric softening temperature can be obtained from the dilatometer curve according to ISO 7884-8 “Viscosity and viscometric fixed point of glass – Part 8: Method for the determination of (dilatometric) transition temperature” standard. The difference between the measurement methods can be observed due to the difference between measurement methods compared to the glass transition temperature and softening temperature obtained from the viscosity/optical dilatometer calculated values.

According to ISO 7884-8 standard; glass transition temperature represents the point where two different linear lines obtained from elongation-temperature curve of dilatometer analysis overlapped, and the peak temperature in the elongation-temperature curve of dilatometer analysis corresponds to the dilatometric softening temperature.

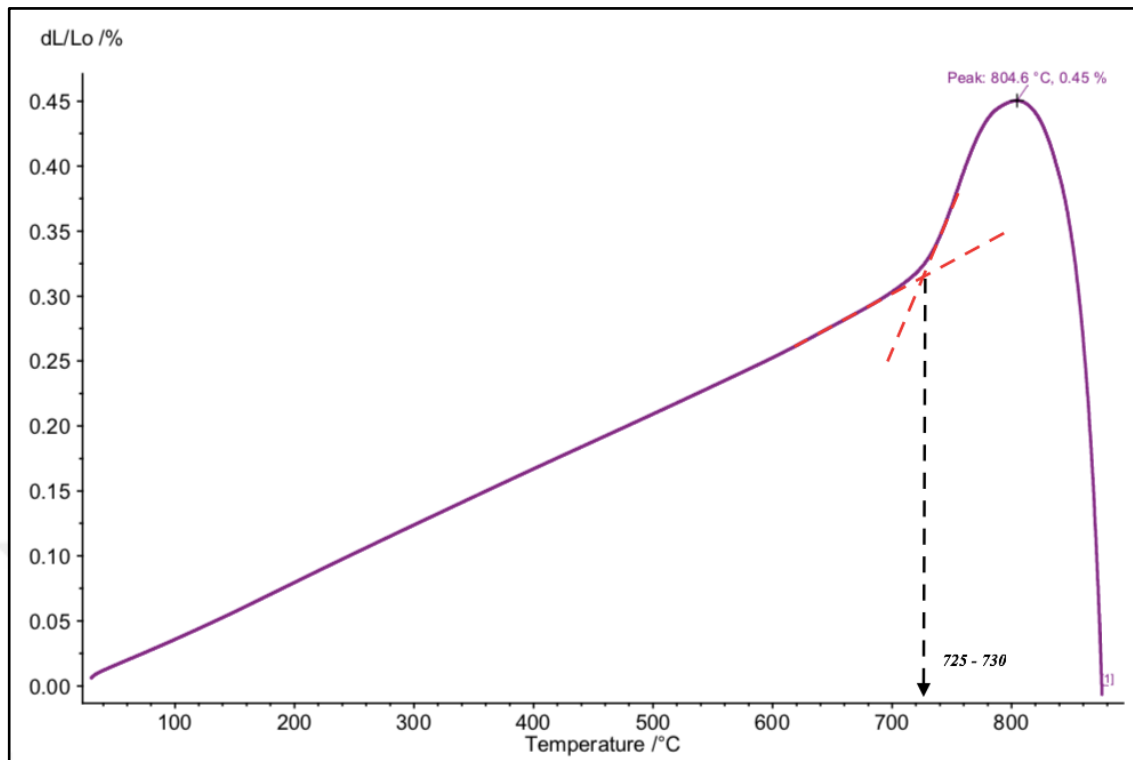


Figure 2.28. Dilatometer analysis result of the parent glass composition

For the parent glass composition,  $T_g$  temperature and dilatometer softening temperature is calculated in the range of 725-730°C and 804,6°C respectively. When the  $T_g$  temperature (740°C) calculated from DTA results compared with  $T_g$  temperature (725-730°C) obtained from dilatometer analysis, it can be seen that the results obtained for both different methods are similar in the parent glass composition.



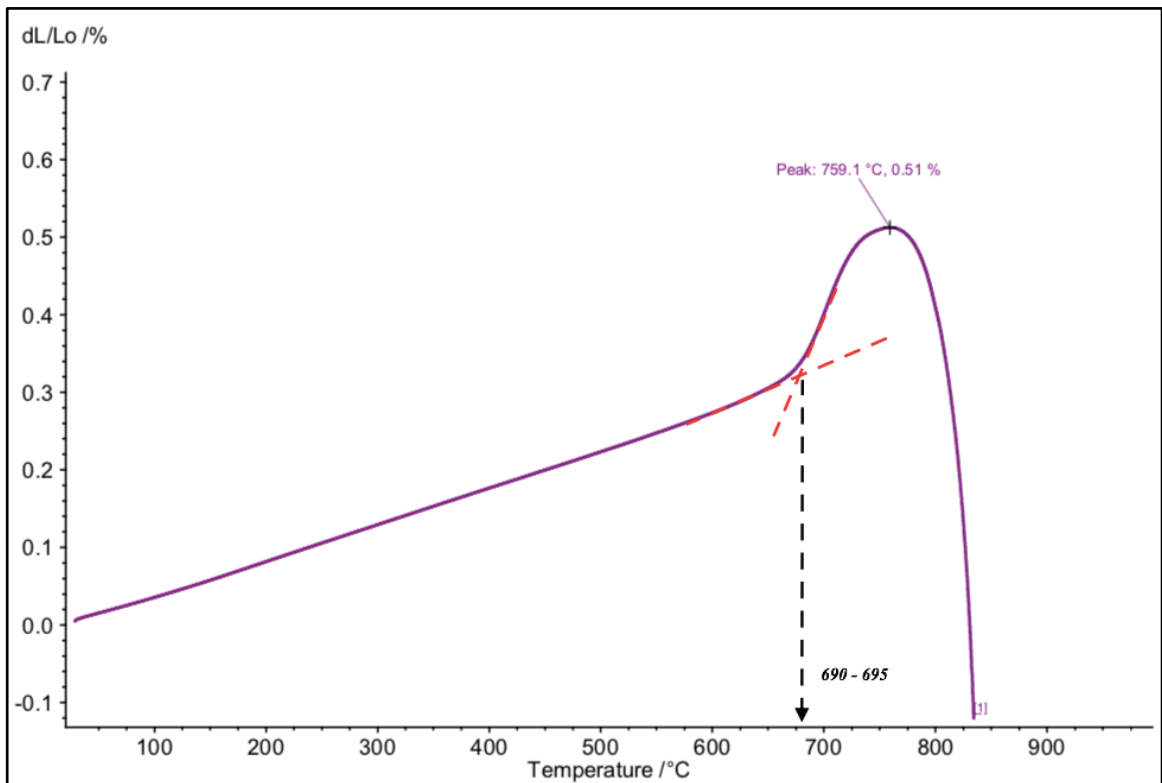


Figure 2.29. Dilatometer analysis result of the doped 1 wt. % LiF glass composition

For the doped 1 wt. % glass composition, T<sub>g</sub> temperature and dilatometer softening temperature is calculated in the range of 690-695°C and 759,1°C respectively. When the T<sub>g</sub> temperature (694°C) calculated from DTA results compared with T<sub>g</sub> temperature (690-695°C) obtained from dilatometer analysis, it can be seen that the results obtained for both different methods are similar in the doped 1 wt. % LiF glass composition.

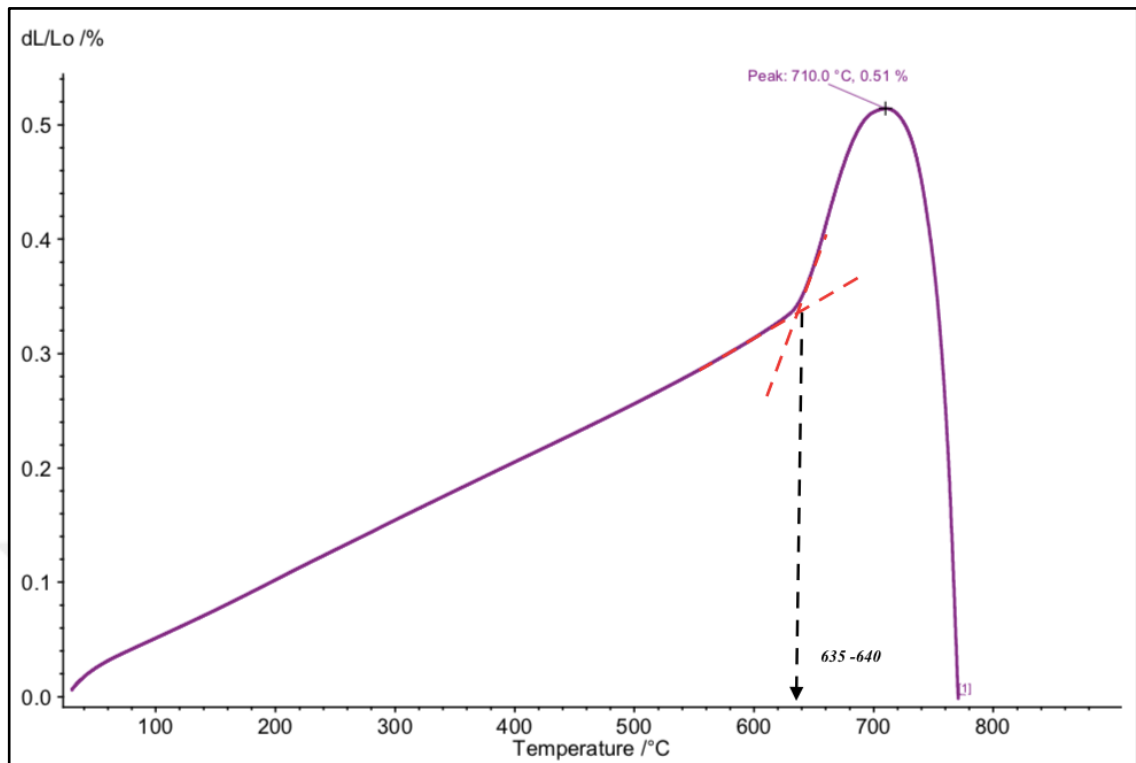


Figure 2.30. Dilatometer analysis result of the doped 2 wt. percent LiF glass composition

For the doped 2 wt. % glass composition, T<sub>g</sub> temperature and dilatometer softening temperature is calculated in the range of 635-640°C and 710°C respectively. When the T<sub>g</sub> temperature (665°C) calculated from DTA results compared with T<sub>g</sub> temperature (635-640°C) obtained from dilatometer analysis, it can be seen that the results obtained for both different methods are similar in the doped 2 wt. % LiF glass composition.

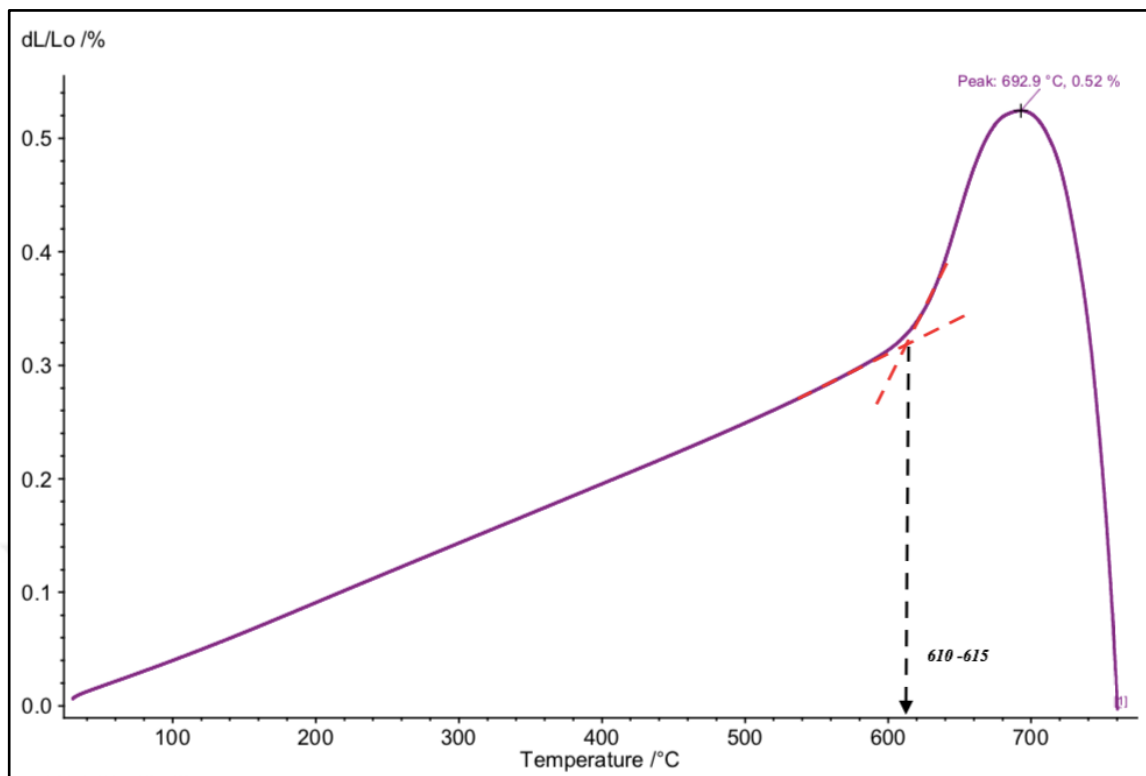


Figure 2.31. Dilatometer analysis result of the doped 3 wt. percent LiF glass composition

For the doped 3 wt. % glass composition,  $T_g$  temperature and dilatometer softening temperature is calculated in the range of 610-615°C and 692,9°C respectively. When the  $T_g$  temperature (633°C) calculated from DTA results compared with  $T_g$  temperature (610-615°C) obtained from dilatometer analysis, it can be seen that the results obtained for both different methods are similar in the doped 3 wt. % LiF glass composition.

To sum up,  $T_g$  values of each composition obtained from the DTA thermal analysis parameter was obtained at 10°C/min heating range, it can be observed that  $T_g$  values for two different methods are close each other and crystallization process of the glasses can be started with respect to these value. In addition to the  $T_g$  temperature, dilatometer softening temperature are key parameter in the crystallization process. When the glass are heated to above softening temperature, it causes to disapper of the crystals formed until the softening temperature again at this temperature. For this reason, crystallization temperature is determined by taking into account softening temperature.

Table 2.10.  $T_g$ , and dilatometer softening temperature for each composition

<b>% LiF</b>	<b><math>T_g</math>(°C) obtained from DTA analysis</b>	<b><math>T_g</math>(°C)</b>	<b>Dilatometer softening temperature</b>
%0	740	~725	804,6
%1	694	~690	759,1
%2	665	~640	710
%3	633	~610	692,9

Various methods such as DTA, DSC and dilatometry are used to determine the glass transition temperature of the materials. Among these methods, DTA or DSC methods are generally used in determining the  $T_g$  temperatures of amorphous-solid/glasses. Dilatometer analysis is used in determining the thermal expansion coefficients, which is another important feature of the glass substrate. With the dilatometry analysis, in addition thermal expansion coefficient of glass samples according to the above-mentioned principle and ISO 7884-8 standard,  $T_g$  temperature and softening temperatures values of glasses can be obtained according to ISO 7884-8 standard. Whereas bulk glasses are used for the measurements performed with the dilatometric method, the powder samples are used for the measurements performed with the DTA.

When thermal analysis of parent glass composition and doped 1-2-3 wt. percent LiF glass compositions results are compared with the given two different studies, it has been observed that  $T_g$  and crystallization temperature of each composition decreased. As mentioned in crystallization kinetic studies, adding of LiF to given glass composition has a lowering effect on  $T_g$  (transition temperature) and  $T_s$  (softening temperature). Because of the lowering of both  $T_g$  and crystallization temperature it made easier to obtain glass-ceramic structure.

Values obtained by using two different methods were close to each other, for differences between measurement results; it is thought to be caused by parameters such as heating rate, sample type analyzed (powder, bulk sample etc.).

In the section, thermal expansion coefficient of the parent glass and doped 1-2-3 wt. percent LiF glass samples was calculated. And next action is that producing of glass-ceramic materials from these glass batch.



### 3. PRODUCTION AND CHARACTERIZATION OF GLASS-CERAMIC MATERIALS

#### 3.1. PRODUCTION OF GLASS-CERAMIC MATERIALS

As stated in crystallization kinetic studies, it is necessary to know the crystallization behavior of the amorphous structure in the process of producing glass-ceramic materials with crystalline structure from amorphous glass materials. According to DTA thermal analysis method performed previous section, it was observed that the temperature of  $T_g$  and  $T_c$  varies depending on LiF content in the composition. In the study, as a first step of crystallization temperature–time was chose  $900^\circ\text{C}$  for 3 hours with heating rate of  $5^\circ\text{C}/\text{min}$  by taking into account  $928^\circ\text{C}$ ,  $888^\circ\text{C}$ ,  $846^\circ\text{C}$ ,  $812^\circ\text{C}$   $T_c$  temperature obtained DTA studies performed with  $10^\circ\text{C}/\text{min}$  heating rate for parent glass composition and doped 1 – 2 – 3 wt. percent LiF glass composition. When the crystallization method at given temperature-time regime was completed, softening in the samples was observed.

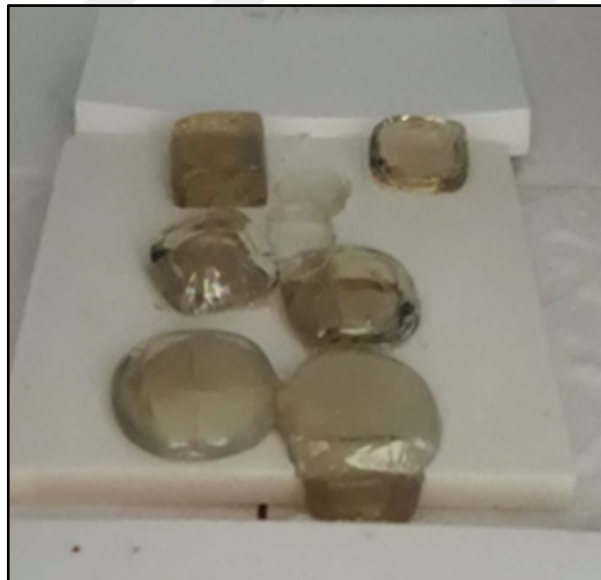


Figure 3.1. Softening of samples at  $900^\circ\text{C}$  for 3 hours

After softening of samples at  $900^\circ\text{C}$  for 3 hours, crystallization temperature was decreased to  $730^\circ\text{C}$  for 2 hours +  $830^\circ\text{C}$  for 3 hours temperature – time regime.

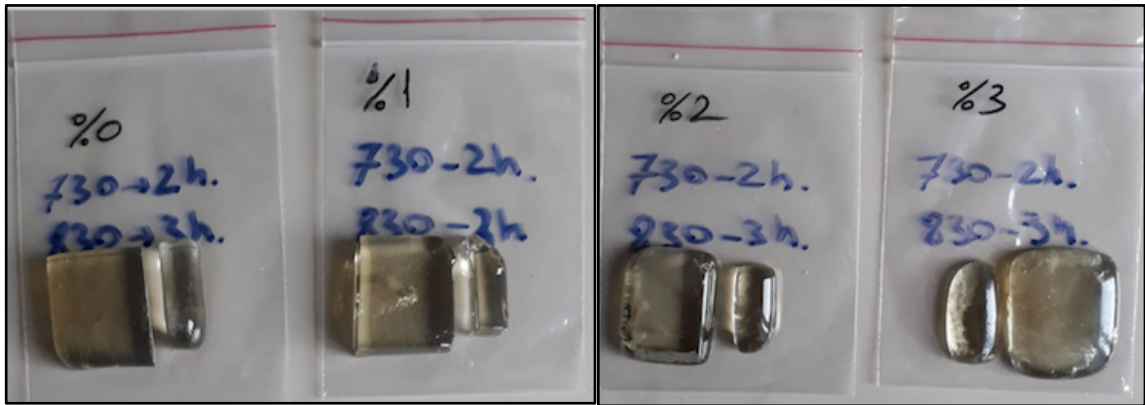


Figure 3.2. The samples nucleated at 730°C for 2h and crystallized at 830°C for 3h. Softening of the sample occurred in the 730°C 2h + 830°C 3h temperature – time regime as well. Because of softening of samples, crystallization temperature were preferred as;

- 630 2h + 640 3 – 6 – 9 – 24h,
- 680 2h + 690 3 – 6 – 9 – 24h,
- 730 2h + 740 3 – 6 – 9 – 24 - 48h,

In different temperature – time crystallization regime, in total 52 samples will be exposed to crystallization process.



Figure 3.3. Image of production process of glass-ceramics in the furnace

After the crystallization process at determined temperature–time regime, softening of samples did not occur at 730°C 2h + 740°C 24h. Since softening didn't occur at this temperature-time regime, crystallization process was applied in other regimes.

After applied the crystallization process at certain temperature-time regime without softening of samples, in order to examine properties of these samples characterizations tests will done in the next section.

### 3.1.1. X-Ray Diffraction Analysis

X-ray Diffraction (XRD) is a technique used for determining the atomic and molecular structure of a crystalline material, that the crystalline structure reflects a beam of incident XRD to diffract into many specific directions. Powder XRD is used extensively for the identification of phases by measuring the diffraction angles and intensities of these diffracted beams, and comparing the resulting diffraction pattern to a reference database of diffracted pattern.



Figure 3.4. PANalytical X'Pert PRO MPD model X-ray diffractometer analyze device

In order to detect crystalline phase and structure of the phase of the glass-ceramic materials produced at determined crystallization regime, XRD analyze method was performed with



PANalytical X'Pert PRO MPD model X-ray diffractometer device by using Cu X-ray tube ( $\lambda=1.5405$  Angstrom). First of all, in powder and bulk form of glass-ceramic materials was analyzed and no phase structure was observed. In this step, that no phase structure was observed, surface crystallization of the samples calculated from Avrami exponent was verify.

In general, phase structure of powder samples or bulk materials are analyzed with the method. Although often used as a technique to work with powders or bulk materials, thin films of deposited on surface of samples from nanometers to micrometers in thickness can be analyzed. In the thin film method with the X-Ray diffraction technology, since the angle of the incoming X-ray beam ( $0,49^\circ$ ) is lower than the angle ( $2,70^\circ$ ) used in analysis of powder and bulk samples, the penetration of X-ray beam to sample surface is diminished, so it can be analyze in between  $3\text{nm}$ - $3\mu\text{m}$  on the surface. For this reason, it was decided to make thin film analysis for each composition and crystallization regime. XRD-Thin Film analysis of the parent glass composition nucleated at  $630^\circ\text{C}$  for 2h and crystallizaed at 640 for 3h-6h-9h-24h is shown in Figure 3.5

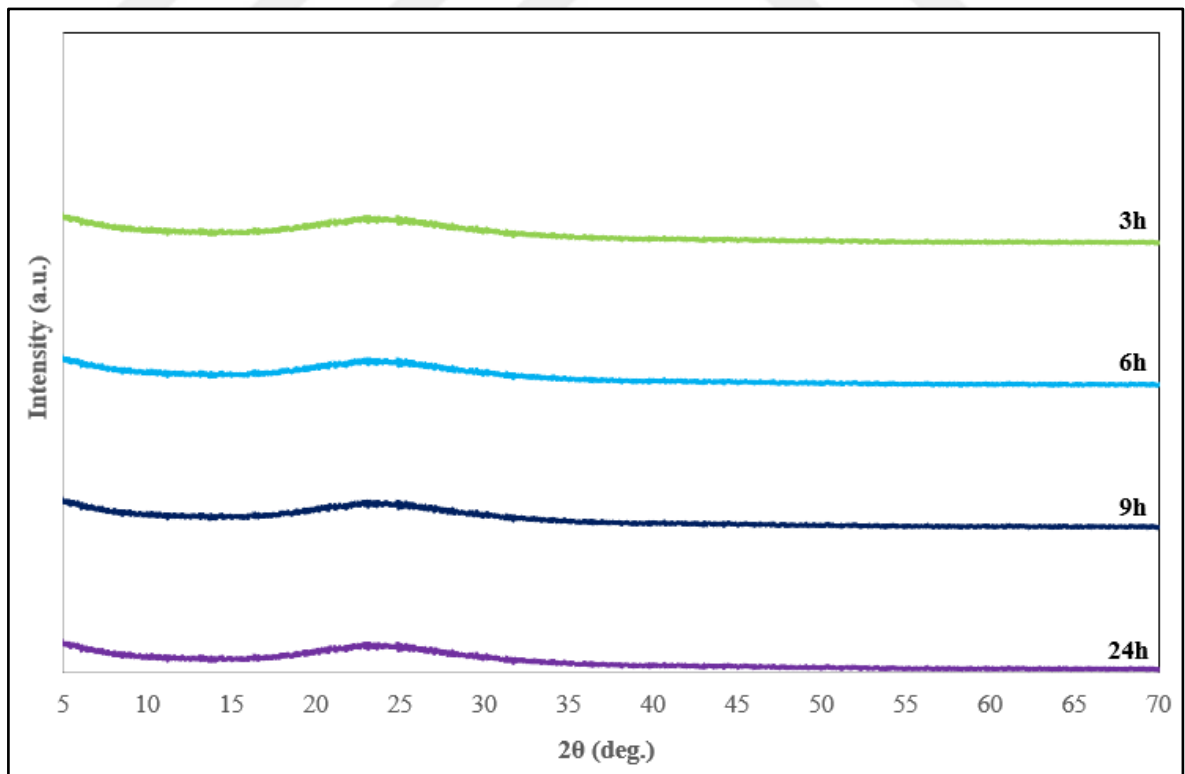


Figure 3.5. XRD-Thin Film pattern of glass compositions without LiF nucleated at  $630^\circ\text{C}$  for 2h and crystallizaed at 640 for 3h-6h-9h-24h.

The crystallization process was applied to the parent glass compositions. No crystal phase was observed in these samples as expected at crystallization regime nucleated at 630°C for 2h and crystallized at 640°C for 3h-6h-9h-24h. In Figure 3.6, XRD-Thin Film analysis of same composition nucleated at 680°C for 2h and crystallized at 690°C for 3h-6h-9h-24h is shown.

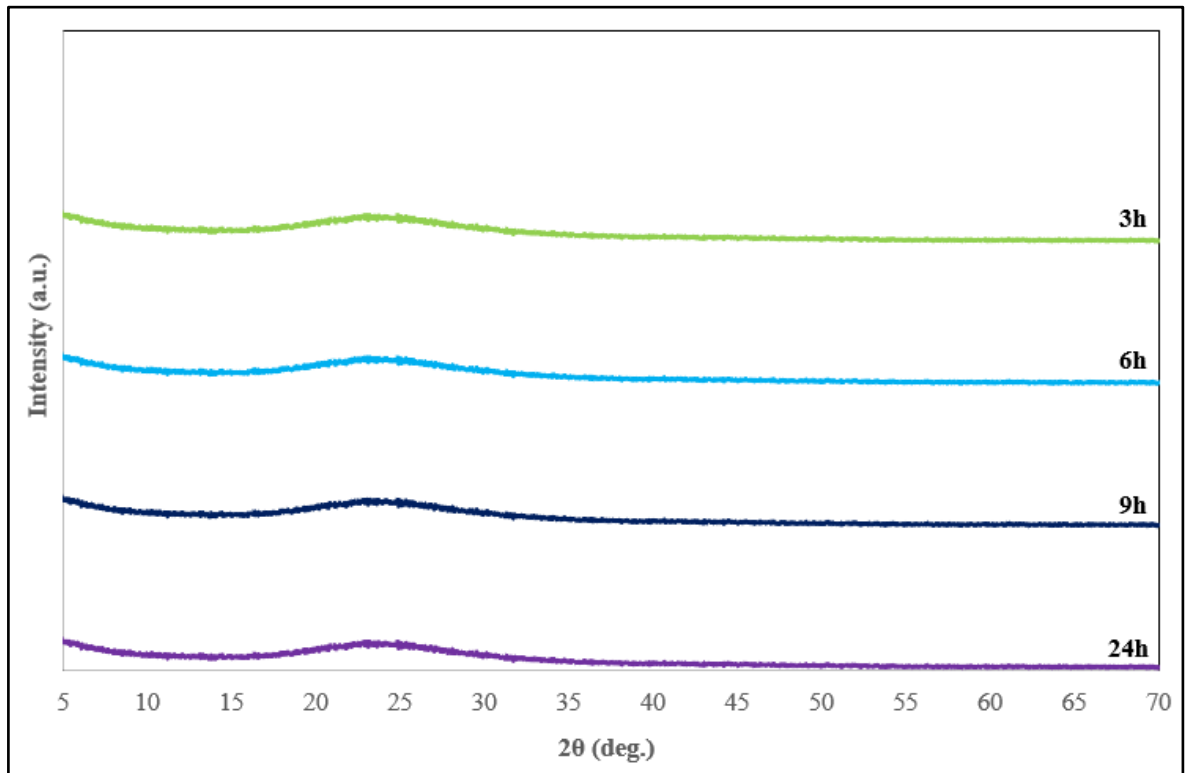


Figure 3.6. XRD-Thin Film pattern of the parent glass compositions nucleated at 680°C for 2h and crystallized at 690 for 3h-6h-9h-24h.

The crystallization process was applied to the parent glass compositions. No crystal phase was observed in these samples as expected at crystallization regime nucleated at 680°C for 2h and crystallized at 690°C for 3h-6h-9h-24h. In the next step, XRD-Thin film analysis of the parent glass compositions nucleated at 730°C for 2h and crystallized at 740°C for 3h-6h-9h-24h-48h is shown in Figure 3.7.

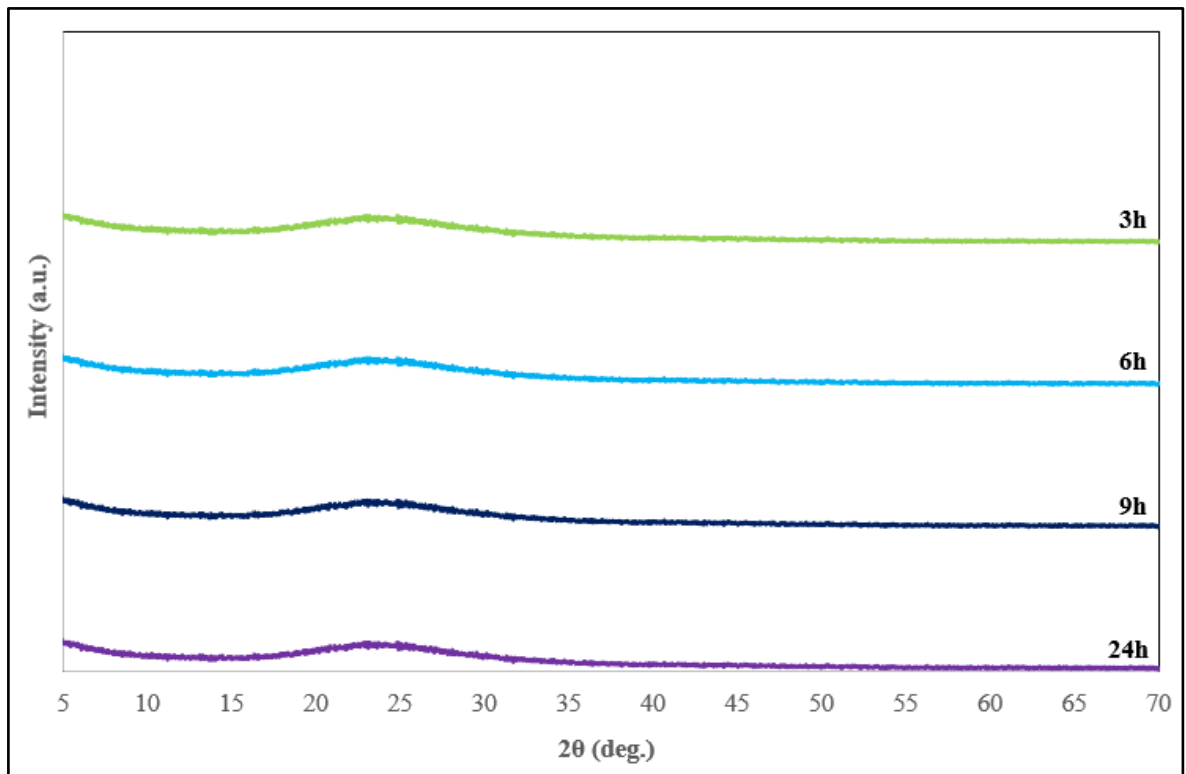


Figure 3.7. XRD-Thin Film pattern of parent glass compositions nucleated at 730°C for 2h and crystallized at 740°C for 3h-6h-9h-24h-48h.

The crystallization process was applied to the parent glass compositions. No crystal phase was observed in these samples nucleated at 730°C for 2h and crystallized at 740°C for 3h-6h-9h-24h-48h as expected due to without additive of any nucleating agent. After XRD-Thin Film of the parent glass compositions was analyzed, the analysis of glass compositions doped 1 wt. percent LiF was started. Analysis results of these compositions at each crystallization regime will be given in following. Next action is XRD-Thin film analysis of doped 1wt. percent LiF glass composition at different crystallization regime. In Figure 3.8, XRD-Thin Film analysis of glass compositions doped 1 wt. percent LiF nucleated at 630°C for 2h and crystallized at 640 for 3h-6h-9h-24h is shown.

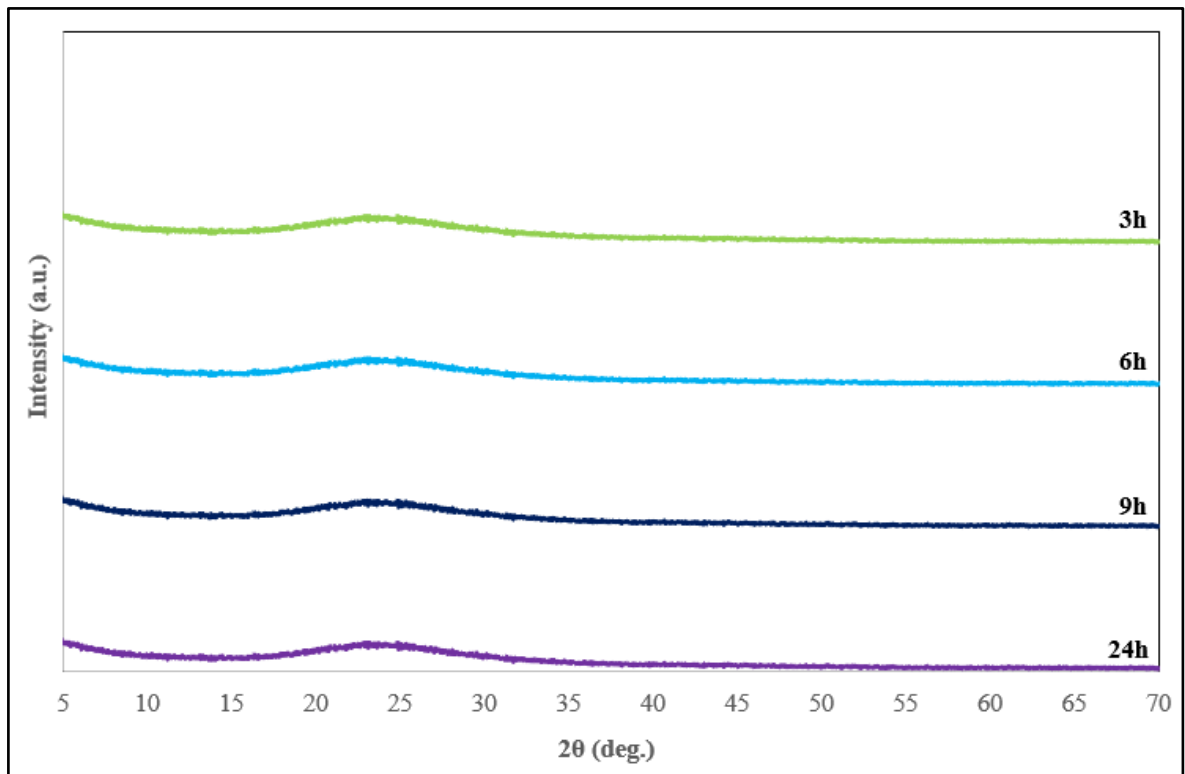


Figure 3.8. XRD-Thin Film pattern of glass compositions doped 1 wt. percent LiF nucleated at 630°C for 2h and crystallized at 640 for 3h-6h-9h-24h.

As a results of XRD-Thin Film analysis of the doped 1 wt. percent LiF glass compositions nucleated at 630°C for 2h and crystallizaed at 640°C for 3h-6h-9h-24h, no any crystal structure was detected. According to the results, it has been concluded that applied crystallization regime for the doped 1wt. percent LiF glass compositions is not sufficient to create a crystalline structure. And then, as shown in Figure 3.9, XRD-Thin Film analysis of the glass compositions doped 1 wt. percent LiF glass compositions nucleated at 680°C for 2h and crystallizaed at 690°C for 3h-6h-9h-24h was performed respectively.

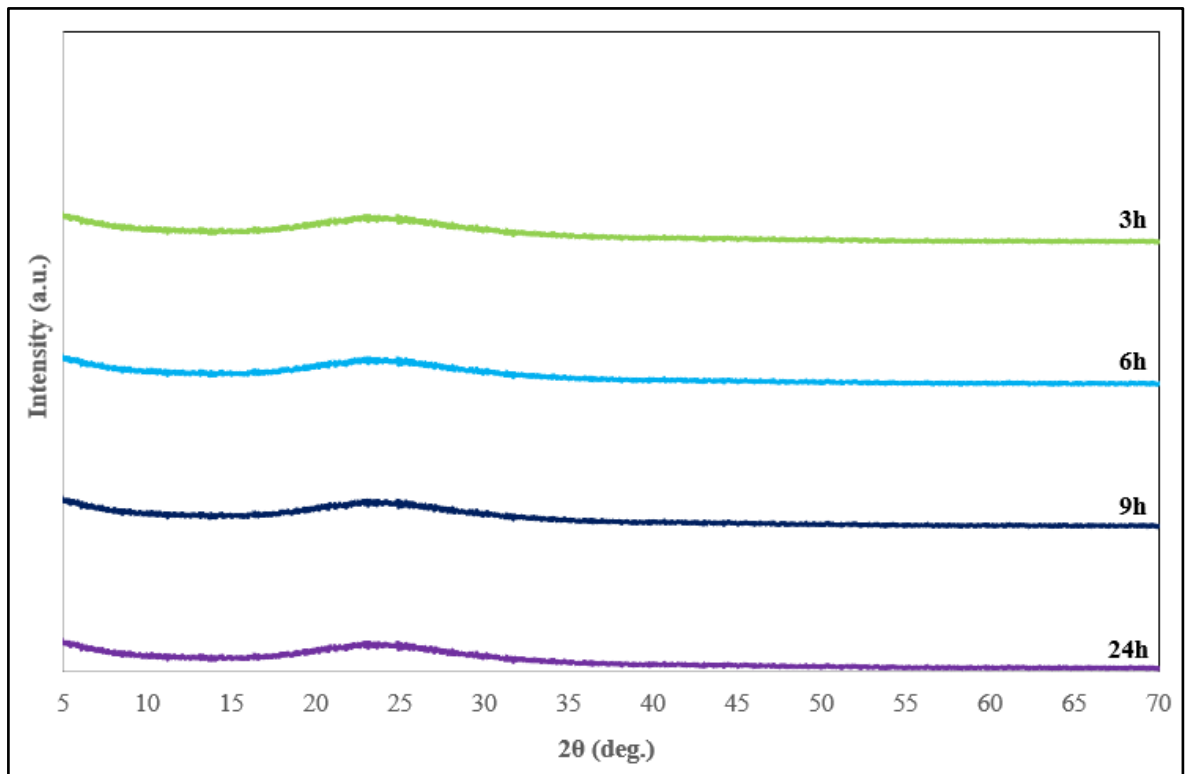


Figure 3.9. XRD-Thin Film pattern of doped 1 wt. percent LiF glass compositions nucleated at 680°C for 2h and crystallized at 690°C for 3h-6h-9h-24h.

When the examined of XRD-Thin Film analysis of the doped 1 wt. percent LiF glass compositions nucleated at 680°C for 2h and crystallized at 690°C for 3h-6h-9h-24h, no any crystal structure was detected. As a results of, it has been concluded that applied crystallization regime for the doped 1 wt. percent LiF glass compositions is not sufficient to create a crystalline structure like in previous one. Finally, XRD-Thin Film analysis for doped 1 wt. percent LiF glass compositions nucleated at 730°C for 2h and crystallized at 740°C for 3h-6h-9h-24h-48h was performed respectively.

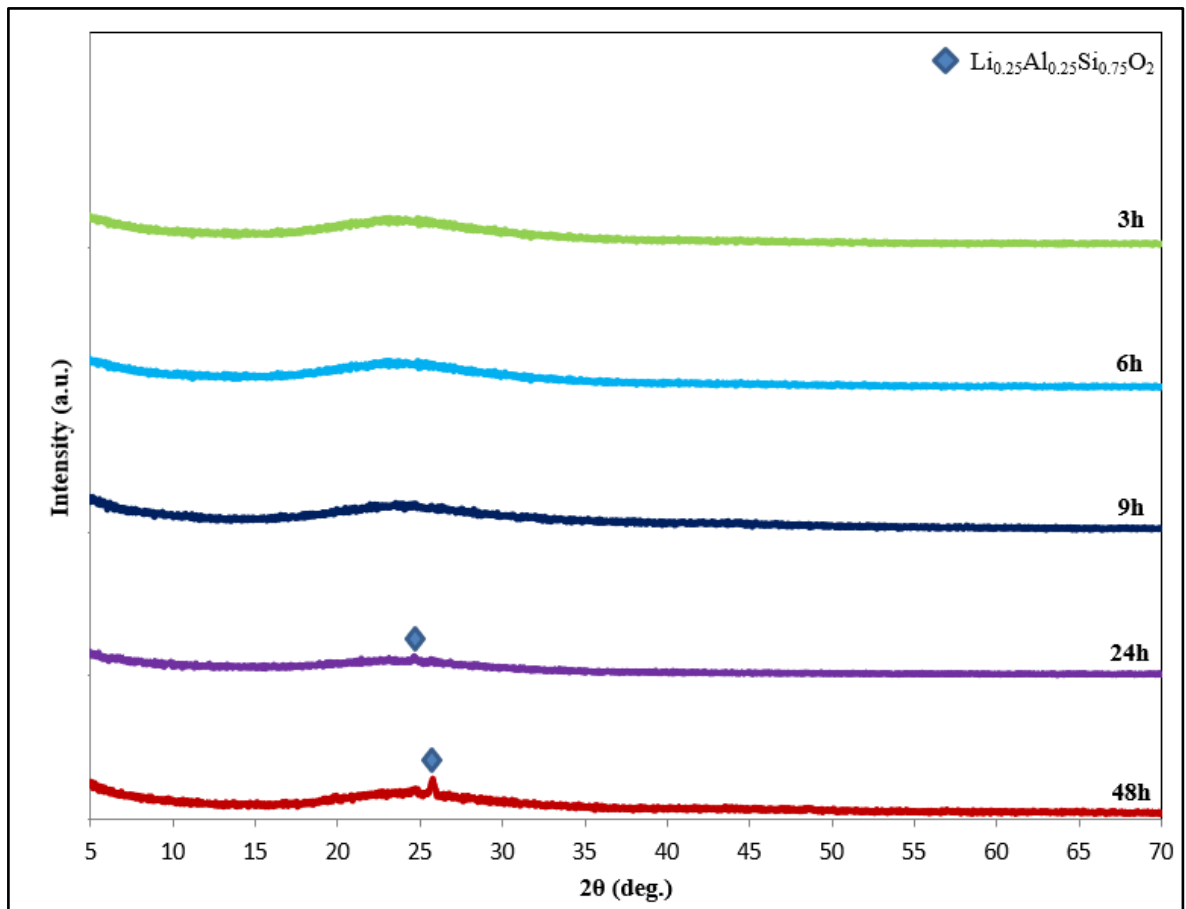


Figure 3.10. XRD-Thin Film pattern of doped 1 wt. percent LiF glass compositions nucleated at  $730^\circ\text{C}$  for 2h and crystallized at  $740^\circ\text{C}$  for 3h-6h-9h-24h-48h.

In the XRD-Thin Film analysis results of doped 1 wt. percent LiF glass compositions nucleated at  $730^\circ\text{C}$  for 2h and crystallized at  $740^\circ\text{C}$  for 3h-6h-9h-24h-48h, no any crystalline structure was detected at crystallization regime nucleated at  $730^\circ\text{C}$  for 2h and crystallized at  $740^\circ\text{C}$  for 3h-6h-9h. When the crystallization time is increased to 24h, it was found that the peak detected at  $2\theta=25.743$  corresponds to (101) plane of  $\text{Li}_{0.25}\text{Al}_{0.25}\text{Si}_{0.75}\text{O}_2$ -Ecryptite (KKD 04-018-8284). After the peak was detected at crystallization regime nucleated at  $730^\circ\text{C}$  for 2h and crystallized at  $740^\circ\text{C}$  for 24h. The crystallization time was increased to 48 hours from 24 hours, increasing in the intensity of peak was detected. As a conclusion, crystalline structure was observed at crystallization regime nucleated at  $730^\circ\text{C}$  for 2h and crystallized at  $740^\circ\text{C}$  for 24h-48h for doped 1 wt. percent LiF glass compositions. After completed XRD-Thin Film analysis of the doped 1 wt. percent LiF compositions, next step is analysis of doped 2 wt. percent LiF glass compositions. XRD-Thin Film analysis of

glass compositions doped 2 wt. percent LiF glass compositions nucleated at 630°C for 2h and crystallized at 640 for 3h-6h-9h-24h is shown in Figure 3.11.

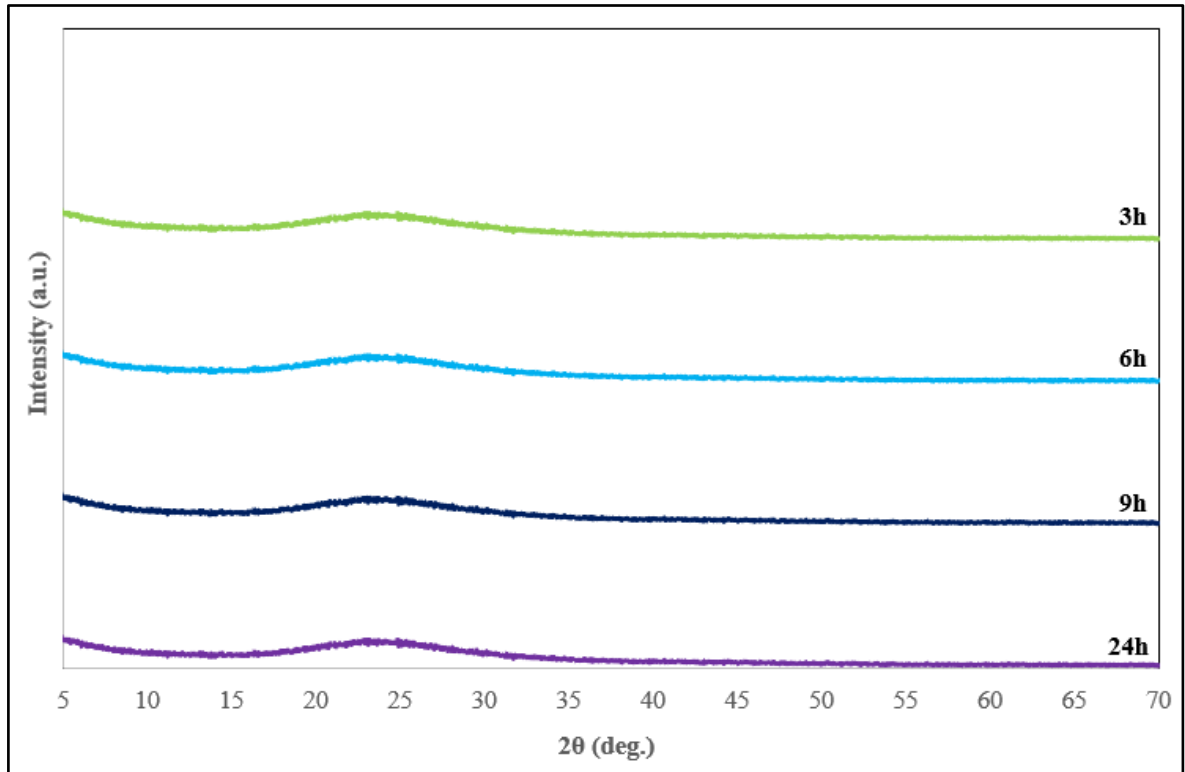


Figure 3.11. XRD-Thin Film pattern of doped 2wt. percent LiF glass compositions nucleated at 630°C for 2h and crystallized at 640 for 3h-6h-9h-24h.

According to XRD-Thin Film analysis of the doped 2 wt. percent LiF glass compositions nucleated at 630°C for 2h and crystallized at 640°C for 3h-6h-9h-24h, no any crystal structure was detected. It has been concluded that applied crystallization regime for the doped 2 wt. percent LiF glass compositions is not sufficient to create a crystalline structure.

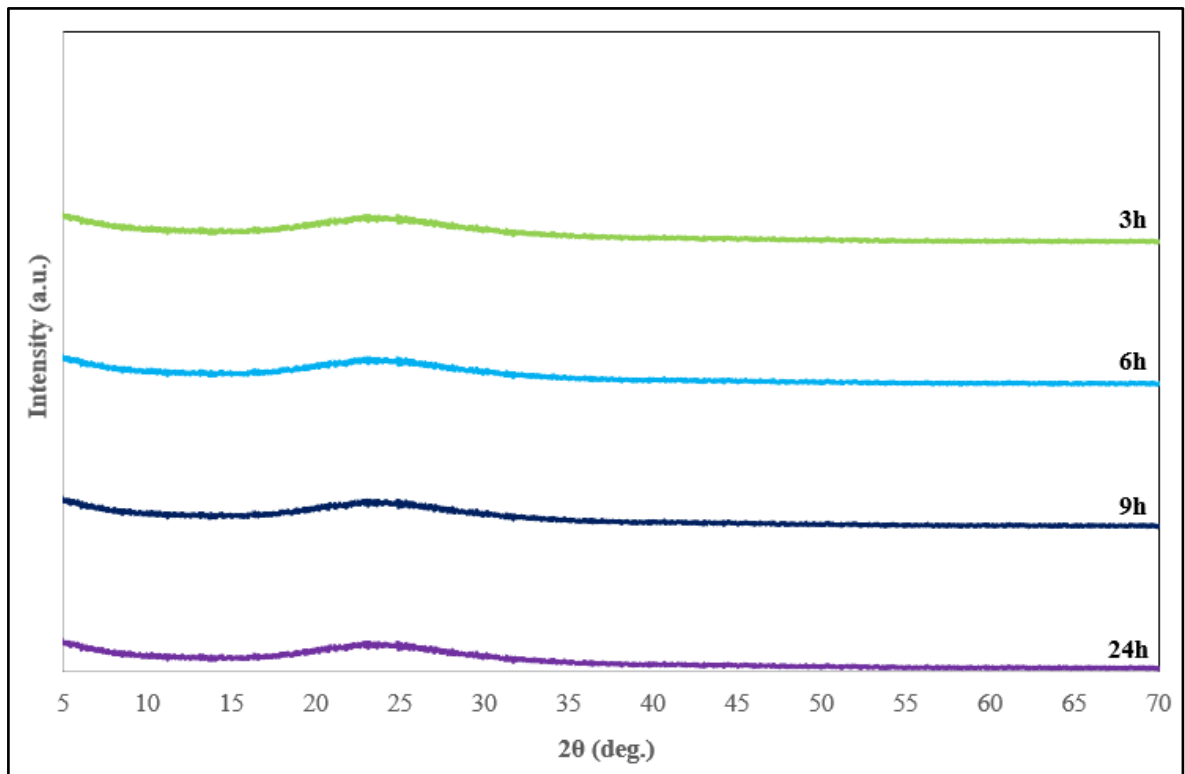


Figure 3.12. XRD-Thin Film pattern of doped 2 wt. percent LiF glass compositions nucleated at 680°C for 2h and crystallized at 690°C for 3h-6h-9h-24h.

When the examined of XRD-Thin Film analysis of the doped 2 wt. percent LiF glass compositions nucleated at 680°C for 2h and crystallized at 690°C for 3h-6h-9h-24h, no any crystal structure was detected. As a conclusion, it is found that applied crystallization regime for the doped 2 wt. percent LiF glass compositions is not sufficient to create a crystalline structure. The next action is XRD-Thin analysis of the doped 2 wt. percent LiF glass compositions nucleated at 730°C for 2h and crystallized at 740°C for 3h-6h-9h-24h-48h.



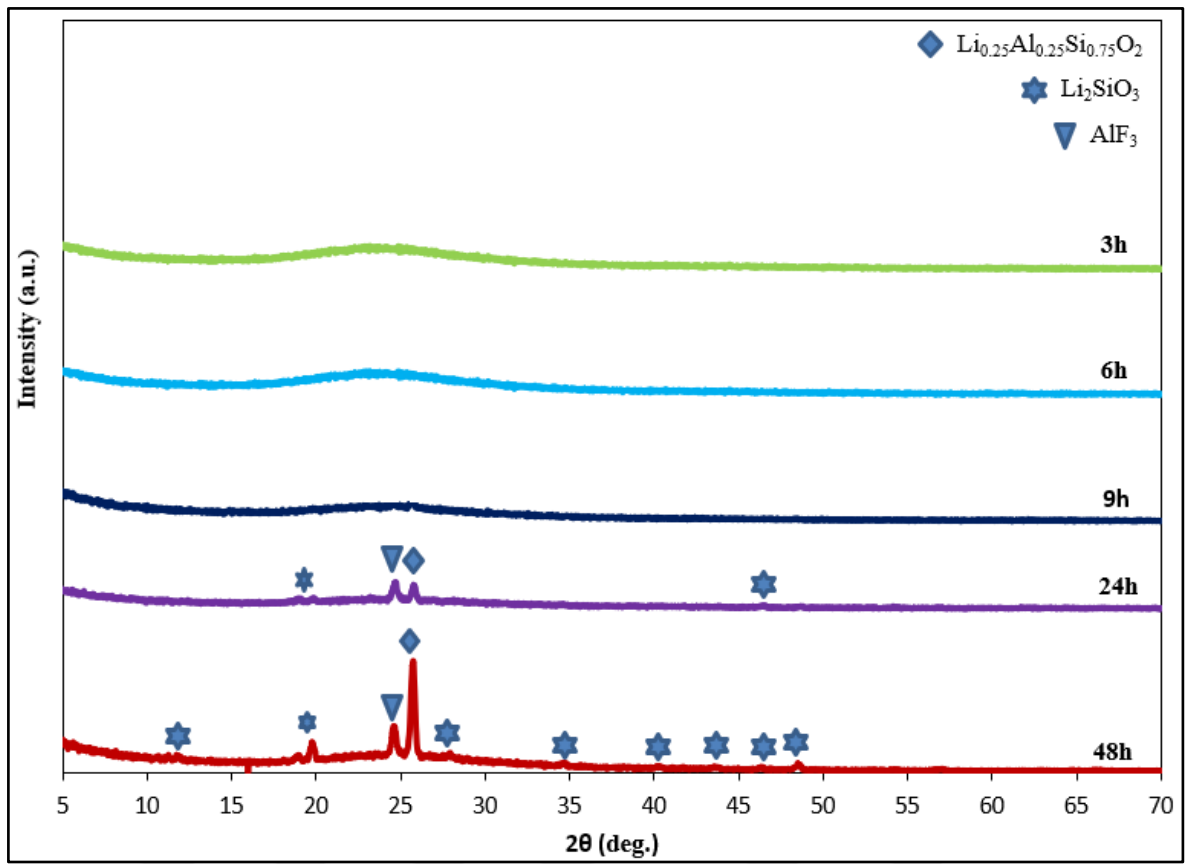


Figure 3.13. XRD-Thin Film pattern of the doped 2 wt. percent LiF glass compositions nucleated at  $730^\circ\text{C}$  for 2h and crystallized at  $740^\circ\text{C}$  for 3h-6h-9h-24h-48h.

When the examined of XRD-Thin Film analysis of the doped 2 wt. percent LiF glass compositions nucleated at  $730^\circ\text{C}$  for 2h and crystallized at  $740^\circ\text{C}$  for 3h-6h-9h-24h-48h, no any crystal structure was detected at crystallization regime nucleated at  $730^\circ\text{C}$  for 2h and crystallized at  $740^\circ\text{C}$  for 3h-6h. When the crystallization time is extended to 9h, it is found that the peak detected at  $2\theta=25.743^\circ$  corresponds to (101) plane of  $\text{Li}_{0.25}\text{Al}_{0.25}\text{Si}_{0.75}\text{O}_2$ -Ecryptite (KKD 04-018-8284). When the crystallization time is 24h, intensity of peak detected at  $2\theta=25.743^\circ$  increased. Besides, a new peak at  $2\theta=24.663^\circ$  corresponds to (100) plane of  $\text{AlF}_3$  (KKD 01-081-8082) was appeared. In addition the these two peaks,  $2\theta=18.87^\circ$  and  $2\theta=46.13^\circ$  corresponds to (101) plane of  $\text{Li}_2\text{SiO}_3$  was observed. When crystallization time reached to 48h, no new phase appeared and it is seen that increasing of intensity of peaks corresponding to  $\text{Li}_{0.25}\text{Al}_{0.25}\text{Si}_{0.75}\text{O}_2$ -Ecryptite,  $\text{AlF}_3$ , and  $\text{Li}_2\text{SiO}_3$  was observed. In Figure 3.14, XRD-Thin Film analysis result of the doped 3 wt. percent LiF glass compositions nucleated at  $630^\circ\text{C}$  for 2h and crystallized at  $640^\circ\text{C}$  for 3h-6h-9h-24h is shown.

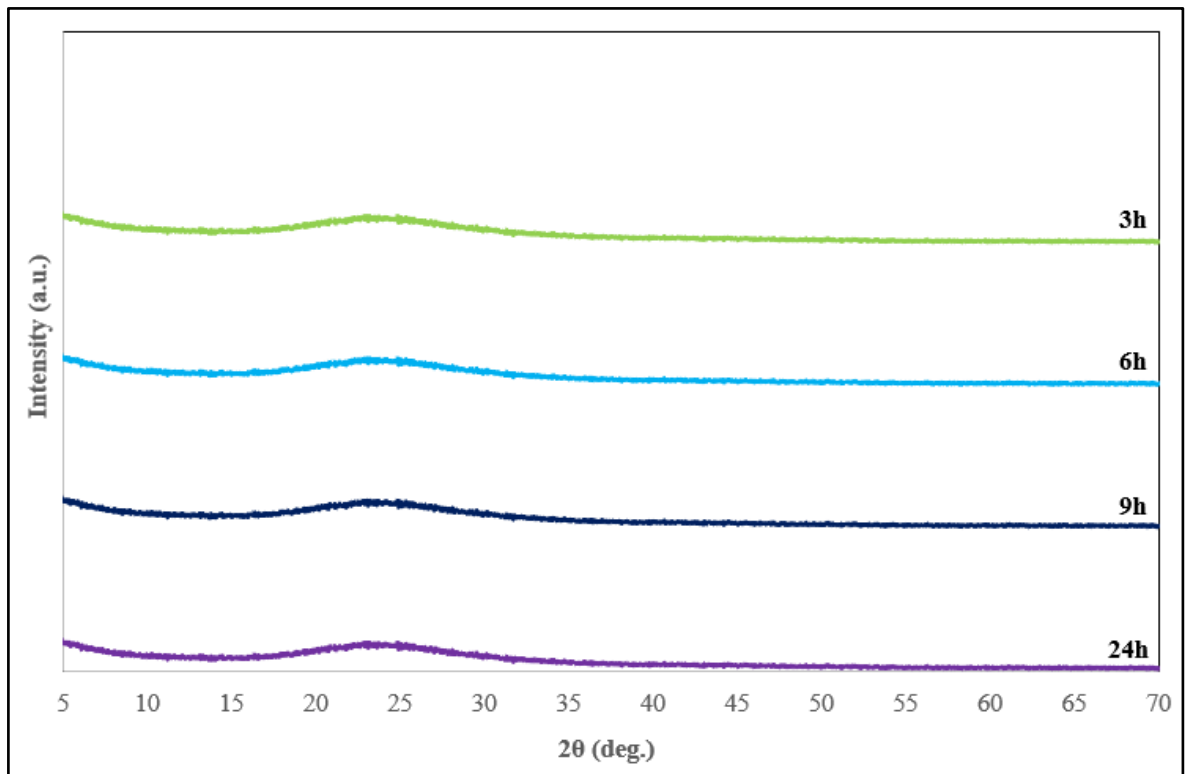


Figure 3.14. XRD-Thin Film pattern of doped 3 wt. percent LiF glass compositions nucleated at  $630^\circ\text{C}$  for 2h and crystallized at  $640^\circ\text{C}$  for 3h-6h-9h-24h.

When the examined of XRD-Thin Film analysis of the doped 3 wt. percent LiF glass compositions nucleated at  $630^\circ\text{C}$  for 2h and crystallized at  $640^\circ\text{C}$  for 3h-6h-9h-24h, no any crystal structure was detected. As a results of, it has been concluded that applied crystallization regime for the doped 3 wt. percent LiF glass compositions is not sufficient to create a crystalline structure.

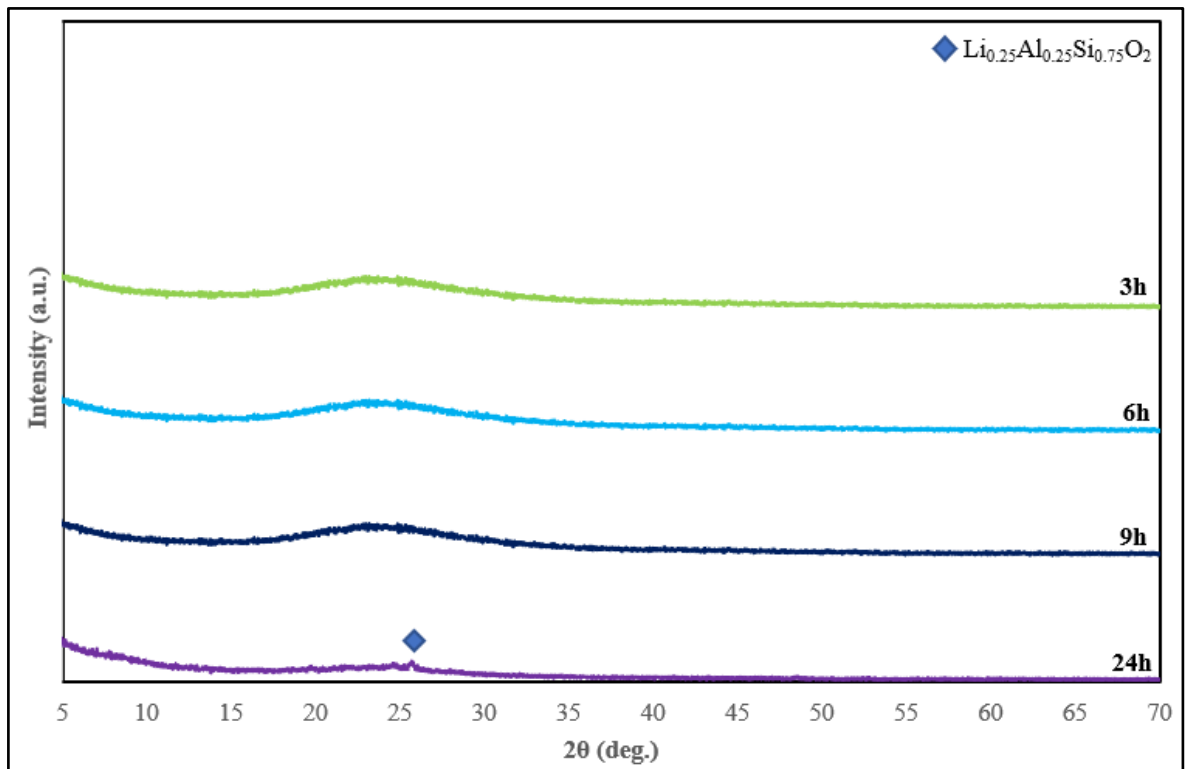


Figure 3.15. XRD-Thin Film pattern of doped 3 wt. percent LiF glass compositions nucleated at 680°C for 2h and crystallized at 690°C for 3h-6h-9h-24h.

When the examined of XRD-Thin Film analysis of doped 3 wt. percent LiF glass compositions nucleated at 680°C for 2h and crystallized at 690°C for 3h-6h-9h, no any crystal structure was detected. When the crystallization time reached to 24h, a new phase was detected at  $2\theta = 25.743^\circ$  corresponds to (101) plane of  $\text{Li}_{0.25}\text{Al}_{0.25}\text{Si}_{0.75}\text{O}_2$ -Ecryptite (KCD 04-018-8284). In the doped 3 wt. percent LiF compositions as lastly action is XRD-Thin Film analysis of the doped 3 wt. percent LiF glass compositions nucleated at 730°C for 2h and crystallized at 740°C for 3h-6h-9h-24h-48h and result of the analysis is shown in Figure 3.16.

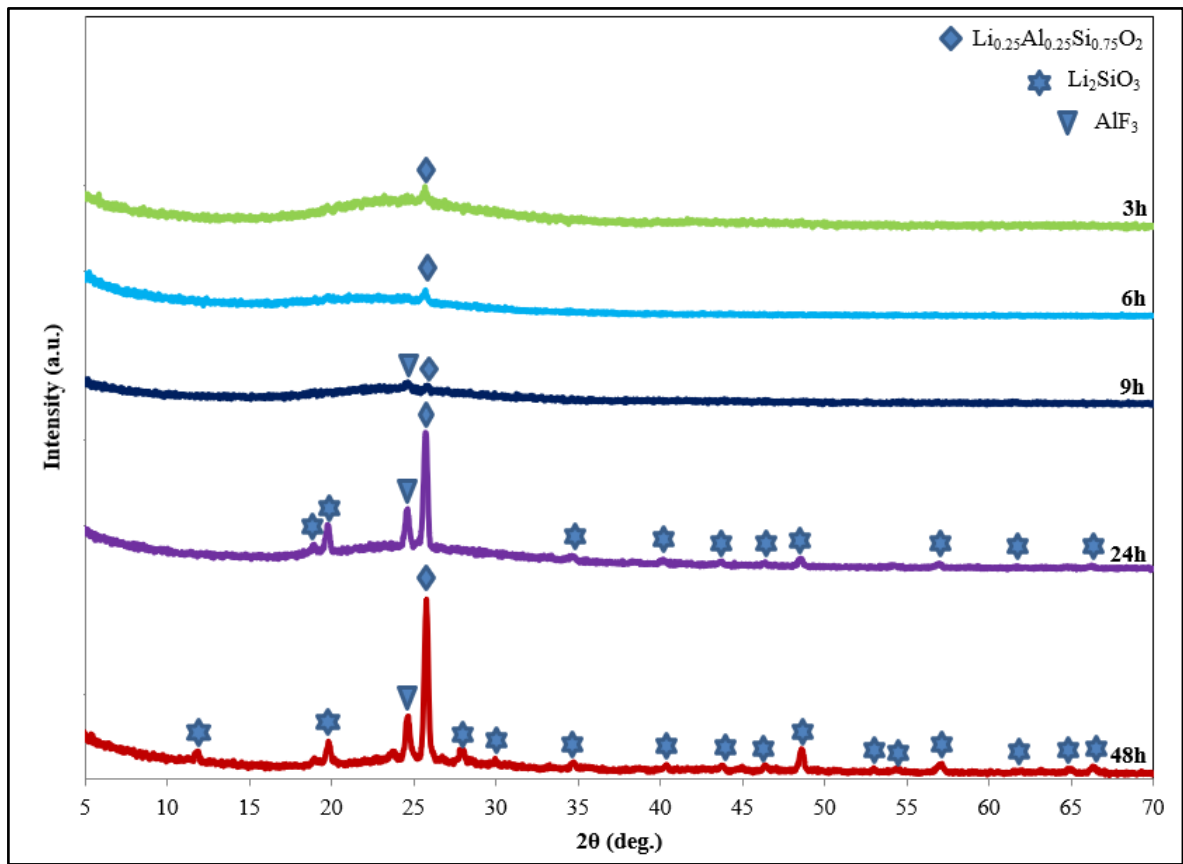


Figure 3.16. XRD-Thin Film pattern of doped 3 wt. percent LiF glass compositions nucleated at 730°C for 2h and crystallized at 740°C for 3h-6h-9h-24h-48h.

When the examined of XRD-Thin Film analysis of doped 3 wt. percent LiF glass compositions nucleated at 730°C for 2h and crystallized at 740°C for 3h-6h-9h-24h-48h, in the crystallization regime nucleated at 730°C for 2h and crystallized at 740°C for 3h, the peak detected at  $2\theta=25.743^\circ$  corresponds to (101) plane of  $\text{Li}_{0.25}\text{Al}_{0.25}\text{Si}_{0.75}\text{O}_2$ -Ecryptite (KKD 04-018-8284). When the crystallization regime is increased to 6h,  $\text{Li}_{0.25}\text{Al}_{0.25}\text{Si}_{0.75}\text{O}_2$ -Ecryptite phase continue to expand. And at 740°C for 9h, a new phase at  $2\theta=24.663^\circ$  corresponds to (100) plane of  $\text{AlF}_3$  (KKD 01-081-8082) was appeared. Beside, these two phase  $2\theta=18.87^\circ$  and  $2\theta=46.13^\circ$  corresponds to (101) plane of  $\text{Li}_2\text{SiO}_3$  was observed at 740°C for 24h. When crystallization time reached to 48h, no new phase appeared and it is seen that expanding of intensity of peaks corresponding to  $\text{Li}_{0.25}\text{Al}_{0.25}\text{Si}_{0.75}\text{O}_2$ -Ecryptite,  $\text{AlF}_3$ , and  $\text{Li}_2\text{SiO}_3$  was observed.

As a results of XRD-Thin Film analysis, it is seen that the formation of  $\text{Li}_{0.25}\text{Al}_{0.25}\text{Si}_{0.75}\text{O}_2$ -Ecryptite,  $\text{AlF}_3$  and  $\text{Li}_2\text{SiO}_3$  in the given compositions varies depending on the crystallization temperature-time and LiF content. To clarify, no any phase was detected at without added

LiF glass compositions. After the adding of 1 wt. percent LiF to glass compositions, a new phase ( $\text{Li}_{0,25}\text{Al}_{0,25}\text{Si}_{0,75}\text{O}_2$ ) was detected at crystallization regime crystallized at  $740^\circ\text{C}$  for 24h and 48h. When the LiF content was increased to 2 wt. percent from 1wt. percent in the glass composition, formation temperature of  $\text{Li}_{0,25}\text{Al}_{0,25}\text{Si}_{0,75}\text{O}_2$  phase decreased to 9h. And, at the  $740^\circ\text{C}$  for 24h the  $\text{Li}_{0,25}\text{Al}_{0,25}\text{Si}_{0,75}\text{O}_2$ ,  $\text{AlF}_3$  phase appeared as well. At this composition crystallized at  $740^\circ\text{C}$  for 48h,  $\text{Li}_2\text{SiO}_3$  was detected in addition to other phases. In composition doped with 3 wt. percent LiF, temperature and time formation of the  $\text{Li}_{0,25}\text{Al}_{0,25}\text{Si}_{0,75}\text{O}_2$  decreased to 3 hours at  $740^\circ\text{C}$  crystallization temperature. In parallel with the increasing of the crystallization time, intensity of formed  $\text{Li}_{0,25}\text{Al}_{0,25}\text{Si}_{0,75}\text{O}_2$  phase increased and  $\text{AlF}_3$  phase started to appear at 9 hours. When the crystallization time reached to 24 hours,  $\text{Li}_2\text{SiO}_3$  was detected with other  $\text{Li}_{0,25}\text{Al}_{0,25}\text{Si}_{0,75}\text{O}_2$ ,  $\text{AlF}_3$ . To sum up, LiF reduced the formation of crystallization temperature and time at the determined glass compositions. Also, Guo X. [62] and Gawronski A. [63] investigated crystalline phase in their studies, they put forward that crystallization regime affects the formation of crystalline phase in glass structure, and observed crystalline phase based on increasing crystallization time and temperature intensively.

### 3.1.2. Optical Microscope Analysis

After XRD – Thin Film analysis, crystal observed samples were examined on OLYMPUS BX53M model optical microscope device.



Figure 3.17. OLYMPUS-BX53M optical microscope device

Before the analysis of samples under the optical microscope, taken bakelite process of samples is necessary. Due to the fragile properties of glasses, cold bakelite is generally preferred. After the cold bakelite process, samples are grinded, polished, lastly prepared for etching at certain time and with chemical solution.

In the cold bakelite process, Epoxy Resin, Epoxy Hardener, Silicon – Spray AK providing removal of samples from mold easily, cold bakelite mold compatible with polishing device, and mixing bowl are used.



Figure 3.18. Materials used in preparing cold bakelite process

Cold bakelite solution used in study is prepared by mixing Epoxy Hardener and Epoxy Resin at 1:2 ratio. For the cold bakelite process of each sample, 12.5 g of Epoxy Resin and 6.25 g of Epoxy Hardener are weighed at analytical balance and poured into mixing bowl. After mixing of the solution in the mixing bowl without creating bubbles, the solution is ready to use.

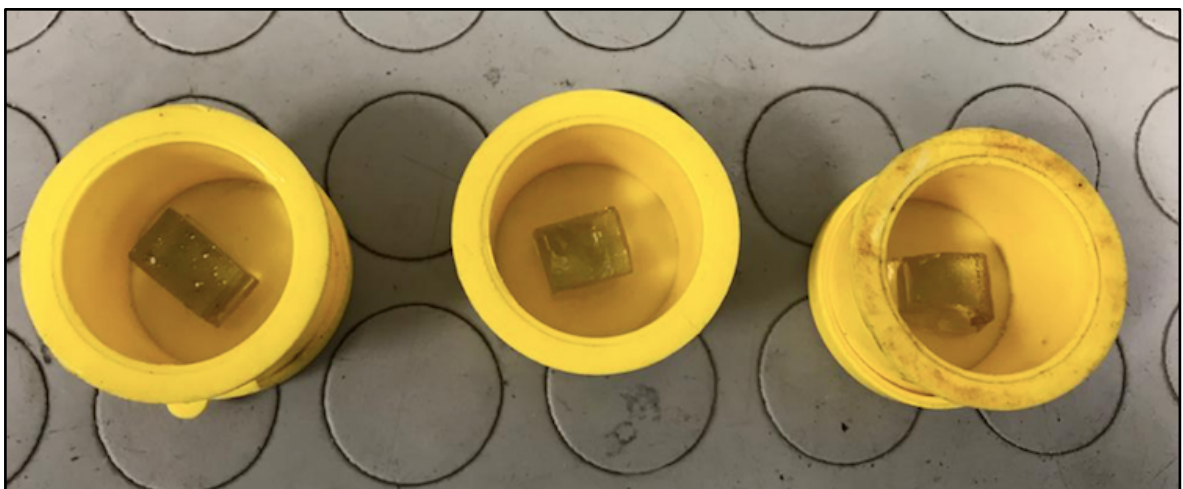


Figure 3.19. Samples placed on cold bakelite molds

In the process of placing of samples in bakelite molds, the surface to be analyzed should be placed in contact with bottom surface of the bakelite mold. After the mold is properly placed in the mold, the prepared solution is poured into the mold to fill it completely, and then waiting for 8 hours for the hardening process to be completed, the samples are ready.

Grinding of process of the samples was started by using 120 mesh sandpaper, and the surface of the samples which will be analyzed was grinded for approximately 3 minutes by using 240 – 320 – 400 – 600 – 800 – 1000 – 1200 – 2500 mesh sandpaper respectively in METKON GRIPO 1V Grinder – Polisher device.



Figure 3.20. Grinding process with METKON GRIPO 1V device

After the grinding process completed, polishing is done by applying 25N load on the samples, at 50 rpm, and using 0.3 micron grain size  $\text{Al}_2\text{O}_3$  with ATA SAPHIR 530 polishing device for 10 minutes.



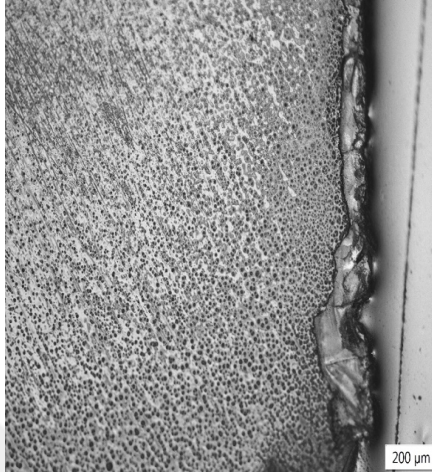
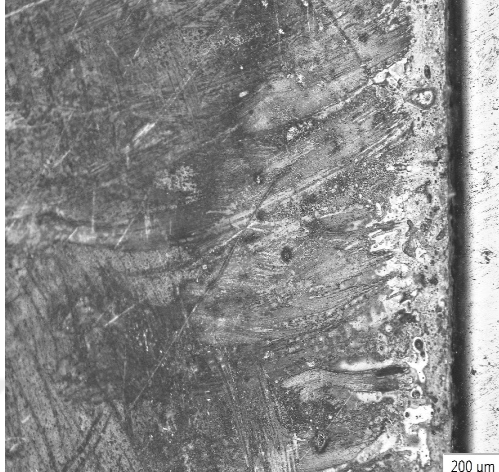
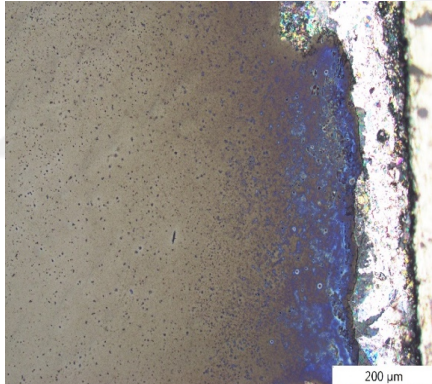
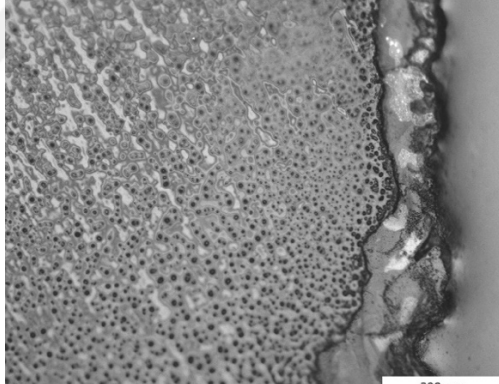
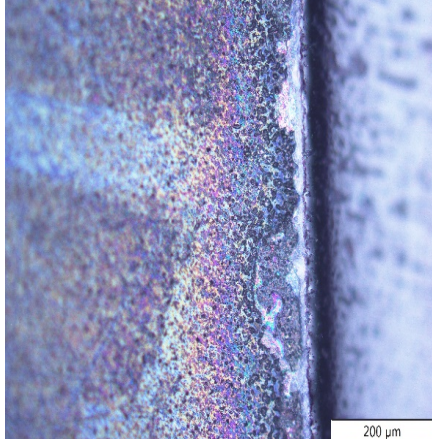



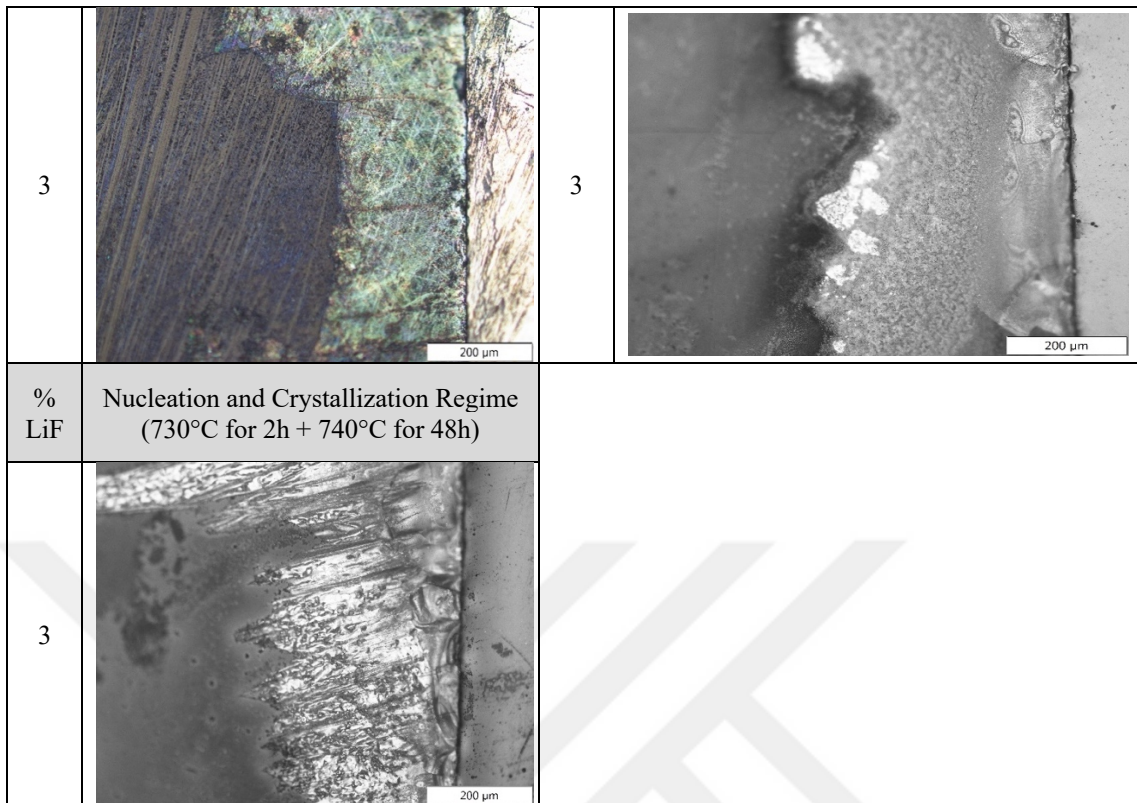
Figure 3.21. ATA SAPHIR 530 polishing device

In order to get clearer images from the sample surfaces in the optical microscope, etching was applied with mixture prepared with 5 vol. percent hydrofluoric (HF) acid in 90 seconds.

The surface of the etched samples were examined on optical microscope at 20x magnification.

Table 3.1. Optical microscope image of crystallized samples

% LiF	Nucleation and Crystallization Regime (730°C for 2h + 740°C for 48h)	% LiF	Nucleation and Crystallization Regime (730°C for 2h + 740°C for 24h)
1		2	
% LiF	Nucleation and Crystallization Regime (730°C for 2h + 740°C for 48h)	% LiF	Nucleation and Crystallization Regime (680°C for 2h + 690°C for 24h)
2		3	
% LiF	Nucleation and Crystallization Regime (730°C for 2h + 740°C for 3h)	% LiF	Nucleation and Crystallization Regime (730°C for 2h + 740°C for 6h)
3		3	
% LiF	Nucleation and Crystallization Regime (730°C for 2h + 740°C for 9h)	% LiF	Nucleation and Crystallization Regime (730°C for 2h + 740°C for 24h)

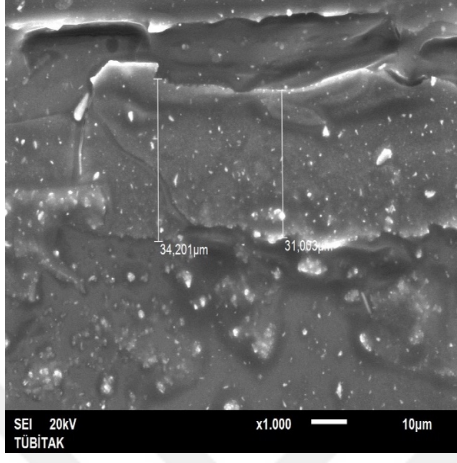
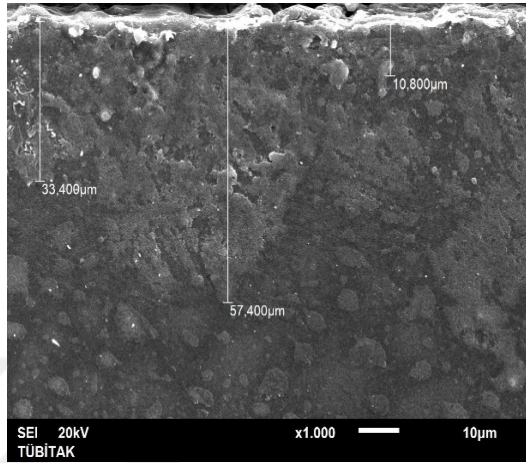
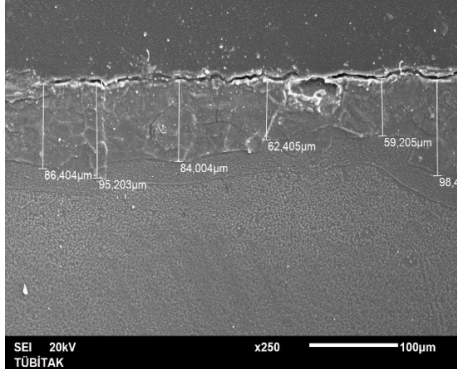
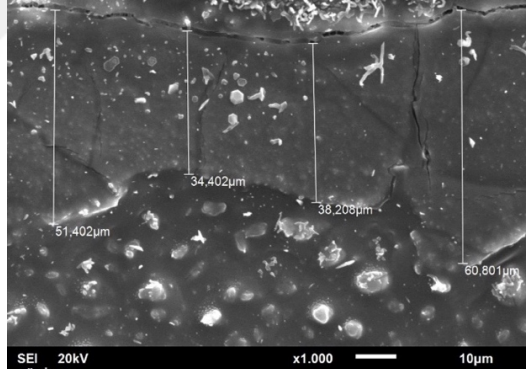
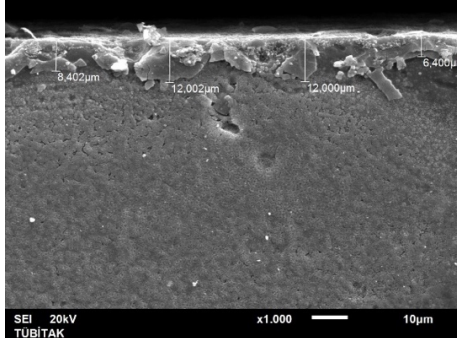
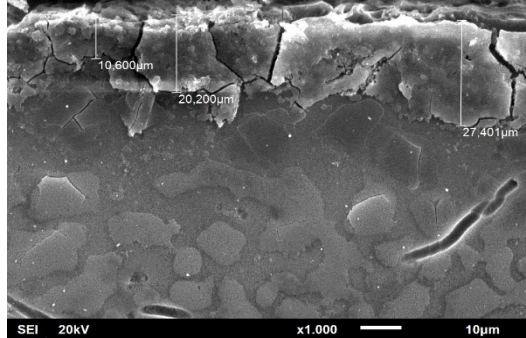


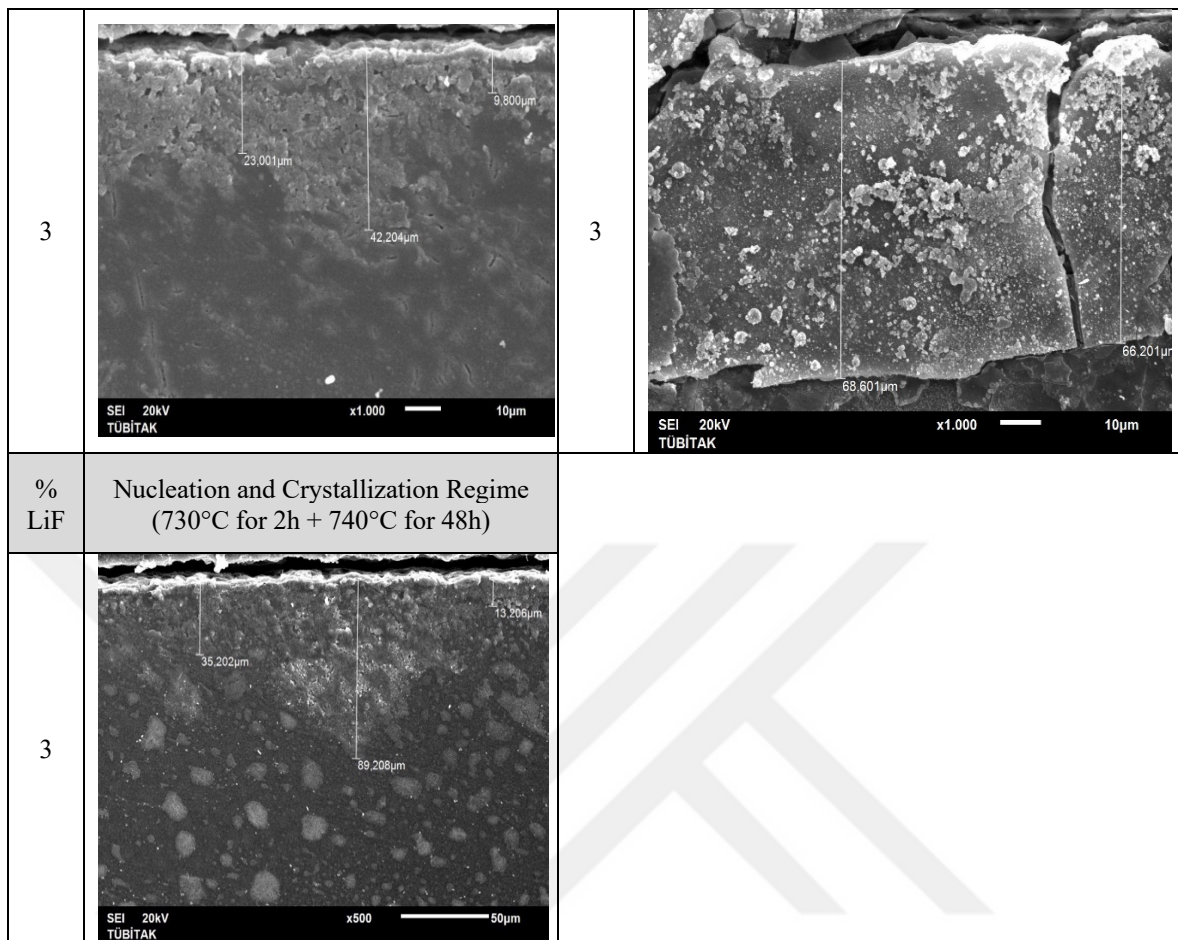
When the samples detected crystals with XRD – Thin Film analyze was examined under optical microscope, it was observed that crystals starting from the edges of the samples to growing certain area appeared on the surface. These results confirmed the surface crystallization calculated from the Avrami constant. Then, Scanning Electron Microscopy (SEM) analyze was performed in order to observe the crystals clearly, and to determine their size. In the next section, detailed information will be given by SEM analysis.

### 3.1.3. Scanning Electron Microscopy (SEM) Analysis

In order to determine the size and get clear image of the surface crystallization seen with optical microscope, SEM analysis was performed at 500x and 1000x magnification with JEOL JSM-6510-LV - Scanning Electron Microscopy (SEM) device. Table 3.2. shows the SEM image of samples observed crystal phase at XRD-Thin Film analysis results at different time and temperature regime.

Table 3.2. SEM image of crystallized samples

% LiF	Nucleation and Crystallization Regime (730°C for 2h + 740°C for 48h)	% LiF	Nucleation and Crystallization Regime (730°C for 2h + 740°C for 24h)
1		2	
% LiF	Nucleation and Crystallization Regime (730°C for 2h + 740°C for 48h)	% LiF	Nucleation and Crystallization Regime (680°C for 2h + 690°C for 24h)
2		3	
% LiF	Nucleation and Crystallization Regime (730°C for 2h + 740°C for 3h)	% LiF	Nucleation and Crystallization Regime (730°C for 2h + 740°C for 6h)
3		3	
% LiF	Nucleation and Crystallization Regime (730°C for 2h + 740°C for 9h)	% LiF	Nucleation and Crystallization Regime (730°C for 2h + 740°C for 24h)



When the SEM analysis results of the given samples examined, it is found that LiF content in the composition and crystallization regime affects the size of crystal phase formed on the surface of the samples. To illustrate, whereas the size of crystalline phases formed on surface of the sample doped 3 wt. percent LiF content and nucleated at 730°C 2h and crystallized at 740°C 3h is in the range 6,4  $\mu\text{m}$  and 12,002  $\mu\text{m}$ , the size of the crystalline phase formed on the surface of the sample doped 3 wt. percent LiF and nucleated at 730°C 2h and crystallized at 740°C 48h is reached to 89,208  $\mu\text{m}$ . It is clearly observed that the size of crystalline phase is increased based on crystallization regime and LiF content. When the effects of crystallization regime and LiF content on size of crystalline phase investigated, while the size of crystalline phase formed on the surface of the samples doped 1 wt. percent LiF and nucleated at 730°C 2h and crystallized at 740°C 48h is roughly 34  $\mu\text{m}$ , the size of crystalline phase formed on the surface of the samples doped 3 wt. percent LiF and nucleated at 730°C 2h and crystallized at 740°C 48h is approximately 90  $\mu\text{m}$ . As a conclusion, when the LiF content is low and crystallization process is performed at high temperature such as in this study, the size of formed crystalline phase is in the low scale relatively.

### 3.1.4. Transmittance Analysis of Glass-Ceramic Materials

As it mentioned in the section where the properties of substrate glasses are given, the transmittance is important in such glasses used in display technology. Transmittance value in display technologies play critical role in reflecting the signal entering display technology system to reach users as image quality. For this reason, transmittance value of glass substrate effect other component performance of display technology system.

It is known that directly transmittance percent of total solar energy at 300 – 2500 nm wavelength range to through glass surface is called as transmittance of solar energy. Transmittance of daylight, transmittance percent of total light at 90° right angle at 380 – 780 nm wavelength range to through glass surface is described. Transmittance percent of light which is at 780-2500 nm wavelength range and is at 300 – 380 nm wavelength range to through glass surface is considered infrared and ultraviolet transmittance respectively.



Figure 3.22. Perkin Elmer UV-Visible-NIR spectrophotometer

UV-Visible analysis of the parent glass and glass-ceramics doped with 1 – 2 – 3 wt. percent LiF and crystallized at different time and temperature was analyzed with Perkin Elmer Lambda 750S model UV-Visible-NIR spectrophotometer device with 5 nm/s surface scanning speed and at 250 – 2500 nm wavelength range.

In the transmittance analysis of each sample crystallized at different crystallization regime were divided into three categories as (1) crystallization regime nucleated at 630°C for 2h

and crystallized at 640°C for 3h-6h-9h-24h, as (2) crystallization regime nucleated at 680°C for 2h and crystallized at 690°C for 3h-6h-9h-24h, as (3) crystallization regime nucleated at 730°C for 2h and crystallized at 740°C for 3h-6h-9h-24h-48h. And then, transmittance of samples was analyzed based on proportion of LiF content on the glass composition, and increasing crystallization temperature-time.

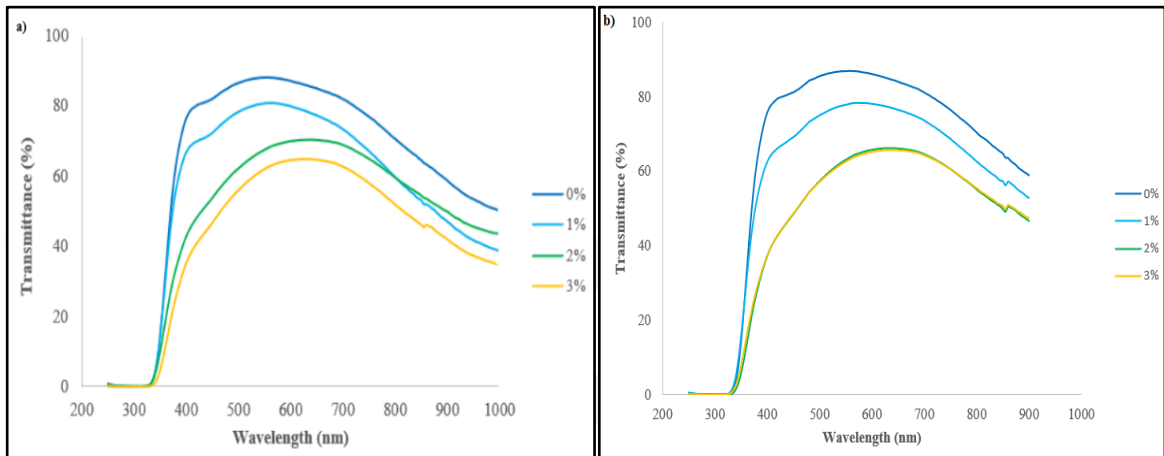


Figure 3.23. Transmittance of samples nucleated at 630°C for 2h and (a) crystallized at 640°C for 3h and (b) crystallized at 640°C for 6h

When the transmittance of samples examined, the transmittance of the samples crystallized at 3h-6h are very close to each other. For example, transmittance value of the glass sample without additive of LiF crystallized at 3h-6h is 83,99 and 83,25 respectively. Additionally, transmittance value of samples doped 3 wt. percent LiF crystallized at 3h-6h is 66,11 and 64,94 respectively.

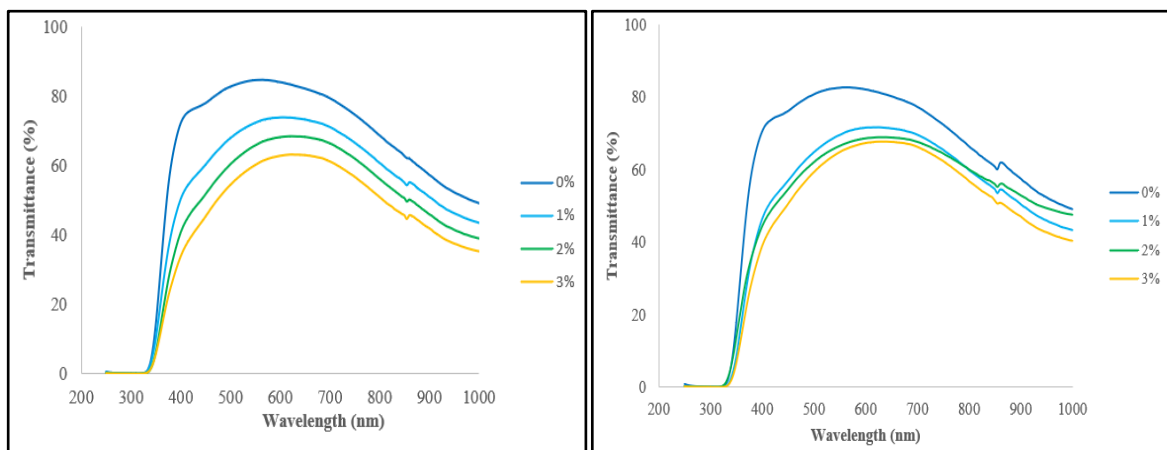


Figure 3.24. Transmittance of samples nucleated at 630°C for 2h and (a) crystallized at 640°C for 9h and (b) crystallized at 640°C for 24h

Transmittance value of glass sample without additive of LiF crystallized at 9h-24h are 82,87 and 82,74 respectively. Also, transmittance value of the glass samples doped 3 wt. percent LiF crystallized at 9h-24h are 64,62 and 63,15. As a result, decreasing of transmittance value in the visible range was observed based on LiF content and crystallization process. However, when the transmittance value of the samples are compared with XRD-Thin Film results, no crystalline phase observed in the given samples. Therefore, it is thought that color changing in the samples effects transmittance value or dimensions of crystalline phase are below  $3\mu\text{m}$ - $3\text{nm}$  which is XRD-Thin Film analysis range. Transmittance value for each composition is given in Table 3.3.

Table 3.3. Transmittance value of the samples nucleated at  $630^{\circ}\text{C}$  for 2h and crystallized at  $640^{\circ}\text{C}$  for 9h-24h and at different LiF content

% LiF	Transmittance Value			
	$630^{\circ}\text{C}$ 2h + $640^{\circ}\text{C}$ 3h	$630^{\circ}\text{C}$ 2h + $640^{\circ}\text{C}$ 6h	$630^{\circ}\text{C}$ 2h + $640^{\circ}\text{C}$ 9h	$630^{\circ}\text{C}$ 2h + $640^{\circ}\text{C}$ 24h
0	83,99	83,25	82,87	82,74
1	79,52	77,12	76,27	74,11
2	68,41	66,52	66,31	65,87
3	66,11	64,94	64,62	63,15

Obtained transmittance value of each compositions shown in Table 3.3 is given in Figure 3.25 comparatively.



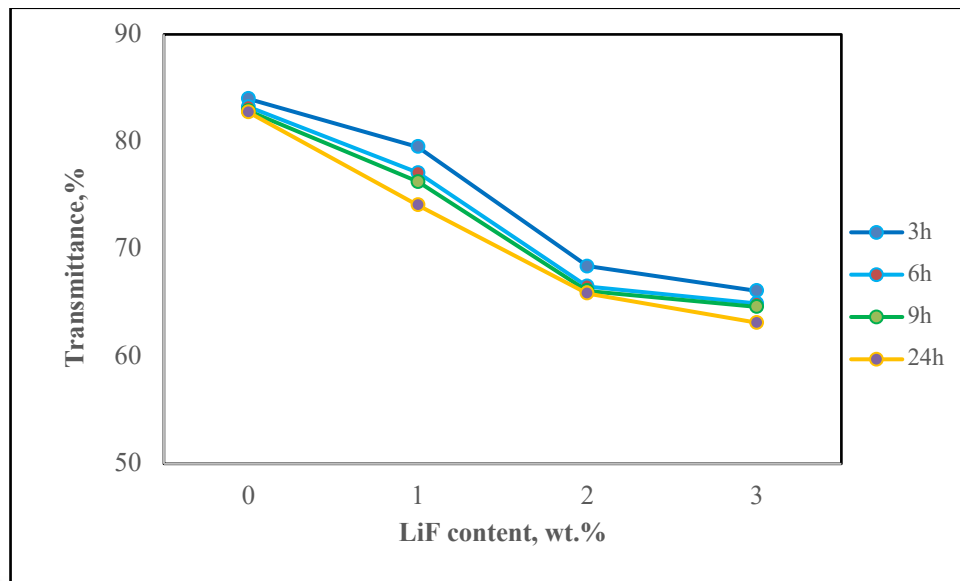


Figure 3.25. The transmittance value of samples nucleated at 630 °C for 2h and crystallized at 640°C for 3h-6h-9h-24h

In summary, as explained above section, transmittance value of samples nucleated at 630 °C for 2h and crystallized at 640°C for 3h-6h-9h-24h decreased based on LiF content and crystallization time. The highest transmittance value was obtained.

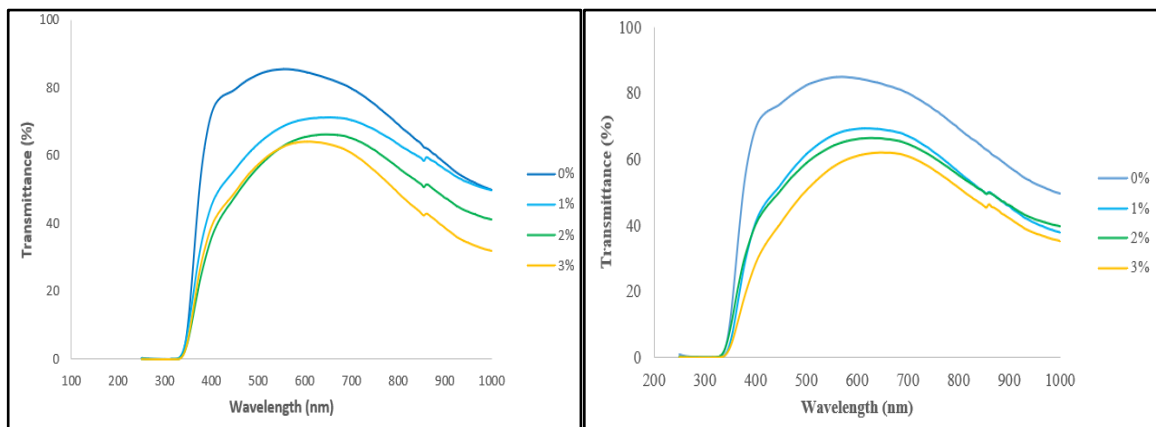


Figure 3.26. Transmittance of samples nucleated at 680°C for 2h and (a) crystallized at 690°C for 3h and (b) crystallized at 690°C for 6h

After the crystallization process was extended to 690°C for 3h-6h, transmittance value of without additive of LiF samples crystallized at 690°C for 3h-6h was obtained 81,86 and 75,1 respectively. It is recognized that these results are lower when the results are compared with transmittance value of samples crystallized at 640°C for 3h-6h. Besides, transmittance value

for the samples doped 3 wt. percent LiF is 62,32 and 62,09 respectively. To these results, it should be added that there is no crystal formation in the XRD-Thin Film analysis.

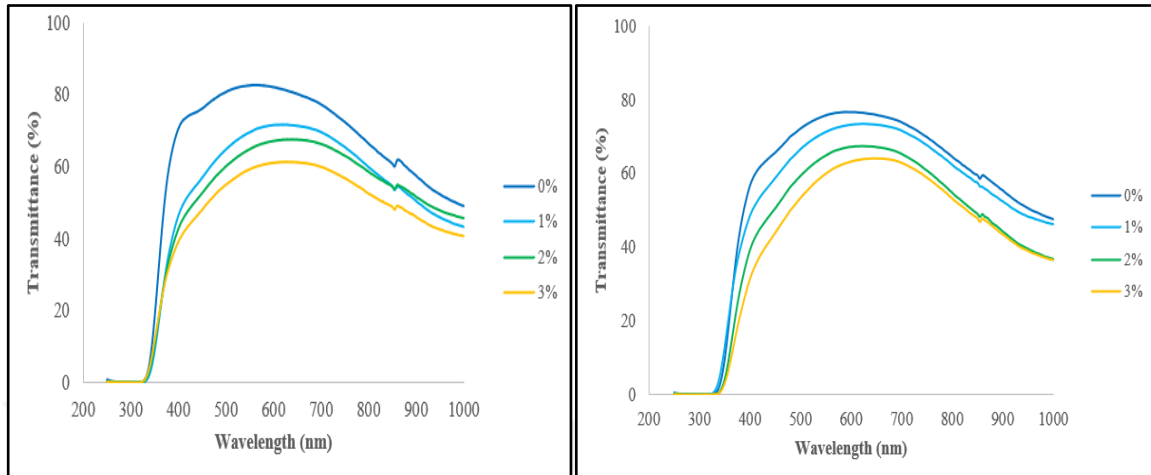


Figure 3.27. Transmittance of samples nucleated at 680°C for 2h and (a) crystallized at 690°C for 9h and (b) crystallized at 690°C for 24h

Transmittance value of samples nucleated at 680°C for 2h and crystallized at 690°C for 9h-24h without LiF is 73,1 and 72,23 respectively. For samples doped 3 wt. percent LiF and crystallized at 690°C for 9h-24h is 61,78 and 61,59 respectively. As in previous results, crystallization temperature-time and LiF content effects transmittance value of samples. However, except sample doped 3wt. percent LiF and crystallized at 690°C for 24h, there is no crystal formation in the XRD-Thin Film analysis. Crystalline phase was detected in the sample doped 3 wt. percent LiF and crystallized at 690°C for 24h with XRD-Thin Film analysis and transmittance value of this samples is 61,59. It is thought that dimensions crystalline phase detected in this sample was enhanced based on crystallization time. Transmittance value for each composition is given in Table 3.4.

Table 3.4. Transmittance value of the samples nucleated at 680°C for 2h and crystallized at 690°C for 9h-24h and at different LiF content

% LiF	Transmittance Value			
	680°C 2h + 690°C 3h	630°C 2h + 690°C 6h	630°C 2h + 690°C 9h	630°C 2h + 690°C 24h
0	81,86	75,1	73,1	72,23
1	77,48	74,2	73,27	72,14
2	67,1	65,41	63,32	63
3	62,32	62,09	61,78	61,59

Obtained transmittance value of each compositions shown in Table 3.4 is given in Figure 3.28 comparatively.

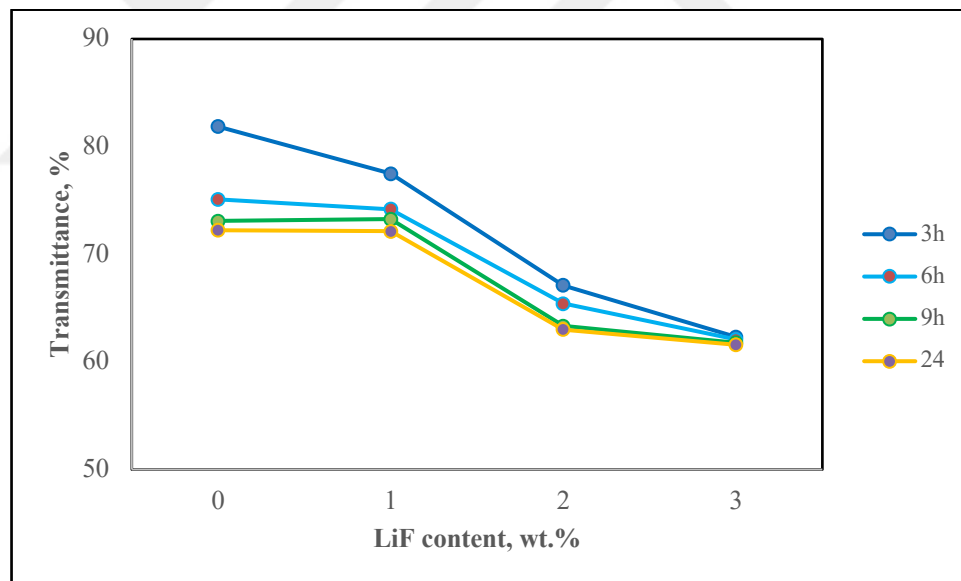


Figure 3.28. The transmittance value of samples nucleated at 680 °C for 2h and crystallized at 690°C for 3h-6h-9h-24h

As a summary, transmittance value of samples nucleated at 680°C for 2h and crystallized at 690°C for 3h-6h-9h-24h decreased based on LiF content and crystallization time like in previous crystalline regime. Finally, transmittance value of samples nucleated at 730°C for 2h and crystallized at 740°C was analyzed.

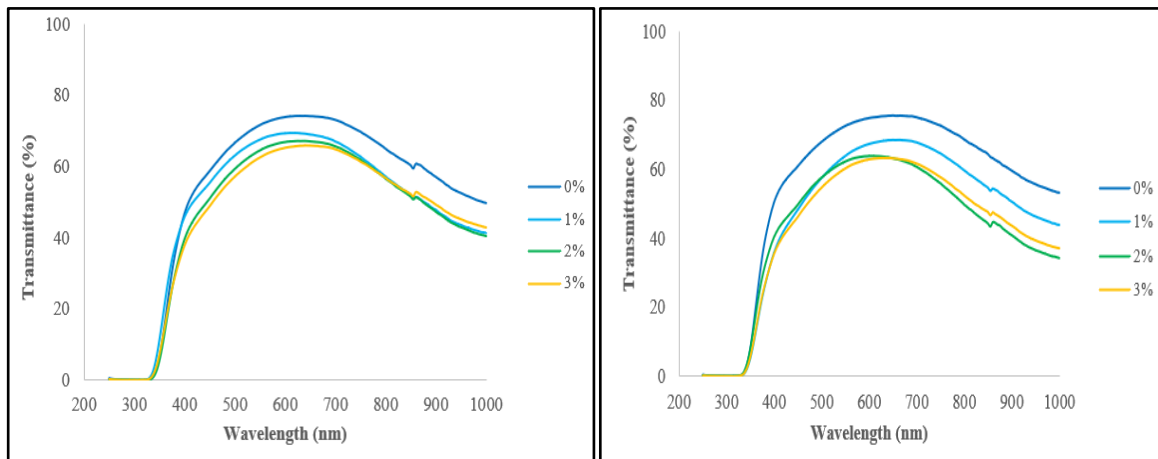


Figure 3.29. Transmittance of samples nucleated at 730°C for 2h and (a) crystallized at 740°C for 3h and (b) crystallized at 740°C for 6h

Transmittance value of samples nucleated at 730°C for 2h and crystallized at 740°C for 3h-6h without LiF is 71,16 and 70,04 respectively. For samples doped 3 wt. percent LiF and crystallized at 690°C for 3h-6h is 61,31 and 61,11 respectively. As in the previous results, the transmittance value of the samples continues to decreased depending on crystallization regime and LiF content.

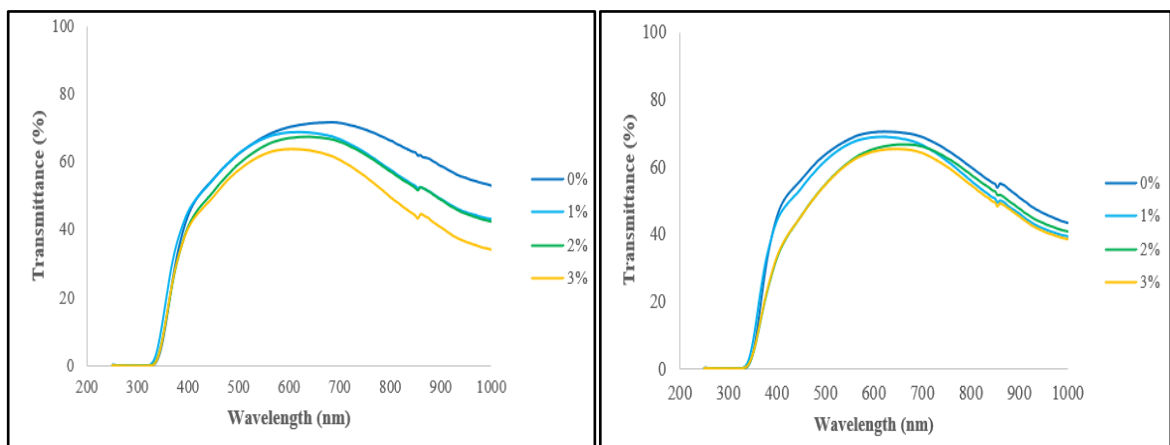


Figure 3.30. Transmittance of samples nucleated at 730°C for 2h and (a) crystallized at 740°C for 9h and (b) crystallized at 740°C for 24h

Transmittance value of samples nucleated at 730°C for 2h and crystallized at 740°C for 9h-24h without LiF is 69,31 and 67,18 respectively. For samples doped 3 wt. percent LiF and crystallized at 740°C for 9h-24h is 60,15 and 59,12 respectively. Crystalline phase was observed in these samples with XRD-Thin Film analysis. Transmittance value of parent glass and glass compositions doped 1-2-3 wt. percent LiF is shown in Figure 3.31.

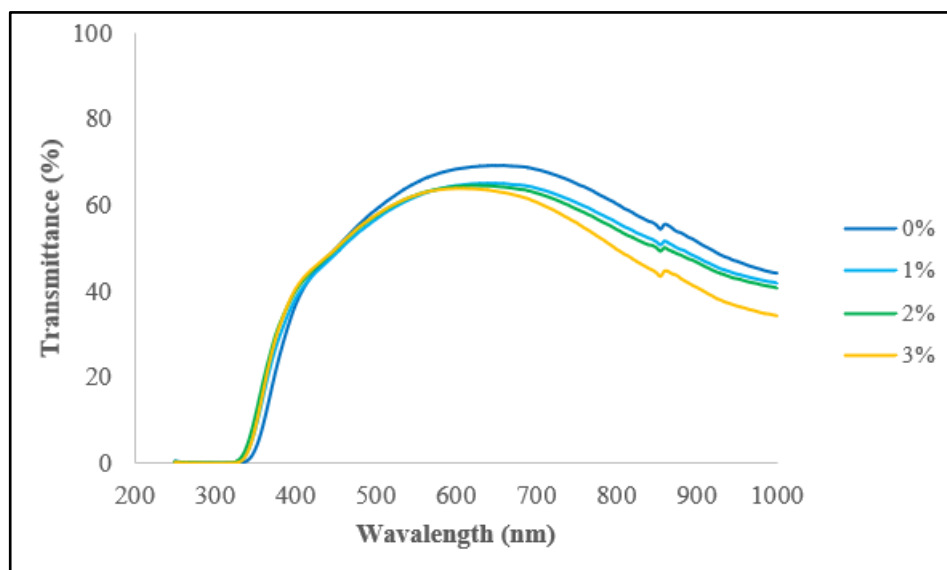


Figure 3.31. Transmittance of sample nucleated at 730°C for 2h and crystallized at 740°C for 48h

Transmittance value for pure glass composition and glass composition doped with 1-2-3 wt. percent LiF and crystallized at different temperature-time regime is given in Table 3.5

Table 3.5. Transmittance value of the samples nucleated at 730°C for 2h and crystallized at 740°C for 3h-6h-9h-24h and at different LiF content

% LiF	Transmittance Value				
	730°C 2h + 740°C 3h	730°C 2h + 740°C 6h	730°C 2h + 740°C 9h	730°C 2h + 740°C 24h	730°C 2h + 740°C 48h
0	71,16	70,04	69,31	67,18	64,69
1	67,41	67,08	65,58	63,36	62,49
2	64,10	64,21	62,54	61,44	60,14
3	61,31	61,11	60,15	59,12	58,79

Obtained transmittance value of each compositions shown in Table 3.5 is given in Figure 3.32 comparatively.

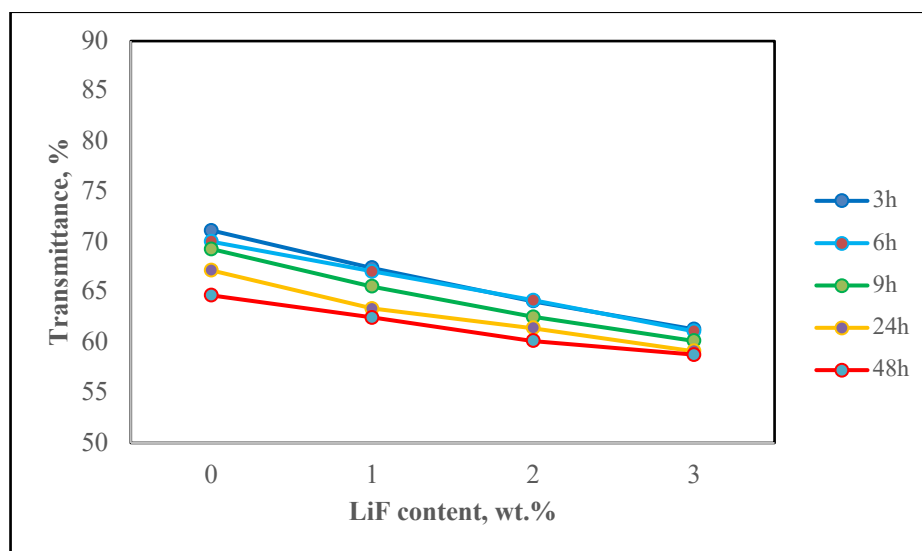


Figure 3.32. The transmittance value of samples nucleated at 730°C for 2h and crystallized at 740°C for 3h-6h-9h-24h-48h

Transmittance value of samples nucleated at 730°C for 2h and crystallized at 740°C for 48h without LiF is 64,69. For samples doped 3 wt. percent LiF and crystallized at 740°C for 48h is 58,79. The lowest transmittance value was obtained in the crystallized at 740°C for 48h crystallization regime.

Transmittance value of all the samples decreased based on crystallization regime and LiF content. When these results are compared with other studies with regard to producing alkali-free glass and glass ceramics, Liu J. [64] proposed that transmittance value of the samples is decreased based on crystallization regime as well. Although transmittance value of the samples crystallized at 640°C and 690°C for 3h-6h-9h-24 except the sample doped 3 wt. percent LiF and crystallized at 690°C decreased, no crystalline phase observed in these samples. There are two reasons for the situation. One of them is color changing of the samples and second of them is dimensions of crystalline phase. In addition to these, as seen in the optical microscope and SEM analysis formed crystals starts from edges of the samples and growth toward the center. It is concluded that there is not clear difference between crystallization regime due to the the surface crystallization formed edge of the samples. In other words, formed crystals did not cover entire sample surfaces. But, it is observed that transmittance values of samples decreased because of LiF addition.

### 3.1.5. Three Point Bending Test of Produced Glass-Ceramics

Since the crystalline phase formed on the surface of the samples was observed clearly at both XRD method and SEM analysis, in the determination of mechanical behavior of glass and glass-ceramic materials, the samples detected crystalline phase at XRD-Thin Film analysis and crystallized at 740°C for 48 h was selected.

Before the testing, the samples were cut into 3x4x50 mm dimensions according to ISO 14704:2008(E) – Fine ceramics (advanced ceramics, advanced technical ceramics). Each experiment was performed with a crosshead speed of 0.5mm/min and under 5kN load cell. Also, each result is the average value of three measurements in each experiment.

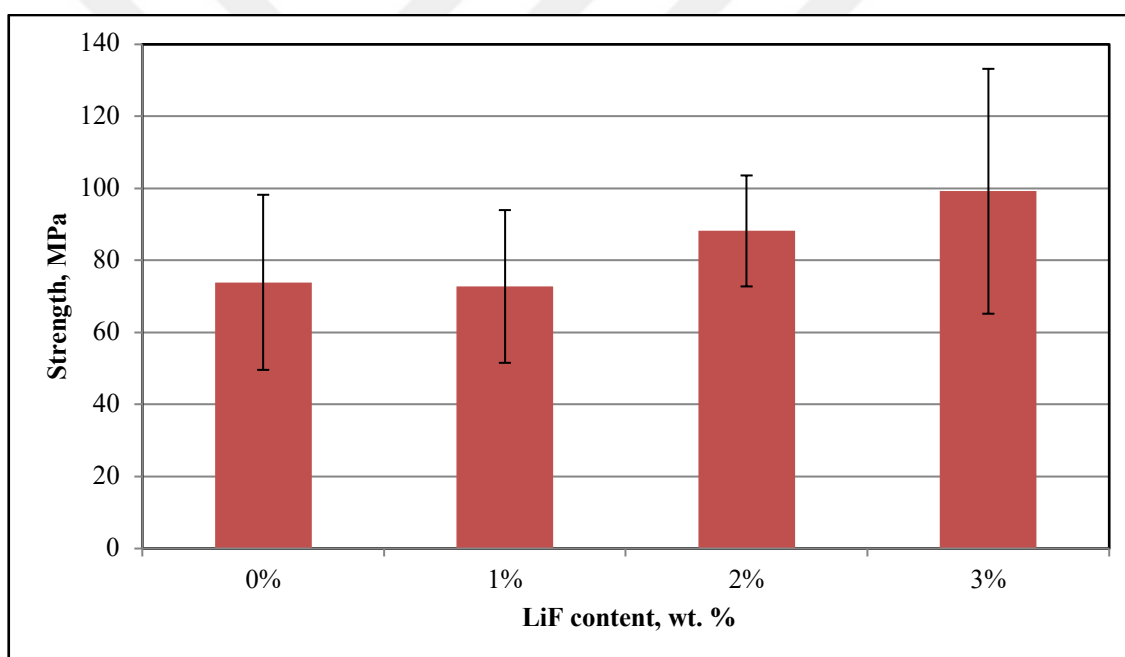


Figure 3.33. Three point bending test of the produced glass and glass-ceramic materials nucleated at 730°C for 2h and crystallized at 740°C for 48h

It is shown that mechanical strength of the samples increase depending upon LiF content in the structure in Figure 3.33. Since LiF is used as nucleation agent in the given composition, it trigger forming of the crystalline phase. For this reason, mechanical properties of the different samples shown in Figure 3.33 was enhanced at certain value. It is thought that there are not clear difference between these samples because of the surface crystallization. Because, surface crystallization did not cover all surface of the samples. Consequently, it is

expect that mechanical properties of the samples are close each other relatively like in Figure 3.33.





## 4. CONCLUSION

The aim of the thesis was to produce and characterization of glass and glass-ceramic materials with compositions obtained from patents including glass substrate properties for display technologies. In characterization tests, physical (thermal expansion coefficient,  $T_g$  and softening temperature), chemical (crystal structure of formed phase), microstructural analysis (optical microscope, SEM), optical (transmittance) properties of glass and glass-ceramics was analyzed depending on LiF content. The obtained findings are summarized below.

1. Crystallization behavior of the glass material produced in desired proportion adding with 1-2-3 wt. percent LiF was examined by using Ozawa-Kissinger crystallization method. Results calculated from both crystallization methods, when the LiF content in the glass composition is increased,  $T_g$  and  $T_c$  temperature of samples is decreased. Correspondingly, activation energy of the samples is decreased with increasing LiF content. To illustrate, activation energy of glass composition without LiF was calculated 421 kJ/mol in Ozawa method. When LiF proportion in composition is increased from 0 to 1 – 2 – 3, activation energy values of each composition was calculated as 388 kJ/mol, 368 kJ/mol, and 301 kJ/mol for each composition respectively. In Kissinger method, similar results was obtained. While activation energy of glass material without added of LiF was calculated 401 kJ/mol, these values decreased to 369 kJ/mol, 349 kJ/mol, 282 kJ/mol depending on 1 – 2 - 3 wt. percent LiF content, respectively.
2. Crystallization process was completed at determined temperature-time regime, phase structure of produced glass-ceramics was analyzed with XRD method. In the first step, XRD analyze of glass-ceramic materials was performed as powdery. As a result, any crystalline phase no observed. Then, thin film analyzed was done with XRD method, crystalline phase was detected the samples firstly, doped 1 wt. percent LiF, nucleated at 730°C for 2h and 740°C for 24h-48h secondly, doped 2 wt. percent LiF, nucleated at 730°C for 2h and 740°C for 9-24-48hours and finally, doped 3 wt. LiF 680°C for 2h and crystallized at 690°C for 24h, and 730°C for 2h and crystallized 740°C for 3h-6h-9h-24h-48h.

3. In order to see the formed crystal structure, surface of the samples was examined with optical microscope. In the optical microscope, crystalline phases growing from the edge of samples at certain dimensions was observed. Because of the growing of the crystals from edge of the samples at certain dimensions, the surface crystallization of samples is confirmed and the result explain why the crystal structure was no observed in XRD analysis in bulk and powder form.
4. The thermal expansion coefficient of glass compositions analyzed at between 0-300°C temperature vary on between  $4,3 \times 10^{-6}/\text{K}$  –  $5,5 \times 10^{-6}/\text{K}$  based on LiF content like previous characterization methods. Whereas thermal expansion coefficient of produced glass no added LiF is  $4,3 \times 10^{-6}/\text{K}$ , in the doped 1-2-3 wt. percent glass compositions  $4,5 \times 10^{-6}/\text{K}$ ,  $5,1 \times 10^{-6}/\text{K}$ ,  $5,5 \times 10^{-6}/\text{K}$  is obtained respectively. It is seen that obtained thermal expansion coefficient of produced samples is in the range of commercial display glass.
5. Dimensions of formed crystalline phase on the surface of glass-ceramics was specify with SEM analyze. Dimensions of the crystalline phase was expended depending on increasing LiF content and temperature-time crystallization regime. Whereas the size of crystalline phases was detected on surface of glass-ceramic sample doped wt.1 % LiF and nucleated at 730°C for 2h and crystallized at 740°C for 48h is approximately 35 $\mu\text{m}$  , the size of crystalline phases was detected on surface of glass-ceramic sample doped wt. 3 % LiF and nucleated at 730°C for 2h and crystallized at 740°C for 48h is roughly 90 $\mu\text{m}$ . It is observed that size of crystalline phase on sample surface's is increased based on LiF content in the determined composition.
6. Transmittance values of glass and glass-ceramics was decreased based on crystallization temperature-time and LiF content, and also, color changing of samples. As transmittances of glass material was in the range of 85-90 percent in the visible range, after crystallization process based on increasing temperature-time and LiF content the transmittance value of the glass-ceramic nucleated at 730°C for 2h and crystallized at 740°C for 48h reduced to 58-60 percent in the visible range. At the same time, it is observed that transmittance value of samples which any phase was not detected at XRD and SEM analysis decreased. For the situation, it is thought

that color changing of samples was observed depending on LiF content and as a result color changing effects transmittance of the samples. Also, it is concluded that there is not clear difference crystallization regime due to the surface crystallization formed edge of the samples at certain dimensions. And the surface crystallization did not cover entire sample surface.



## 5. SUGGESTIONS AND FUTURE WORKS

Within the scope of this thesis, glass-ceramics materials were produced at different heat treatment process by using LiF as nucleating agent. As a results of the studies, it is observed that LiF affects the  $T_g$ ,  $T_c$ , and softening temperature of the given glass compositions decreasingly. According to  $T_g$  and  $T_c$  temperatures obtained crystallization kinetics results, heat treatment process was determined and produced glass-ceramics materials. After the heat treatment process, doped 1-2-3 wt percent LiF glass materials have surface crystallization detected on the surface of samples by using XRD, optical microscope, SEM analysis methods. Also, transmittance value of the parent glass and glass-ceramic materials decreased based on doped 1-2-3 wt. percent LiF.

It is observed that crystallization temperature-time is significant properties in the glass-ceramics production process. Crystallization regime affects the formation of new phases on the structure. For this reason, crystallization temperature and time can be extended by taking into account the  $T_g$ ,  $T_c$ , and softening temperature. Then, phase transformation and effects of new phases can be investigated in the new structure.

For the future works, nucleating agent can be changed and effects of a new nucleating agent on the crystallization behavior and other properties of the glass materials can be investigated. Different nucleating agent except LiF can cause to form bulk crystallization and transmittance, mechanical properties of produced glass-ceramics can be examined.

Glass composition worked on the thesis was determined from patents include properties of glass substrate materials. For the future works, components of the determined glass composition can be decreased or increased and chemical durability, thermal stability, etc. of the created new compositions can be explored.

## REFERENCES

1. Chen HW, Lee JH, Lin BY, Chen S, Wu ST. Liquid crystal display and organic light-emitting diode display: present status and future perspectives. *Light: Science & Applications*. 2018;7(3):17168-17168.
2. Gurski J, Quach LM. *Display technology overview*. Ottawa: Lytica White Paper Press; 2005.
3. Hopper DG. Display science and technology for defense and security. *International Society for Optics and Photonics*. 2004;52(14):1-10
4. Molinaroli CJ, inventor. Light emitting diode display device. United States patent US 6,265,984. 2001 Jul 24.
5. Larach SI, Hardy AE. Cathode-ray-tube phosphors: principles and applications. *Proceedings of the IEEE*. 1973;61(7):915-26.
6. Bagher AM, Vahid MM, Mohsen M. A Review of Challenges in Display Technology. *Int. J. Electr. Compon. Energy Convers*. 2017;19(3):26-39.
7. Dielectric Material Market by Technology; 2014 [Cited 2014 15 March] Available from: <https://www.marketsandmarkets.com/Market-Reports/display-materials-market-42841002.html>
8. Ellison A, Cornejo IA. Glass substrates for liquid crystal displays. *International Journal of Applied Glass Science*. 2010;1(1):87-103.
9. Eichmeier JA, Thumm M. *Vacuum Electronics: Components and Devices*. M $\ddot{u}$ nich: Springer Science & Business Media Press; 2008.
10. Weber LF. History of the plasma display panel. *IEEE Transactions on Plasma Science*. 2006;34(2):268-278.

11. Jandt KD, Mills RW. A brief history of LED photopolymerization. *Dental Materials*. 2013;29(6):605-17.
12. King CN. Electroluminescent displays. *Journal of Vacuum Science & Technology A: Vacuum, Surfaces, and Films*. 1996;14(3):1729-35.
13. Chang MH, Das D, Varde PV, Pecht M. Light emitting diodes reliability review. *Microelectronics Reliability*. 2012;52(5):762-82.
14. Kawamoto H. The history of liquid-crystal displays. *Proceedings of the IEEE*. 2002;90(4):460-500.
15. Kunić S, Šego Z. OLED technology and displays. In *Proceedings ELMAR-2012, International Symposium on Electronics in Marine on*; 2012
16. Lee DK, Kim SK, Hong IK, Ko JM, Im SH, inventors; LG Chem Ltd, assignee. Alkali-free glass and preparation thereof. United States patent US 8,883,665. 2014 Nov 11.
17. Shin D, Kim Y, Chang N, Pedram M. Dynamic voltage scaling of OLED displays. *IEEE Council on Electronic Design Automation CEDA, In Proceedings of the 48th Design Automation Conference on*; 2011.
18. Amin J, Ellison AJ, Glaesemann GS, Gross TM, inventors; Corning Inc, assignee. Glass articles/materials for use as touchscreen substrates. United States patent application US 13/291,567. 2012 May 31.
19. Organic Electronics Market by Material; 2014 [Cited 2014 20 August]. Available from: <http://www.marketsandmarkets.com/Market-Reports/organic-electronics-market-144113962.html>
20. Shelby JE. *Introduction to glass science and technology*. New York: Royal Society of Chemistry Press; 2005.

21. Günay V, Yılmaz Ş. *Cam-Seramikler: Bilim ve Teknolojisi*. Kocaeli: TÜBİTAK MAM Press; 2010.
22. Seramik ve Cam Teknolojisi, Camın Kimyasal Yapısı; 2006 [Cited 2006 6 June] Available from: [http://ismek.ist/files/ismekOrg/file/2013\\_hbo\\_program\\_modulleri/camin\\_kimyasal\\_yapisi.pdf](http://ismek.ist/files/ismekOrg/file/2013_hbo_program_modulleri/camin_kimyasal_yapisi.pdf)
23. Sakamoto A, Yamamoto S. Glass–ceramics: engineering principles and applications. *International Journal of Applied Glass Science*. 2010;1(3):237-47.
24. Montazerian M, Singh SP, Zanotto ED. An analysis of glass-ceramic research and commercialization. *American Ceramic Society Bulletin*. 2015;94(4):30-5.
25. Davis MJ. Practical aspects and implications of interfaces in glass-ceramics: A review. *International Journal of Materials Research*. 2008;99(1):120-9.
26. Holand W, Beall GH. *Glass-ceramic technology*. New York: John Wiley & Sons Press; 2019.
27. Zanotto ED. Bright future for glass-ceramics. *American Ceramics Society Bulletin*. 2010;89(8):19-27.
28. Miwa S, inventor; Nippon Electric Glass Co Ltd, assignee. Alkali-free glass substrate. United States patent US 5,851,939. 1998 Dec 22.
29. Miwa S, inventor; Nippon Electric Glass Co Ltd, assignee. Alkali-free glass substrate. United States patent US 5,811,361. 1998 Sep 22.
30. Murata T, Miwa S, inventors; Nippon Electric Glass Co Ltd, assignee. Alkali-free glass. United States patent US 8,835,335. 2014 Sep 16.

31. Dumbaugh Jr WH, inventor; Corning Inc, assignee. Substrate glass for liquid crystal displays. United States patent US 4,824,808. 1989 Apr 25.
32. Bocko PL. Handbook of Visual Display Technology. *Glass Substrates for AMLCD, OLED and Emerging Display Platforms*. 2012:559-623
33. Lapp JC, Bocko PL, Nelson JW. Advanced glass substrates for flat panel displays. In Advanced Flat Panel Display Technologies. *International Society for Optics And Photonics, IS&T/SPIE 1994 International Symposium on Electronic Imaging: Science and Technology on*; 1994.
34. Faulkner EK, Whitney RK, Zeman JE. Alkali extraction as a determinant in the selection of a glass for displays. *IEEE Transactions on Electron Devices*. 1983;30(5):545-8.
35. Moffatt DM. Glass substrates for flat panel displays. *MRS Bulletin*. 1996;21(3):31-4.
36. Castellano JA, editor. *Handbook of display technology*. San Jose, California: Elsevier Press; 2012.
37. Dumbaugh Jr WH, inventor; Corning Inc, assignee. Thin silicon film electronic device. United States patent US 4,180,618. 1979 Dec 25.
38. Kantur U. Kurşun geçirmez cam üretim sürecinin incelenmesi [M.Sc Thesis]. Edirne: Trakya University; 2009.
39. Musgraves JD, Hu J, Calvez L, editors. *Handbook of Glass*. New York: Springer Press; 2019.
40. Advanced Optics, Capabilities, Melting & Hot Forming, Up-Draw Process SCHOTT AG's homepage 2005 [Cited 2005 4 May]. Available from: [https://www.schott.com/advanced\\_optics/english/capabilities/up-draw-process.html](https://www.schott.com/advanced_optics/english/capabilities/up-draw-process.html)



41. Loeffelbein B, Buellesfeld F, Langsdorf A, inventors; Schott AG, assignee. Method of production of high-refractive thin glass substrates. United States patent US 10,505,129. 2019 Dec 10.
42. Pitbladdo RB, inventor; Corning Inc, assignee. Overflow downdraw glass forming method and apparatus. United States patent US 8,042,361. 2011 Oct 25.
43. Pitbladdo RB, inventor. Overflow downdraw glass forming method and apparatus. United States patent US 6,748,765. 2004 Jun 15.
44. Hou Y, Cheng J, Kang J, Cui J, Xue X, Zuo D. Effect of Parameters of Isopipe on the Quality of Glass Sheet Produced from Overflow Fusion Process by Numerical Simulation. *InMATEC Web of Conferences* on 2017.
45. McIntosh JJ, inventor; Corning Inc, assignee. High delivery temperature isopipe materials. United States patent US 8,028,544. 2011 Oct 4.
46. Lin HJ, Hsu FY, Chang WK. Effect of isopipe temperature on the glass sheet forming for overflow fusion process by numerical simulation. *In Advanced Materials Research* 2008;39(1):517-522.
47. Lin HJ, Chang WK. Design of a sheet forming apparatus for overflow fusion process by numerical simulation. *Journal of Non-crystalline Solids*. 2007;353(30-31):2817-25.
48. Murata T, Yanase T, Miwa S, Yamazaki H. Ultra thin glass roll for flexible AMOLED display. *Nippon Electronic Glass Co., Ltd. In 18th International Display Workshops* on; 2011.
49. Milillo SM, Rhoads RL, inventors; Corning Inc, assignee. Overflow down-draw with improved glass melt velocity and thickness distribution. United States patent US 8,973,402. 2015 Mar 10.

50. Karlsson S, Jonson B, Stålhandske C. The technology of chemical glass strengthening—a review. *Glass Technology*. 2010;51(2):41-54.
51. Shi ZM, Ji GJ. A method to improve mechanical properties of glass plates by surface-coating titania nanofilms with sol–gel technique. *Surface and Coatings Technology*. 2008;202(8):1350-6.
52. Es'kin SV, Kosobudsky ID, Zhimalov AB, Ushakov NM, Gribov AN. Strengthening coating based on silica nanoparticles for soda-lime-silica glass. *Inorganic Materials*. 2014;50(1):63-7.
53. Kirtay S, Oktay E, Avcı GG, Gunay V. Strengthening of SLS glasses by hybrid ormosil coatings. *In Key Engineering Materials*. 2004;264:419-422.
54. Norville HS, King KW, Swofford JL. Behavior and strength of laminated glass. *Journal of Engineering Mechanics*. 1998;124(1):46-53.
55. Khatib J, editor. *Sustainability of Construction Materials*. Kidlington: Woodhead Publishing; Press; 2016.
56. Varshneya AK. Chemical strengthening of glass: lessons learned and yet to be learned. *International Journal of Applied Glass Science*. 2010;(2):131-42.
57. Donald IW. Methods for improving the mechanical properties of oxide glasses. *Journal of Materials Science*. 1989;24(12):4177-208.
58. Güzel AS, Sarıgüzel M, Yanık MC, Günay E, Usta M, Öztürk Y. Enhancing mechanical endurance of chemical-tempered thin soda-lime silicate float glass by ion exchange. *Journal of the Australian Ceramic Society*. 2020;56(1):185-201.
59. Shim GI, Eom HW, Kim SH, Park JK, Choi SY. Fabrication of lightweight and thin bulletproof windows using borosilicate glass strengthened by ion exchange. *Composites Part B: Engineering*. 2015;69:44-9.

60. Höland W, Deubener J. *Nucleation and Crystallization of glasses and glass-ceramics*. Germany: Frontiers Media SA Press; 2017.
61. Weinberg M.C. *Nucleation and Crystallization in Liquids and Glasses*. New York: American Ceramic Society Press; 1993.
62. Guo X, Cai X, Song J, Yang G, Yang H. Crystallization and microstructure of CaO–MgO–Al<sub>2</sub>O<sub>3</sub>–SiO<sub>2</sub> glass–ceramics containing complex nucleation agents. *Journal of Non-crystalline Solids*. 2014;405:63-7.
63. Gawronski A, Patzig C, Höche T, Rüssel C. Effect of Y<sub>2</sub>O<sub>3</sub> and CeO<sub>2</sub> on the crystallisation behaviour and mechanical properties of glass–ceramics in the system MgO/Al<sub>2</sub>O<sub>3</sub>/SiO<sub>2</sub>/ZrO<sub>2</sub>. *Journal of Materials Science*. 2015;50(4):1986-95.
64. Liu J, Han L, Luo Z, Huang Q, He X, Lin C, Liu T, Li C, Lu A. Non-alkali glass substrate with improved mechanical properties for display devices. *Journal of Non-Crystalline Solids*. 2019;524:119610.
65. Römer H, Kiefer W, Köpsel D, Nass P, Rodek E, Kolberg U, Pfeiffer T, inventors; Schott AG, assignee. Method for refining molten glass. United States patent US 6,698,244. 2004 Mar 2.
66. Nishizawa M, Nakao Y, inventors; Asahi Glass Co Ltd, assignee. Alkali-free glass and flat panel display. United States patent US 6,169,047. 2001 Jan 2.
67. ElBatal FH, Marzouk MA, ElBatal HA. Crystallization and spectroscopic characterizations of binary SrO–B<sub>2</sub>O<sub>3</sub> glasses doped with LiF, NaF, CaF<sub>2</sub>, or TiO<sub>2</sub>. *Journal of the Australian Ceramic Society*. 2019;55(4):1039-49.
68. Hamzawy EM, El-Meliegy EM. Crystallization in the Na<sub>2</sub>O–CaO–Al<sub>2</sub>O<sub>3</sub>–SiO<sub>2</sub>–(LiF) glass compositions. *Ceramics International*. 2007;33(2):227-31.

69. Laporte P, Subtil JL, Courbon M, Bon M, Vincent L. Vacuum-ultraviolet refractive index of LiF and MgF<sub>2</sub> in the temperature range 80-300 K. *JOSA*. 1983;73(8):1062-9.
70. Han L, Song J, Zhang Q, Luo Z, Lu A. Crystallization, structure and characterization of MgO-Al<sub>2</sub>O<sub>3</sub>-SiO<sub>2</sub>-P<sub>2</sub>O<sub>5</sub> transparent glass-ceramics with high crystallinity. *Journal of Non-Crystalline Solids*. 2018;481:123-31.
71. Zhao MJ, Zou XY, Wei QL, Meng S, Zhang HB, Su CH. Preparation and characterization of Na<sub>2</sub>O-Y<sub>2</sub>O<sub>3</sub>-P<sub>2</sub>O<sub>5</sub>-SiO<sub>2</sub> transparent glass ceramics. *In Solid State Phenomena* 2018;281:692-698.
72. Ellison AJ, Kiczenski TJ, inventors; Corning Inc, assignee. Alkali-free glass compositions having high thermal and chemical stability. United States patent US 8,598,056. 2013 Dec 3.
73. Ellison AJ, inventor; Corning Inc, assignee. Alkali-free glasses containing iron and tin as fining agents. United States patent US 7,534,734. 2009 May 19.
74. Dumbaugh Jr WH, inventor; Corning Inc, assignee. Alkaline earth aluminoborosilicate glasses for flat panel displays. United States patent US 5,116,788. 1992 May 26.
75. Brix P, Lautenschlager G, Schneider K, Kloss T, inventors; Schott Glaswerke AG, assignee. Alkali-free aluminoborosilicate glass and its use. United States patent US 5,770,535. 1998 Jun 23.
76. Miwa S, inventor; Nippon Electric Glass Co Ltd, assignee. Alkali-free glass substrate. United States patent US 5,811,361. 1998 Sep 22.
77. Miwa S, inventor; Nippon Electric Glass Co Ltd, assignee. Alkali-free glass substrate. United States patent US 5,851,939. 1998 Dec 22.

78. Peuchert U, Brix P, inventors; Schott AG, assignee. Alkali-free aluminoborosilicate glass and uses thereof. United States patent US 6,329,310. 2001 Dec 11.
79. Nishizawa M, Nakao Y, inventors; Asahi Glass Co Ltd, assignee. Alkali-free glass and display substrate. United States patent US 5,885,914. 1999 Mar 23.
80. Lautenschlager G, Schneider K, Kloss T, Brix P, inventors; Schott AG, assignee. Alkali metal-free aluminoborosilicate glass and its use. United States patent US 6,096,670. 2000 Aug 1.
81. Nishizawa M, Nakao Y, inventors; Asahi Glass Co Ltd, assignee. Alkali-free glass and flat panel display. United States patent US 6,169,047. 2001 Jan 2.
82. Nishizawa M, Nakao Y, Koike A, Kase J, inventors; Asahi Glass Co Ltd, assignee. Alkali-free glass. United States patent US 6,537,937. 2003 Mar 25.
83. Fechner J, Brix P, inventors; Schott AG, assignee. Aluminoborosilicate glass. United States patent application US 11/692,358. 2007 Oct 4.
84. Peuchert U, Gaschler L, inventors; Schott AG, assignee. Aluminoborosilicate glass devoid of alkali and uses thereof. United States patent application US 10/472,528. 2005 May 12.
85. Amin J, Ellison AJ, Glaesemann GS, Gross TM, inventors; Corning Inc, assignee. Glass Articles/Materials For Use As Touchscreen Substrates. United States patent application US 14/448,143. 2014 Nov 20.
86. Ellison AJ, inventor; Corning Inc, assignee. Boroalumino silicate glasses. United States patent US 8,598,055. 2013 Dec 3.
87. Lee DK, Kim SK, Hong IK, Ko JM, Im SH, inventors; LG Chem Ltd, assignee. Alkali-free glass and preparation thereof. United States patent US 8,883,665. 2014 Nov 11.

88. Naka J, Narita T, Miwa S, Yamamoto S, inventors; Nippon Electric Glass Co Ltd, assignee. Method of producing an alkali-free glass. United States patent US 6,546,753. 2003 Apr 15.
89. Peuchert U, Brix P, inventors; Schott AG, assignee. Alkali-free aluminoborosilicate glasses, and uses thereof. United States patent US 7,157,392. 2007 Jan 2.
90. Narita T, Takaya T, Tomamoto M, inventors; Nippon Electric Glass Co Ltd, assignee. Alkali-free glass substrate. United States patent US 7,358,205. 2008 Apr 15.
91. Chacon LC, Ellison AJ, Hares GB, Kohli JT, Lapp JC, Morena R, inventors; Corning Inc, assignee. Glasses for flat panel displays. United States patent US 6,831,029. 2004 Dec 14.
92. Komori H, Miwa S, inventors; Nippon Electric Glass Co Ltd, assignee. Glass substrate. United States patent US 7,968,482. 2011 Jun 28.
93. Takaya T, Tomamoto M, inventors; Nippon Electric Glass Co Ltd, assignee. Glass for display substrate. United States patent US 7,888,276. 2011 Feb 15.
94. Nishizawa M, Kase J, Suzuki K, Maeda K, inventors; AGC Inc, assignee. Alkali-free glass and liquid crystal display panel. United States patent US 7,838,451. 2010 Nov 23.
95. Kurachi J, Koyama A, Hachitani Y, inventors; Hoya Corp, AvanStrate Inc, assignee. Glass substrate for display and display. United States patent US 7,763,559. 2010 Jul 27.
96. Murata T, Miwa S, inventors; Nippon Electric Glass Co Ltd, assignee. Alkali-free glass. United States patent US 8,835,335. 2014 Sep 16.

97. Chacon LC, Ellison AJ, Hares GB, Kohli JT, Lapp JC, Morena R, inventors; Corning Inc, assignee. Glasses for flat panel displays. United States patent US 7,365,038. 2008 Apr 29.
98. Chacon LC, Ellison AJ, Hares GB, Kohli JT, Lapp JC, Morena R, inventors; Corning Inc, assignee. Glasses for flat panel displays. United States patent US 7,524,784. 2009 Apr 28.
99. Maehara T, Nishizawa M, Kase J, Matsumoto S, inventors; AGC Inc, assignee. Alkali-free glass substrate, method for producing it and liquid crystal display panel. United States patent US 7,754,631. 2010 Jul 13.
100. Danielson PS, Ellison AJ, Venkataraman N, inventors; Corning Inc, assignee. Glass compositions having high thermal and chemical stability and methods of making thereof. United States patent US 7,833,919. 2010 Nov 16.
101. Yinnon H, Uhlmann DR. Applications of thermoanalytical techniques to the study of crystallization kinetics in glass-forming liquids, part I: theory. *Journal of Non-Crystalline Solids*. 1983;54(3):253-75.
102. Henderson DW. Thermal analysis of non-isothermal crystallization kinetics in glass forming liquids. *Journal of Non-Crystalline Solids*. 1979;30(3):301-15.
103. Salama SN, Salman SM, Darwish H. Effect of nucleation catalysts on crystallisation characteristics of aluminosilicate glasses. *Ceramics-Silikáty*. 2002;46(1):15-23.